STRATIGRAPHY AND RESERVOIR-ANALOG MODELING OF UPPER MIOCENE SHALLOW-WATER AND DEEP-WATER CARBONATE DEPOSITS: AGUA AMARGA BASIN, SOUTHEAST SPAIN

BY

Submitted to the graduate degree program in Geology
and the Graduate Faculty of the University of Kansas
in partial fulfillment of the requirements for the degree of
Master of Sciences.

____
Robert H. Goldstein, Co-chairperson

____
Evan K. Franseen, Co-chairperson

Committee members* ______________________________*
George Tsoflias

Date defended: March 9, 2009

The Thesis Committee for Rachel Ana Dvoretsky certifies
that this is the approved Version of the following thesis:

STRATIGRAPHY AND RESERVOIR-ANALOG MODELING OF UPPER MIOCENE SHALLOW-WATER AND DEEP-WATER CARBONATE DEPOSITS, AGUA AMARGA BASIN, SOUTHEAST SPAIN

Committee:

____
Robert H. Goldstein, Co-chairperson

____
Evan K. Franseen, Co-chairperson

____
George Tsoflias

Date approved: March 9, 2009

Abstract

Rachel Ana Dvoretsky, M.S.
Department of Geology, March 2009
The University of Kansas

This study documents the basin-wide stratigraphic characterization and 3-D reservoir-analog modeling of upper Miocene carbonate deposits in the Agua Amarga basin, Cabo de Gata volcanic province, southeast Spain. In the basin, paleotopography and relative fluctuations in sea level were primary controls on the deposition of shallow-water heterozoan and subsequent deep-water photozoan-dominated, coarse- and fine-grained gravity flow deposits and interstratified hemipelagic-pelagic sediments.

Gently sloping basin paleotopography in conjunction with two successive periods of shallow marine inundation promoted *in situ* deposition of shallow-water strata in high-energy subtidal environments. This lower succession consists dominantly of Units 1 and 2 volcaniclastic skeletal packstone-grainstones and skeletal grainstones, respectively. Skeletal assemblages within these facies are of the heterozoan association and suggest a regionally temperate climate and/or local upwelling of nutrient-rich waters. Distribution of these deposits was important in modifying paleotopography prior to deposition of deep-water strata, particularly in the northwest portion of the basin where thick accumulations of sediment resulted in a gently sloping ramp-like surface.

Deep-water carbonate strata consist of Units 3 through 7 interstratified fine- to coarse-grained sediment gravity flow deposits and hemipelagic-pelagic sediment. This upper succession contains abundant photozoan material, evidence of reef development on the La Rellena paleohigh during a subtropical-tropical climate after a relative rise in sea level. The majority of sediment-gravity flows sourced from the La Rellena platform were focused into and along a large flooded, margin-parallel paleovalley and ultimately distributed into the basin. These sediments are referred to as focused-flow deposits and resemble point-sourced deep-water siliciclastic systems.

Sediment-gravity flows were also dispersed into the basin (dispersed-flow deposits) along the ramp-like surface produced from deposition of older shallow-water carbonates.

The deep-water deposits in the Agua Amarga basin are particularly important because they challenge paradigms about deep-water carbonate deposition. Traditional models for deposition of coarse-grained deep-water carbonate sediments portray line-sourced and laterally restricted sediment gravity flow deposits that accumulate along the toe-of-slope adjacent of a carbonate platform. The focused-flow and dispersed-flow systems documented in this study differ significantly from traditional models. The major control on focused-flow deposition was the presence of a “funneling mechanism,” a paleotopographic feature (such as the large paleovalley) that focused debris shed from the linear platform margin into the basin. Resulting facies distributions, depositional geometries, and ratios of coarse- to fine-grained sediment within this system suggest that similar deposits in the subsurface would make prolific hydrocarbon reservoirs. On the other hand, dispersed-flow systems occurred where there was no funneling mechanism and sediment gravity-flows were widely distributed across a depositional surface

Outcrop characterization and 3-D modeling reveal that three reservoir analogs may be present: shallow water units (97.7 x 10^6 m^3 of reservoir pore volume); dispersed-flow deep-water deposits (5.71 x 10^6 m^3 of reservoir pore volume) that are heterogeneous and widespread; focused-flow deep-water deposits (14.6 x 10^6 m^3 of reservoir pore volume) that are less heterogeneous and located by substrate paleotopography. The reservoir-analog models should prove useful in future subsurface exploitation of carbonate reservoirs.

Table of Contents

List of Figures & Tables

Chapter 2:

Chapter 3:

Acknowledgements

Above all, I would like to thank my advisors, Dr. Bob Goldstein and Dr. Evan Franseen for their guidance and support during my time at the University of Kansas. I feel honored to have been a part of their ongoing research in southeast Spain, and I am absolutely indebted to them for the ways in which my understanding of and appreciation for carbonate systems has developed. I would also like to thank all of the KU professors I have had the pleasure of interacting with and learning from. Your teachings in the classroom and the field, unique in their own ways, have helped me to become a better geologist. I would like to send a special thanks to the scientists at the Kansas Geological survey, particularly Alan Byrnes, Dr. Marty Dubois and Geoff Bohling, for their help collecting petrophysical data and guidance in Petrel™. This project would not have progressed as it did without their expertise. Thank you Ian Rowell and the entire departmental office staff for your support and invaluable assistance since my arrival.

I would not be here today without the encouragement and enthusiasm of my undergraduate professor and mentor at Franklin & Marshall college, Dr. Carol DeWet. Carol – thank you for introducing me to carbonate sedimentology and for a variety of incredible opportunities, particularly two independent research projects and the chance to go to the Australian outback as a field assistant. The ways in which you supported and challenged me during my undergraduate years meant a great deal to me.

Finally, thank you to my friends and family for being the wonderful people you are, and without knowing, keeping me happy and forward-looking in my endeavors here at KU. To my friends in Lawrence – it has been an incredible few years with you and leaving will surely be one of my tougher experiences. I look forward to future visits and many years of friendship to come. To my family – What can I say? You are the best family in the world and I love you. You have helped me become who I am today, and I am constantly grateful for your unwavering love and support.

Chapter 1:
Introduction

This thesis documents the stratigraphic characterization and outcrop-to-reservoir modeling of upper Miocene *in situ* shallow-water and resedimented deep-water carbonate deposits in the Agua Amarga basin, southeast Spain. Exceptional 3-D outcrop exposures in the basin provide a unique opportunity to evaluate the controls on depositional environments, large-scale geometries and lithofacies architectures, and lateral distributions of carbonate deposits. Detailed stratigraphic studies are an important predictive tool in understanding distribution of reservoir-quality porosity and permeability in subsurface deposits, as well as the construction of geologically constrained reservoir-analog models.

Reservoir-analog facies in the Agua Amarga basin include shallow-water packstone-grainstone deposits and deep-water coarse-grained sediment-gravity flow deposits. The deep-water sediment-gravity flow deposits are particularly significant in that they challenge traditional depositional models. Most deep-water carbonate systems consist of line-sourced narrow aprons of sediment gravity flow deposits that are distributed laterally along the toe-of-slope and have limited subsurface exploitation potential. In the Agua Amarga basin, there are areas where substrate paleotopographic features focus sediment-gravity flows, and areas where there is no paleotopographic focus, allowing flows to be more widely dispersed. Paleotopographic features that focus sediment-gravity flows result in facies distributions that are significantly different from typical slope-apron deposits. Focused-flow deposits display complex and channelized geometries that resemble aspects of point-sourced deep-water siliciclastic deposits and are suggestive of good subsurface reservoir potential. Further, where substrate paleotopography is known and focusing features drain a significant portion of platform margin, focused-flow deep-water systems can be predicted. The increasing outcrop recognition of deep-water carbonate sediment-gravity flows that do not conform to traditional paradigms has sparked interest in the occurrence and reservoir potential of these systems in the subsurface.

The results of this thesis are presented in two papers: the first paper is formatted according to Journal of Sedimentary Research publication style and the second according to AAPG Bulletin publication style. The first paper (Chapter 2) classifies the major lithofacies and depositional units within the basin and discusses the interaction of basin paleotopography and relative sea level on the types, distributions, and lithofacies and sequence-stratigraphic architecture of carbonate deposits. The second paper (Chapter 3) documents the construction of a 3-D reservoir-analog model in Petrel™ using outcrop and core plug petrophysical data, and evaluates the hydrocarbon potential of the resulting reservoir-analog plays. Initial volumetric calculations indicate that ample hydrocarbon potential exists within both shallow-water and deep-water reservoir plays. Further, coarse-grained sediment volumes within the deep-water plays suggest quantitative relationships between internal facies heterogeneity and sediment source area.

Chapter 2:
Stratigraphic Characterization and Documentation of the Controls on the Distributions and Geometries of Shallow-water and Deep-water Carbonate Deposits: Agua Amarga Basin, Southeast Spain

Rachel A. Dvoretsky[1)], Robert H. Goldstein[2)] and Evan K. Franseen[3)]

1) Department of Geology, University of Kansas, Lindley Hall, 1475 Jayhawk Blvd., Lawrence, KS, 66044, Ph. # (785) 766-6995, e-mail: rdvorets@ku.edu

2) Department of Geology, University of Kansas, Lindley Hall, 1475 Jayhawk Blvd., Lawrence, KS, 66044, Ph. # (785) 864-2738, e-mail: gold@ku.edu

3) Department of Geology, University of Kansas, Lindley Hall, 1475 Jayhawk Blvd., Lawrence, KS, 66044, Ph. # (785) 864-2723, e-mail: evanf@kgs.ku.edu

CHAPTER SUMMARY

In situ shallow-water and resedimented deep-water carbonate deposits within the Agua Amarga basin, SE Spain, provide an opportunity to evaluate the effects of sea level, paleotopography, and paleoclimate on the lithofacies architecture of carbonate strata. Units 1 and 2 packstone-grainstone facies are high-energy shallow-water deposits that lap out against gently sloping basement paleotopography during two successive periods of relative sea level rise. These deposits contain heterozoan skeletal grains and suggest a temperate climate during the late Tortonian. Units 3 - 7 deep-water carbonate breccia facies, graded skeletal packstone facies, and foraminifera-rich facies are interstratified fine- to coarse-grained sediment-gravity flows and hemipelagic-pelagic sediments, indicating marine inundation of the basin and shallow-water carbonate production on surrounding paleohighs. Sediment gravity flow deposits contain abundant photozoan constituents and suggest a subtropical-tropical climate by the early-middle Messinian.

The deep-water carbonate deposits in the Agua Amarga basin are exceptional outcrop analogs for both focused-flow and dispersed-flow sediment-gravity flow systems. Focused-flow deposits were funneled into and along the axis of a large margin-parallel paleovalley and point-sourced into the basin. Deposits in proximal paleovalley locations display compensation geometries, channelization, facies truncation, lapout against paleovalley walls, and drape as a result of lateral confinement and proximity to the sediment source and steeply dipping valley walls.

Deposits in distal paleovalley locations display increasingly tabular geometries as a result of decreasing lateral confinement and concentration of coarse-grained sediment-gravity flows down depositional dip. North of the large paleovalley, dispersed-flow deposits were transported into the basin along a gently inclined ramp-like surface produced from earlier deposition of Units 1 and 2 packstone-grainstones. The less complex sheet-like depositional geometries and locations of these deposits result from the absence of lateral confinement and subtle changes in substrate slope. The focused-flow and dispersed-flow accumulations document predictable differences in lithofacies architecture that reveal a strong correlation between paleotopography and the geometries and concentrations of coarse-grained sediment gravity flow deposits. Fluctuations in relative sea level also result in predictable lithofacies architectures and demonstrate a direct correlation between carbonate production on the platform and basin sedimentation.

INTRODUCTION

Upper Miocene carbonate exposures throughout the Cabo de Gata volcanic province in SE Spain serve as the basis for multiple studies on the depositional history, lithofacies architecture, and sequence stratigraphic controls of heterozoan shallow-water ramps and subtropical-tropical reef systems (Dabrio et al. 1981; Goldstein and Franseen 1995; Esteban 1996; Esteban et al. 1996; Franseen and Goldstein 1996; Mankiewicz 1996; Franseen et al. 1997b; Franseen et al. 1998;

Dillett 2004; Johnson et al. 2005). In addition to shallow-water deposits, a deep-water accumulation consisting of hemipelagic-pelagic sediments and sediment gravity flow deposits characterizes the stratigraphy of the Agua Amarga basin, offering a regionally unique example of deep-water carbonate deposits that formed in close association with an extensive reefal platform. Previous work in the basin has mainly focused on the upper Tortonian shallow-water deposits (Betzler et al. 1997; Brachert et al. 1998; Brachert et al. 2001), with general reference to the overlying deep-water deposits (Martin et al. 1996; Franseen and Goldstein 1997). This study develops new ideas on how climate and sea level interact with paleotopography to distribute shallow-water and deep-water carbonates in the Agua Amarga basin.

The deep-water accumulation within the Agua Amarga basin challenges traditional paradigms of deep-water carbonate distribution. Although the typical depositional model for deep-water carbonates involves line-sourced, debris aprons and wedges (Cook and Enos 1977; Mullins and Cook 1986), Payros and Pujalte (2008) have shown recently that funneling mechanisms along carbonate platforms can focus resedimented material and lead to point-sourced deposition at and beyond the toe of slope. A large paleovalley in the Agua Amarga basin, oriented parallel to a major reefal platform, drains a long linear distance of the platform margin and focuses a large volume of coarse-grained sediment into the basin. These focused-flow deposits reveal coarser-grained and laterally more extensive deposits than those predicted by traditional deep-water carbonate models. One goal of this study is to evaluate the paleotopographic control on sediment dispersal patterns and lithofacies architectures of focused-flow deposits in comparison to deposits without a funneling mechanism (dispersed-flow deposits). Another goal is to document the effect of relative sea-level change on the depositional geometries and facies distributions of both shallow-water and deep-water accumulations in relation to the variable paleotopography.

Point-sourced deep-water siliciclastic systems have been widely recognized as prolific hydrocarbon reservoirs, however, comparatively little is known about similar carbonate-dominated systems and the geologic conditions that control their development. This study predicts that where funneling topographic features are located in close proximity, and oriented approximately parallel to carbonate platform margins, high-volume focused-flow deep-water carbonate systems will likely occur. The focused-flow deposits in the Agua Amarga basin display coarser-grained and laterally more extensive sediment gravity flows than those predicted by traditional deep-water carbonate models, and suggest reservoir-potential similar to deep-water siliciclastic systems.

GEOLOGIC SETTING

The Agua Amarga basin is located in the northeastern portion of the Cabo de Gata volcanic province, 35 km northeast of Almeria, Spain (Fig. 1). The Carboneras fault, a major sinistral strike-slip fault system, separates Neogene volcanic basement of the Cabo de Gata region from Mesozoic-Paleozoic metamorphic basement of the

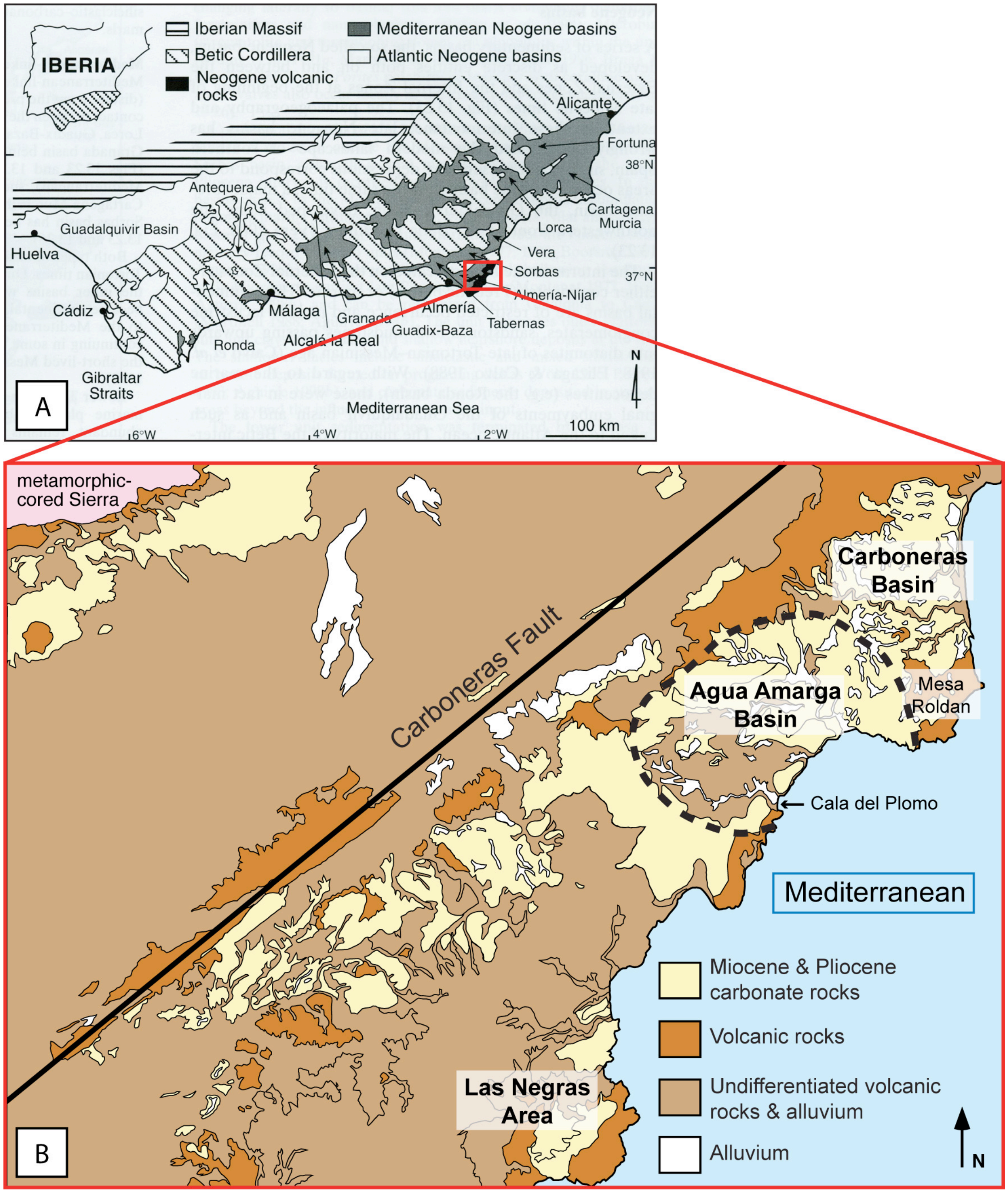

Fig. 1. – **A)** Location map of Neogene basins within the Betic Cordillera of southern Spain. Red Box outlines the Cabo de Gata volcanic province. *After: Gibbons and Moreno, 2003.* **B)** Generalized geologic map of the Cabo de Gata region and location of the Agua Amarga basin (dashed black line), the Carboneras and Las Negras basins, and the Carboneras fault. *Modified from Mapa Geologico de Espana (1981).*

Betic range to the northwest (Platt and Vissers 1989; Montenant and Ott d'Estevou 1990; Fernandez-Soler 2001; Martin et al. 2003). An archipelago of emergent highs and small submarine basins with interconnected straits and passageways characterized the Cabo de Gata region during the middle to late Miocene (Franseen and Goldstein 1996; Franseen et al. 1998). Heterozoan shallow-water deposits followed by subtropical-tropical reef systems were deposited on the Neogene volcanic basement during the late Miocene, and have been the focus of many studies (Dabrio et al. 1981; Goldstein and Franseen 1995; Esteban 1996; Esteban et al. 1996; Franseen and Goldstein 1996; Martin et al. 1996; Franseen et al. 1997a; Franseen et al. 1997b; Brachert et al. 1998; Franseen et al. 1998; Brachert et al. 2001; Martin et al. 2003; Dillett 2004; Martin et al. 2004; Johnson et al. 2005). Argon/Argon dating of an inter-bedded volcanic unit within lower carbonate strata in the Las Negras area indicate an absolute age of 8.5 ± 0.1 Ma (Tortonian) for deposition of some of the oldest marine carbonates in the area (Franseen et al. 1997a; Franseen et al. 1998).

The Agua Amarga basin is approximately 4 km by 8 km and is bound to the north, east, and west by Neogene volcanic highs. To the south, an extensive cliff section from Cala del Plomo to Mesa Roldan abuts the present-day Mediterranean Sea. Tortonian and Messinian-age carbonate deposits unconformably overlie volcanic basement and are the focus of this study (Fig. 1). The Carboneras basin (to the northeast) and the small basins of the Las Negras area (to the southwest) are adjacent to the Agua Amarga basin and contain similar carbonate successions.

METHODOLOGY

Field methodology included measurement of stratigraphic sections for identification of major lithofacies, 3-D documentation of lithofacies architecture using photomosaics, and collection of hand samples for selective petrography.

Twenty-eight stratigraphic sections document the skeletal and non-skeletal constituents and sedimentary structures of existing lithofacies within the Agua Amarga basin (Appendix I). Section location and elevation with respect to sea level was noted using a hand-held GPS. Seven of these sections (1 – 7) are located along the axis of a large paleovalley, the rest of the sections are scattered around the basin (Fig. 2A). Distribution of measured sections was based on outcrop accessibility, quality, and spacing to other sections. Genetic units were traced by walking out major contacts in the field or correlated using photomosaics.

Photomosaics were taken in the field and used to trace lithofacies architecture between stratigraphic sections throughout the basin. Photomosaics were particularly useful on inaccessible outcrops, such as the modern coastline from Cala del Plomo to Agua Amarga, where steep cliff faces prohibited tracing geometries on foot.

Petrographic analysis of thin sections from hand samples of representative lithofacies was done at the University of Kansas using a binocular microscope and 1.25X, 4X, and 10X lenses. 61 thin sections were prepared at the University of Kansas; 25 were prepared in Vancouver, WA by Spectrum Petrographics, Inc. All samples were embedded in standard blue epoxy and polished to 30 microns.

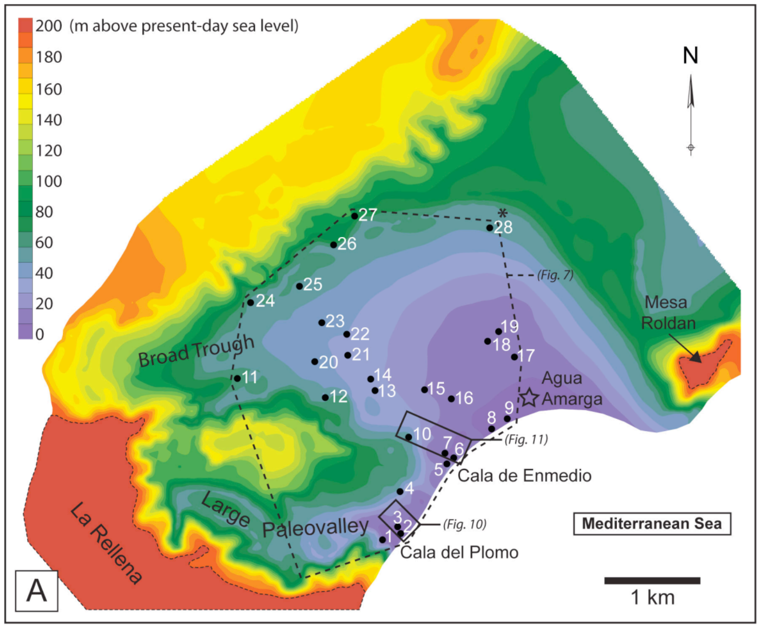

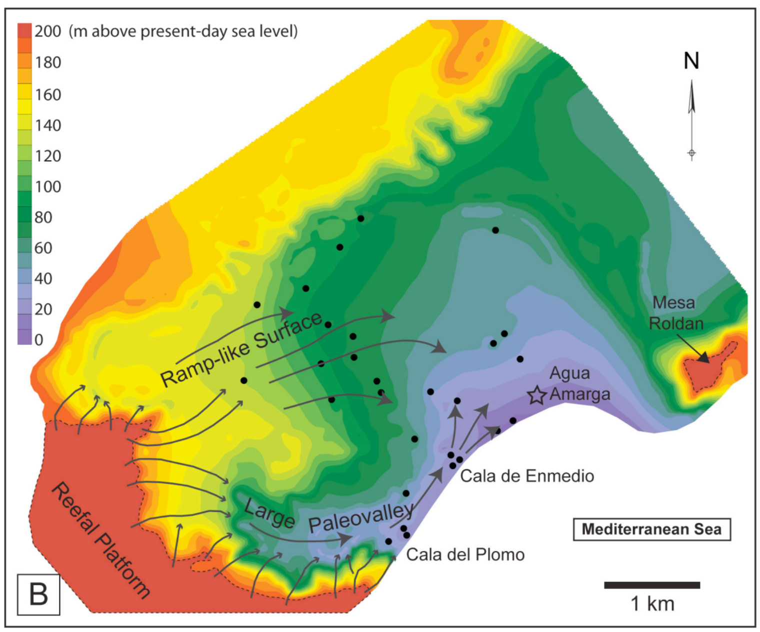

Fig. 2. – **A)** Neogene volcanic basement paleotopography of the Agua Amarga basin. Topographic features have been largely preserved since the Late Miocene and play an important role in the distribution of carbonate deposits. Numbered black dots represent locations of measured stratigraphic sections. **B)** Modified paleotopography after deposition of Units 1 and 2 shallow-water packstone-grainstone deposits. Notice that the broad trough was largely filled, whereas the large paleovalley remained relatively unfilled. The reefal platform (La Rellena) on the western margin of the basin served as the main source of Units 3 – 7 resedimented material into the basin. Sediment gravity-flows were focused into the paleovalley (focused-flow deposits) and dispersed along the packstone-grainstone ramp-like surface created by deposition of Units 1 and 2 (dispersed-flow deposits), (dark grey arrows).

SUBSTRATE PALEOTOPOGRAPHY

Previous studies in the Cabo de Gata region have demonstrated that paleotopography plays a major role in predicting the location, depositional mechanism, and lithofacies architecture of late Miocene carbonate deposits, (Goldstein and Franseen 1995; Franseen and Goldstein 1996; Franseen et al. 1997a; Franseen et al. 1998; Dillett 2004; Johnson et al. 2005). Considering this importance, there is some debate about the nature and degree of syndepositional tectonic deformation. Proximity of the active Carboneras fault system to the small Neogene basins in the Cabo de Gata region (Fig. 1B) suggests a significant tectonic control on existing geometries and facies relationships. Detailed studies of carbonate outcrops in the Las Negras area (Franseen and Goldstein 1996; Franseen et al. 1997a; Franseen et al. 1998; Johnson et al. 2005), the Carboneras basin (Dillett 2004), and the Nijar basin (Dabrio et al. 1981; Mankiewicz 1996) indicate that there is little deformation of the majority of carbonate strata in these areas.

The hypothesis for regional differential uplift of the entire Cabo de Gata volcanic province, with maximum uplift in the western areas since the late Miocene (Martin et al. 2003) is generally accepted. Martin et al. (2003) state that the bioclastic carbonates (Azagador Member) throughout the Cabo de Gata region display a difference in outcrop elevations of greater than 200 meters, suggesting differential uplift of these strata since their deposition during the late Tortonian/early Messinian. An estimated 60 to 70 meters of global sea level change during the Tortonian-

Messinian (Hardenbol et al. 1998; Miller et al. 2005) supports this hypothesis. In the Agua Amarga basin, lower Azagador-equivalent Unit 1 volcaniclastic skeletal packstone-grainstone deposits have a maximum difference in their basal elevations of approximately 150 to 160 meters and display stratigraphic offsets from faulting indicating some structural uplift. Significant fault offsets (Fig. 3) are recorded within Unit 1 deposits immediately south of section 1, between sections 5 and 6 at Cala de Enmedio, and along the southwest edge of the basin (Fig. 2A). This deformation of early carbonate strata is similarly recognized in the Agua Amarga basin by Betzler et al. 1997 and Brachert et al. 2001, although these authors differ in their interpretation of timing of deformation. Betzler et al. (1997) and Brachert et al. (2001) suggest a topography that produced gently dipping carbonate ramps during early carbonate deposition (equivalent Units 1 and 2 deposits) in conjunction with synsedimentary tectonic activity (largely differential subsidence in the western portions of the basin), as well as post depositional uplift. These authors have also attributed late Tortonian to Pliocene synsedimentary low-amplitude (basin center) and high-amplitude (basin margin) block faulting as a significant control on stratigraphic architectures in the basin. Results from this study, however, indicate that the faults cutting through Unit 1 do not continue through subsequent (younger) carbonate units, but rather are healed over by Unit 2. Detailed basin-wide examination of Units 2 – 7 display little evidence of large-scale faulting or deformation, indicating that depositional geometries are preserved for the most part. Some later (Pliocene?) meter-scale faulting occurred in the surrounding areas and cut through the entire Miocene section. Results from this

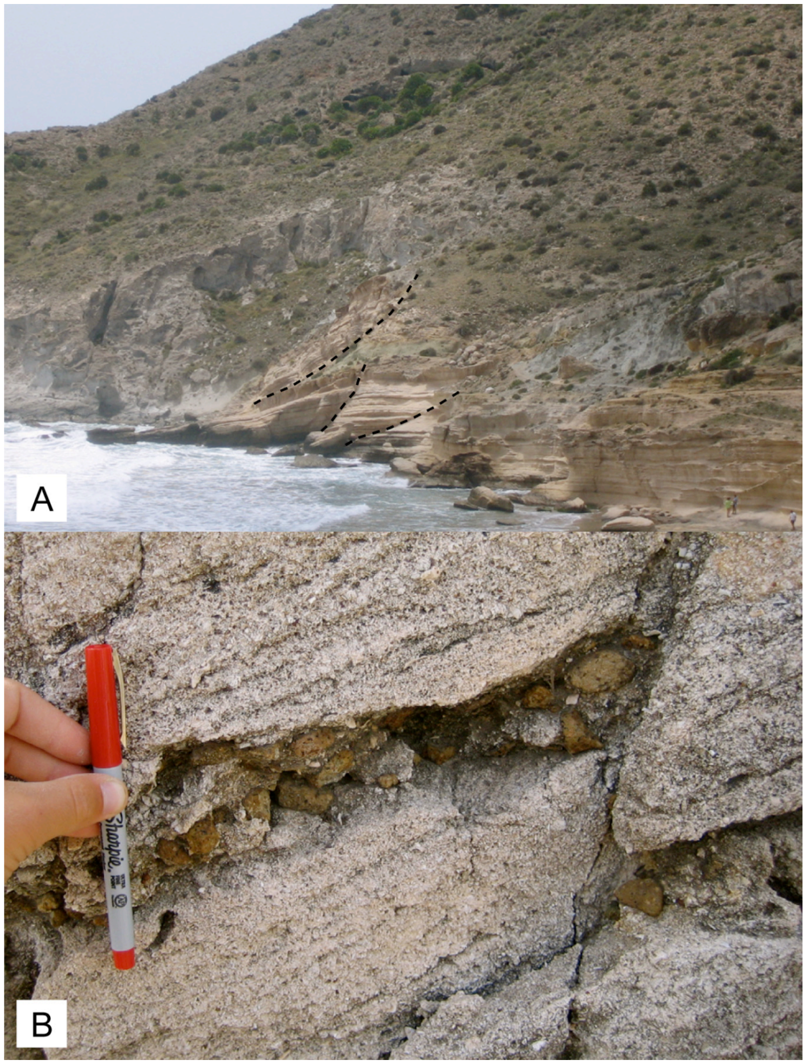

Fig. 3. – **A)** Meter to tens of meter-scale bed offset south of section 1 as a result of faulting through Unit 1 volcaniclastic skeletal packstone-grainstone facies. **B)** A closer look at deposits in this location reveals centimeter-scale offset within Unit 1 as well. Pen is 13.5 cm in length.

study, however, indicate that internal geometries post-Unit 1 largely preserve paleotopography. Additionally, whereas others interpret volcanic basement topography to have been significantly deformed since deposition of Unit 1 (Betzler et al. 1997; Brachert et al. 2001), this study indicates that present-day volcanic basement topography (Fig. 2A) largely reflects preserved paleotopography during the majority of late Miocene carbonate deposition. This study and those of others in the area indicate that subaerial exposure and erosion of volcanic substrate prior to deposition of carbonate strata (Franseen et al. 1993) contributed to a complex paleotopography that exerted significant control on carbonate deposition (e.g. the large paleovalley in the southwest corner of the basin and the various small paleovalleys oriented perpendicular to and dissecting the La Rellena platform margin; Fig. 2A) (Franseen and Goldstein 1997).

Evidence of a major unconformity on top of basement exists throughout the Agua Amarga basin (Martin et al. 1996; Betzler et al. 1997; Franseen and Goldstein 1997), as well as regionally in small Neogene basins of the Cabo de Gata volcanic province (Franseen and Mankiewicz 1991; Franseen et al. 1993; Goldstein and Franseen 1995; Franseen and Goldstein 1996; Franseen et al. 1997a; 1997b; Franseen et al. 1998; Martin et al. 2003; Johnson et al. 2005). Fluvial processes during subaerial exposure contributed to the formation of the various paleodrainage features noted along the southwestern margin of the basin. In addition to subaerial processes, tectonic activity prior to, during, and perhaps immediately following deposition of Unit 1 packstone-grainstones had an effect on topographic features in the basin. In particular, faulting likely enhanced the northern and northeastern margin of the La Rellena platform (Fig. 2A), helping to constrain the location of the large margin-parallel paleovalley and acting as an important topographic control in the distribution of Units 2 – 7 deposits.

The paleotopographic map illustrated in Figure 2A represents the elevations (in meters above sea level) of the contacts between volcanic basement and overlying carbonate strata. Contact elevations were collected during previous mapping in the basin (Franseen and Goldstein 1997) and measurement of stratigraphic sections (this study and initial work by Franseen and Goldstein (1997)). The basin is approximately 4 km (N-S) by 8 km (E-W) and is characterized, in its center, by a gently sloping substrate that dips approximately 1.3 degrees to the south/southeast where it disappears below the present-day Mediterranean in the vicinity of Agua Amarga (Fig. 2A). Along the coastline at Cala del Plomo, volcanic basement is present several meters above sea level and rises steeply to define the southern side of the large paleovalley (Figs 2A and 10). Toward Agua Amarga, basement in the large paleovalley gently dips toward the northeast (Figs 2A and 9). On the northern side of the large paleovalley, a paleohigh separates two major topographic depressions: the large paleovalley to the south and the broad trough to the north (Fig. 2A). The large paleovalley, which is approximately 3,900 meters long and 850 meters wide, is characterized by steeply dipping walls (~36 degrees) and a valley floor that dips approximately 1.2 degrees to the southeast/east. The broad trough, which is approximately 3,200 meters long and 1,100 meters wide, is characterized by more gently dipping walls (~12 degrees) and a valley floor that dips approximately 4 degrees toward the east/southeast. Numerous small and narrow paleovalleys dissect the La Rellana platform margin and lead into the large paleovalley. The northwestern and northeastern margins of the basin are characterized by elongated paleoridges (Fig. 2A). The northwestern ridge is 160 meters above sea level; the northeastern ridge is topographically lower (80 meters above sea level) and passes into the steeply sloping margins of the Mesa Roldan platform to the southeast.

LITHOFACIES AND DEPOSITIONAL ENVIRONMENT

A lower succession consisting of upper Tortonian carbonate deposits and an upper succession consisting of Messinian carbonate deposits characterize the stratigraphy in the Agua Amarga basin (Fig. 4). The lower stratigraphic succession comprising Units 1 and 2 is divided into two major facies on the basis of composition: a volcaniclastic skeletal packstone-grainstone facies (Unit 1) and a skeletal grainstone facies (Unit 2). In addition to dominant packstone-grainstone facies, a minor red fossiliferous wackestone facies comprises a localized pre-Unit 2 interval. The upper stratigraphic succession, comprising Units 3 – 7, is divided into facies on the basis of composition, grain size and/or observed sedimentary structures. These facies include foraminiferal wacke-packstones, volcaniclastic foraminiferal wacke-packstones, skeletal foraminiferal wacke-packstones, graded fine- to very coarse-grained skeletal packstones, and carbonate breccias (fine- to very coarse-

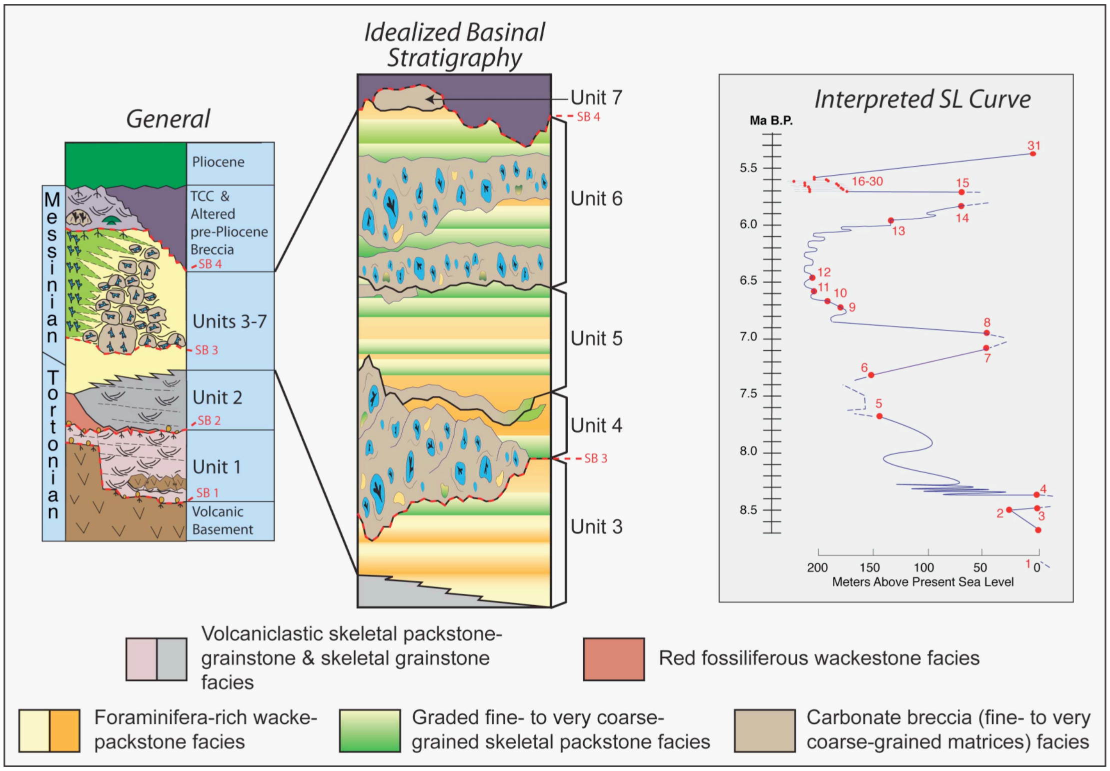

Fig. 4. – General and idealized stratigraphy of carbonates in the Agua Amarga basin (left) *Modified from Franseen et al. (1997)*. Relative sea level curve (Goldstein and Franseen 1995; Franseen et al. 1998) constructed from "pinning points" in the Las Negras area (right). The lower stratigraphic succession is composed of late Tortonian Units 1 and 2 shallow-water volcaniclastic skeletal packstone-grainstone and skeletal grainstone facies, and a localized and deeper water pre-Unit 2 red fossiliferous wackestone facies. The upper stratigraphic succession is composed of Units 3 – 7 interstratified deep-water foraminifera-rich wacke-packstone, graded skeletal packstone and carbonate breccia facies. The relative sea-level curve correlates to the stratal patterns seen in the Agua Amarga basin: points 1 – 5 represent deposition of dominant shallow-water units; points 5 – 12 represent deposition of deep-water units. SB = sequence boundary.

grained matrices) (Table 1). Lithofacies are named following Dunham's classification scheme (Dunham 1962).

The Lower Succession (Units 1 and 2)

Volcaniclastic Skeletal Packstone-grainstone Facies (Unit 1)

The volcaniclastic skeletal packstone-grainstone facies (Table 1) contains abundant silt- to cobble-sized volcanic grains and inter-granular clay particles. Dominant skeletal grains include medium- to well-sorted fragments of bryozoans, echinoids, and red algae. Lesser constituents include fragments of mollusks, solitary corals, benthic foraminifera, and planktonic foraminifera (Fig. 5A). Dominant sedimentary structures include meter-scale trough cross-stratification (Fig. 5B), and dm-scale low-angle planar beds. Local horizons display cm-scale *Skolithos* burrows. Stratigraphically older horizons are alternately coarser-grained (10 to 15 mm) and poorly sorted with well-preserved grain ornamentation, or finer-grained (less than 5 mm) and well sorted with poor preservation of grain ornamentation. Toward the top of the unit (upper-most 5 meters), beds are predominantly composed of finer-grained, well-sorted and highly abraded skeletal fragments. Deposits onlap volcanic basement along basin margins, are thickest in the northwest portion of the basin, and thin substantially toward the present-day Mediterranean. Observed sedimentary features, low percentages of planktonic foraminifera and carbonate mud, and overall facies geometries are indicative of deposition from nearby sources in a shallow-subtidal

	Lithofacies Description							
	Lower Stratigraphic Succession (Units 1 & 2)			Upper Stratigraphic Succession (Units 3 - 7)				
Lithofacies Classification (Dunham, 1962)	Volcaniclastic skeletal packstone-grainstone (Unit 1)	Red fossiliferous wackestone (pre-Unit 2 interval)	Skeletal grainstone (Unit 2)	Foraminiferal wacke-packstone	Volcaniclastic foraminiferal wacke-packstone	Skeletal foraminiferal wacke-packstone	Graded fine- to very coarse-grained skeletal packstone	Carbonate breccia (fine- to very coarse grained matrices)
Characteristic Skeletal Constituents	bryozoans; echinoids; red algae; mollusks; solitary corals; benthic forams; planktonic forams. **Non-skeletal:* volcanic grains	solitary corals; octacorals; hydrozoans; gastropods; mollusks; bryozoans; echinoids; red algae; serpulid worms; small & large benthic forams; planktonic forams **Non-skeletal:* volcanic pebbles to boulders	bryozoans; red algae; echinoids; mollusks; benthic forams; solitary corals; planktonic forams.	planktonic forams; diatoms; sponge spicules; echinoid spines; whole pectin & echinoid shells; fish scales & vertebrae.	plaktonic forams; sponge spicules; echinoid spines. **Non-skeletal:* volcanic grains	planktonic forams; echinoid spines & plates; mollusks.	mollusks; red algae; rhodoliths; bryozoans; echinoids; benthic forams; serpulid worms; gastropods; planktonic forams; *Porites* (rare); *Tarbellastreae* (rare).	mollusks; red algae; rhodoliths; gastropods; serpulid worms; echinoids; benthic forams; planktonic forams; *Halimeda*; *Porites*; *Tarbellastreae*.
Carbonate Mud (Relative Abundance)	Very Low	High	n/a	High	High	Medium	Low	Low - Medium
Dominant Grain Size	5 - 10 mm	whole: 2 - 4 cm fragments: 0.5 - 2 mm	5 - 10 mm	0.2 - 0.5 mm	0.2 - 1 mm	0.5 - 2 mm	fn-med: 1 - 3 mm crs: 3 - 5 mm v.crs: > 5 mm	fn: 2 - 4 mm med: 4 - 6 mm crs-v.crs: > 6 mm
Structures and Bedding	trough cross beds; low-angle planar beds; *Skolithos* burrows	massive beds; fissure-fill	trough cross beds; low-angle planar beds	massive beds with *Zoophycus* burrows; fissile laminated beds	massive beds; normally graded beds (subtle)	normally graded beds (subtle); basal scouring (minor)	normally graded beds; basal scouring; mm- to cm-scale foraminifera-rich ws/ps clasts (rare)	massive & chaotic beds; internal & basal scouring; flame & fold structures; m-scale clasts
Depositional Mechanism	shallow-subtidal sedimentation	deeper water sedimentation	shallow-subtidal sedimentation	Pelagic-hemipelagic sedimentation	Pelagic-hemipelagic sedimentation or low-density turbidity currents	Low-density turbidity currents	High-density turbidity currents	Debris flows

Table 1. – Classification of the major lithofacies in the Agua Amarga basin

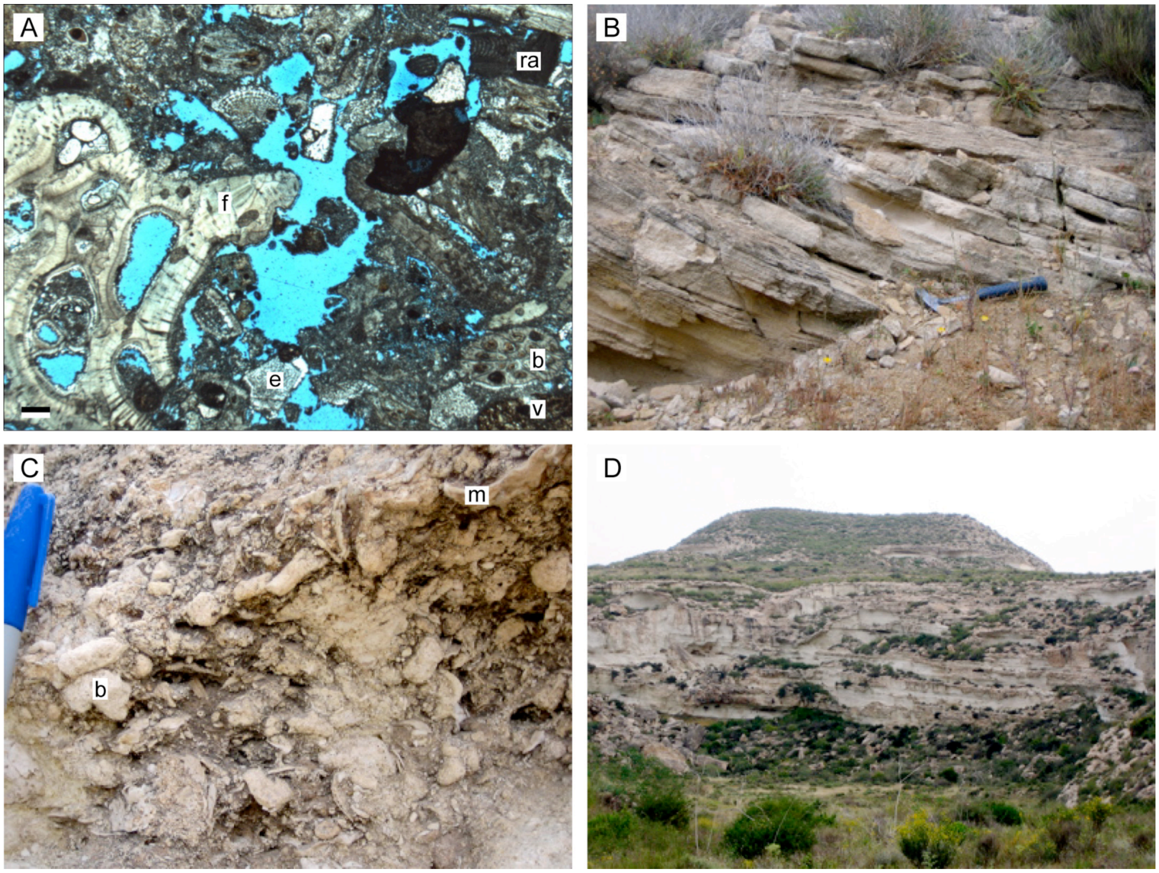

Fig. 5. – Lithofacies photographs and photomicrographs. Scale bar in the lower left corner of photomicrographs is 400 micrometers. Hammer in field photographs is 32 cm in length; marker cap is 5 cm in length. **A)** Photomicrograph of a volcaniclastic skeletal packstone-grainstone facies containing large, encrusting benthic foraminifera (f), echinoid plates (e), volcanic grains (v), red algae (ra), and bryozoans (b). **B)** Outcrop photograph (section 24) of meter-scale trough cross-stratification within volcaniclastic skeletal packstone/grainstone deposits. **C)** Outcrop photograph of a poorly sorted interval containing large, globular bryozoans (b) and mollusk shells (m) within the skeletal grainstone facies. **D)** Outcrop photograph (section 18) of low-angle clinoforms within the skeletal grainstone facies (view to the NE).

high-energy environment (Franseen et al. 1997b). An increase in grain abrasion and sorting within beds toward the top of Unit 1 are suggestive of shoaling conditions prior to subaerial exposure.

Red Fossiliferous Wackestone (pre-Unit 2 Interval)

The red fossiliferous wackestone facies (Table 1) is compositionally and texturally distinct from both the volcaniclastic skeletal packstone-grainstone (Unit 1) and skeletal grainstone facies (Unit 2). Krautworst and Brachert (2003) studied deposits of this facies in detail in the Agua Amarga basin and other locations and attributed them to the regionally extensive Breche Rouge de Carboneras (BRC). Unlike other areas, however, the BRC-equivalent red fossiliferous wackestone facies in the Agua Amarga basin occur as a minor facies with only localized deposits.

Red fossiliferous wackestones contain a distinct reddish lime mudstone matrix containing scattered planktonic foraminifera tests and volcanic grains. Dominant skeletal grains include solitary corals, octacorals, hydrozoans, gastropods, mollusks, and bryozoans. Lesser constituents include echinoids, red algae, small and large benthic foraminifera, and serpulid worms. A more regional examination of the BRC by Krautworst and Brachert (2003) recognizes a similarly diverse faunal assemblage overall consisting of multiple species of hydrozoans and scleractinian corals, brachiopods, and crabs, in addition to the aforementioned fauna. Skeletal constituents within red fossiliferous wackestone deposits are poorly sorted. Whole gastropods, mollusks, octacorals and solitary corals dominantly comprise the coarse-grained (cm-scale) component of this facies. These coarse skeletal grains, in addition to benthic and planktonic foraminifera, commonly exhibit whole and well-preserved shells; other skeletal grains commonly occur as fragments less than 2 mm.

The red fossiliferous wackestone facies is divided into two subfacies on the basis of depositional thicknesses and distributions. A fissure-filling subfacies forms a thin (cm-scale) veneer and everywhere fills cm-scale fissures in the underlying substrate (Fig. 6A). A massive subfacies overlies the fissure-filling subfacies in local areas. The massive subfacies ranges in thickness from 1 to 8 meters and lacks conspicuous sedimentary structures. Sub-rounded to well-rounded volcanic cobbles and boulders are characteristically scattered throughout this subfacies, but are commonly concentrated in basal and upper portions (Fig. 6B). Outcrops of the massive subfacies are tightly cemented and in thin sections reveal micrite in the matrix and blocky calcite cements in molds and intraparticle pores of skeletal grains. Moldic porosity is preserved where calcite does not completely fill dissolved shells (Fig. 6C).

The fissure-filling and massive subfacies that characterize red fossiliferous wackestone deposits in the Agua Amarga basin are similar to Krautworst and Brachert's (2003) LF3 hydrozoan floatstone and LF6 volcaniclastic conglomerate facies of the BRC. A diverse faunal assemblage, whole and poorly sorted skeletal grains, and an abundance of lime mud within both subfacies indicate deposition in an open lower-energy marine environment. Further, the abundance of planktonic foraminifera within the mud matrix suggests significant water depths. Abundant and

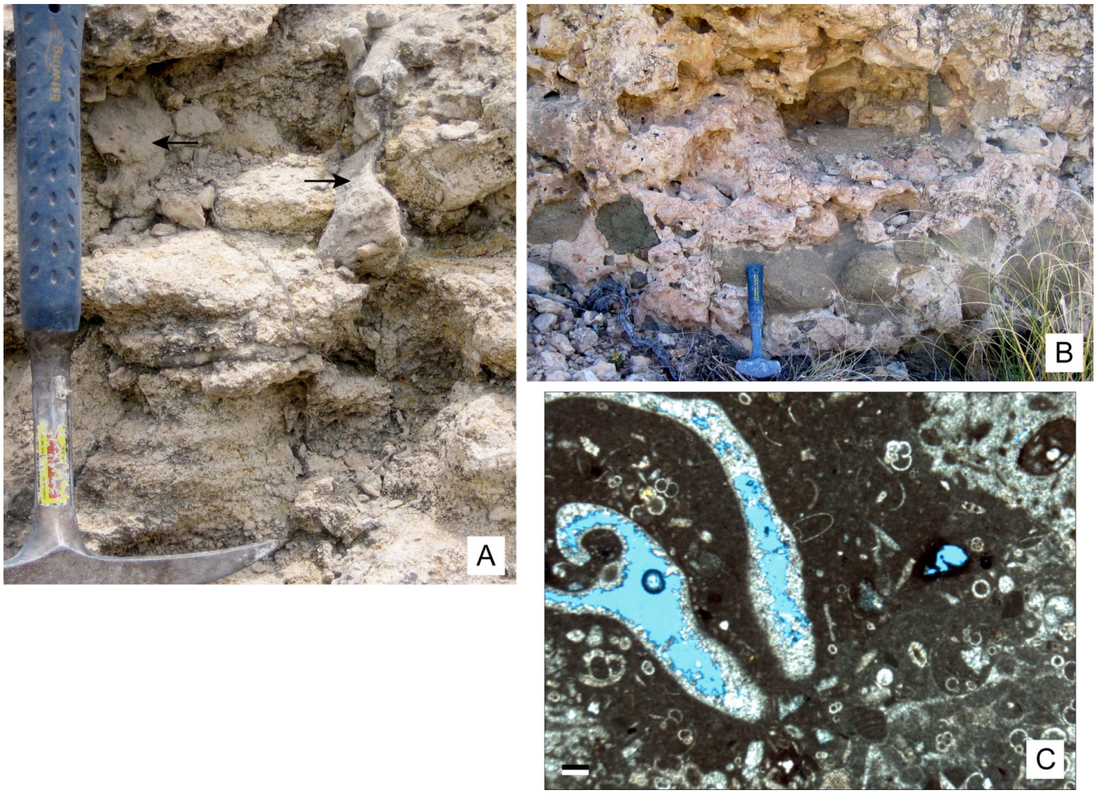

Fig. 6. – Photographs and photomicrograph of the red fossiliferous wackestone facies. Hammer in field photographs is 32 cm in length. Scale bar in the lower left corner of the photomicrograph is 400 micrometers. **A)** The fissure-fill subfacies (black arrows) infiltrating cm-scale fissures in volcaniclastic skeletal packstone-grainstone deposits at the top of Unit 1 at Location 4. **B)** Base of the massive subfacies at location 3 displaying basal concentrations of sub-rounded to rounded volcanic cobbles to boulders in a characteristically red lime mudstone matrix. **C)** Photomicrograph displaying gastropod mold.

well-rounded volcanic cobbles to boulders within the massive subfacies suggest influx of already-abraded volcaniclastic material through debris flows. These interpretations are in agreement with those by Brachert et al. (2001) and Krautworst and Brachert (2003).

Skeletal Grainstone Facies (Unit 2)

The skeletal grainstone facies (Table 1) contains finer-grained and significantly less volcanic constituents than the volcaniclastic skeletal packstone-grainstone facies. Dominant skeletal grains include fragments of bryozoans, red algae, echinoids, mollusks and small benthic foraminifera. Lesser constituents include solitary corals and planktonic foraminifera. Local horizons are poorly sorted and contain large (2-4 cm) globular bryozoans and mollusks (Fig. 5C), however, the majority of horizons are medium to well sorted and contain grains that range from 5 to 10 mm. This facies is composed of low-angle 0.2 to 1 m-thick master beds that onlap underlying Unit 1 deposits and dip gently (~ 6-9°) toward the present-day Mediterranean (Fig. 5D). Meter-scale trough cross-stratification and planar bedding within these onlapping bedforms indicate deposition in a shallow-subtidal high-energy environment similar to that of Unit 1 (Franseen et al. 1997b).

The Upper Succession (Units 3 - 7)

Foraminiferal Wacke-packstone Facies

The foraminiferal wacke-packstone facies (Table 1) contains abundant planktonic foraminifera (Globigerina), diatoms, sponge spicules and echinoid spines (Fig. 7A). Lesser skeletal constituents include whole echinoid and pectin shells, sponges, and fish scales and vertebrae. Dm-scale beds are either massive with *Zoophycos* (and other unidentified) traces, or contain mm-scale laminations. The tops of some massive beds are discolored, heavily burrowed, and are filled with sediment from the overlying deposits (Fig. 7B). Finely laminated intervals are fissile and commonly preserve fish scales and other organic remains. Dominant sedimentary features indicate hemipelagic-pelagic deposition in an oxygenated to slightly dysoxic (at least some of the time) deep-water environment (Scholle et al. 1983). Finely laminated horizons also suggest periods of relative anoxia and non-deposition in the basin (Scholle et al. 1983). Heavily burrowed horizons displaying sediment infilling from the overlying layer may represent firmground formation, similarly indicating periods of non-deposition.

Volcaniclastic Foraminiferal Wacke-packstone Facies

The volcaniclastic foraminiferal wacke-packstone facies (Table 1) contains skeletal grains similar to the foraminiferal wacke-packstone deposits, only silt-sized detrital volcanic grains are present, carbonate mud is less abundant, and diatoms are typically absent. Volcaniclastic foraminiferal wacke-packstone deposits typically occur as dm-scale massive and bioturbated beds, however, some deposits display very subtle normal grading (Fig. 7C). Normal grading, the presence of volcaniclastic

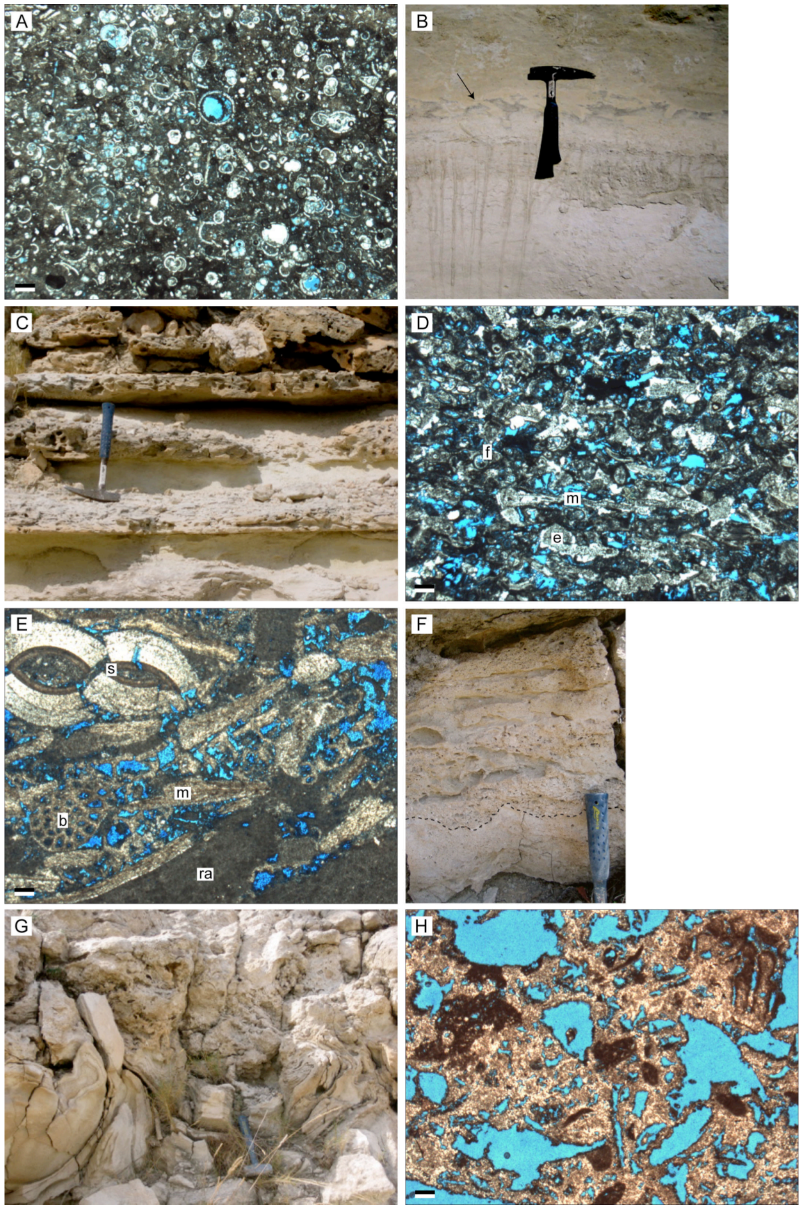

Fig. 7. – Lithofacies photographs and photomicrographs. Scale bar in the lower left corner of photomicrographs is 400 micrometers. Hammer in field photographs is 32 cm in length. **A)** Photomicrograph of a foraminiferal wacke-packstone facies containing abundant planktonic foraminifera, sponge spicules, and carbonate mud. **B)** Outcrop photograph (Section 28) of a discolored and heavily burrowed horizon within a foraminiferal wacke-packstone facies (arrow). **C)** Outcrop photograph (section 26) of subtly graded beds within the volcaniclastic foraminiferal wacke-packstone facies. **D)** Photomicrograph of the skeletal foraminiferal wacke-packstone facies containing planktonic foraminifera (f), mollusks (m), and echinoid plates (e). **E)** Photomicrograph of graded very coarse-grained skeletal packstone facies containing serpulids (s), bryozoans (b), mollusks (m) and red algae (ra). **F)** Outcrop photograph (section 5) of a scoured, amalgamated base (dashed black line) within a graded skeletal packstone facies. **G)** Outcrop photograph (section 14) of a carbonate breccia facies. **H)** Photomicrograph of carbonate breccia matrix displaying microdolomite and moldic porosity.

grains, and the lesser percentages of carbonate mud compared to the foraminiferal wacke-packstone facies suggest deposition from low-density turbulent currents that suspend and sort fine-grained sediment (Lowe 1982; Cook and Mullins 1983; Stelting et al. 2000; Payros and Pujalte 2008). The absence of coarse grains suggests that these graded deposits could have been triggered on the basin margin as low-density events, or they could represent the waning stage of high-density events (Lowe 1982; Posamentier and Walker 2006). Where no grading is present in this facies, two explanations are likely: 1) bioturbation homogenized an originally graded deposit, or 2) non-graded deposits with a significant volcaniclastic component are the result of winds that supplied detrital volcanic grains, and winnowing deep-water currents that removed diatoms and carbonate mud (Scholle et al. 1983).

Skeletal Foraminiferal Wacke-packstone Facies

The skeletal foraminiferal wacke-packstone facies (Table 1) contains abundant planktonic foraminifera, sponge spicules, echinoid spines, and fragments of echinoid plates and mollusks (Fig. 7D). These deposits are coarser-grained, better sorted, and have less carbonate mud than the foraminiferal- and volcaniclastic foraminiferal wacke-packstone facies. Normal grading and minor scoured bases characterize these deposits. Grain size, sorting, and sedimentary structures observed in this facies are indicative of deposition by low-density turbulent sediment-gravity flows, either as low-density events, or during the waning stage of high-density events (Lowe 1982; Posamentier and Walker 2006).

Graded Fine- to Very Coarse-grained Skeletal Packstone Facies

The graded skeletal packstone facies (Table 1) contains abundant fine- to very coarse-grained fragments of mollusks, red algae, rhodoliths, bryozoans, echinoids, benthic foraminifera and serpulids (Fig. 7E). Lesser skeletal constituents include fragments of echinoid spines, gastropods, *Porites* and *Tarbellastreae*. Graded coarse and very coarse-grained skeletal packstone deposits are typically amalgamated (Fig. 7F) and contain mm- to cm-scale clasts of the underlying facies. Beds range in thickness from 0.2 to 1 m, and display prominent scoured bases and normal grading. This facies commonly displays a gradational vertical transition into massive or finely laminated foraminifera-rich beds, and a gradational lateral transition into skeletal foraminiferal wacke-packstone deposits. Grain constituents and sedimentary structures characteristic of this facies indicate deposition from high-density turbidity currents (Lowe 1982; Payros and Pujalte 2008). A shallow-water platform provenance is evident from the abundant bioclasts and relative absence of planktonic foraminifera within these deposits (Ruiz-Ortiz 1983; Franseen et al. 1997; James 1997). Clasts within the coarser-grained skeletal packstone facies suggest a direct relationship between the size of the transported grains and the energy and erosive tendencies of the turbidity current. Basal amalgamated beds suggest the influence of tractive currents (Lowe 1982), or indicate multiple high-density pulses that erode the graded portion of previously deposited beds. Further, a gradual transition into overlying finely laminated or bioturbated foraminifera-rich facies toward the tops of these graded beds likely reflects Bouma Td and Te divisions, respectively. Some graded packstone beds display a more abrupt coarse to fine-grained transition, indicating nuances in sediment-gravity-flow processes. It is not uncommon for carbonate turbidites to lack most of the characteristic Bouma sequence developed for siliciclastic turbidites. The differences in grain densities, shapes, and the relative absence of lubricating clay minerals in carbonate gravity flows result in different and often variable fluid-flow behavior (Davies 1968; Payros and Pujalte 2008). Lateral gradation into skeletal foraminiferal wacke-packstone indicates an eventual transition into low-density turbulent flow conditions. Vertical and lateral facies transitions are common during sediment-gravity flow processes and represent a somewhat predictable continuum of flow conditions from proximal to distal portions of the basin (Mullins and Cook 1986; Mulder and Alexander 2001; Gani 2004).

The concept of high-density turbidites is controversial in deep-water siliciclastic studies (Shanmugam and Moiola 1995; Shanmugam 1996; Bouma et al. 1997; Lowe 1997; Mulder and Alexander 2001). Lowe (1982) proposed an ideal high-density turbidite sequence that includes basal phases of traction sedimentation (S_1), mixed frictional freezing and sediment suspension (S2 traction carpets), and direct suspension sedimentation (S_3). Shanmugam and Moiola (1995) and Shanmugam (1996) maintain that Lowe's S_1 and S_2 phases are actually the result of sandy debris flow processes based on depositional features and inferred sediment-support mechanisms during deposition. Unlike siliciclastic deposits with comparable grain sizes and concentrations, deposits of the graded skeletal packstone facies in this study are confidently classified as high-density turbidites for two reasons: 1) There are no indications of deposition from laminar plastic flow conditions associated with non-Newtonian flows. Rather, normal grading indicates rapid deposition from suspension (Lowe 1982; Shanmugam 1996); 2) High concentrations of coarse grains tend to hinder fluid turbulence and promote non-turbulent sediment-support mechanisms typically attributed to debris flows (Shanmugam 1996). However, the irregular shapes and porous nature of most carbonate grains make them more buoyant than siliciclastic grains of comparable densities and thus validate the concept of a highly concentrated current with fluid turbulence as the dominant sediment-support mechanism (Payros and Pujalte 2008).

Carbonate Breccia (Fine- to Very Coarse-grained Matrices) Facies

Abundant breccia facies (Table 1) occur with matrices that consist of fine- to very coarse-grained fragments of mollusks, red algae, rhodoliths, gastropods, serpulids, echinoids, benthic foraminifera, *Halimeda*, *Porites*, and *Tarbellastreae*. Carbonate mud and low percentages of planktonic foraminifera constitute the fine-grained portion of breccia matrices. The matrices of some breccia deposits are heavily dolomitized and preserve the majority of skeletal grains as molds (Fig. 7G). Breccia deposits are characterized by massive and chaotic matrix textures displaying internal and basal scouring, flame and fold structures, deformation of underlying sediment, and randomly distributed, decimeter- to meter-scale *Porites* and *Tarbellastreae* reef framework clasts, skeletal packstone-grainstone clasts, and foraminifera-rich wacke-packstone clasts (Fig. 7H). These features are unequivocally indicative of deposition from cohesive debris flows, (Lowe 1982; Mullins and Cook 1986; Mulder and Alexander 2001; Gani 2004; Payros and Pujalte 2008). Deposits occur as either single breccia events, or as multiple, coalescing breccia events. Contrary to deep-water siliciclastic and carbonate models (Mullins and Cook 1986; Posamentier and Walker 2006; Payros and Pujalte 2008), breccias are the dominant coarse-grained facies of the deep-water lithofacies assemblage in the Agua Amarga basin. A shallow-water platform provenance is evident from the presence of photozoan constituents such as *Halimeda* and abundant *Porites* and *Tarbellastreae* reef clasts within breccia deposits. Fabric-destructive dolomitization and moldic porosity indicate that dolomite precipitation occurred in association with grain dissolution after sediments were deposited in the basin.

STRATIGRAPHIC UNITS AND THEIR DISTRIBUTION

Units 1 and 2

The text below, presents data on Units 1 and 2. In summary, they are composed of facies that were mainly deposited as *in situ* shallow-water sediments (separated by an interval of deep-water sedimentation) when the heterozoan association was dominant (Fig. 8). These deposits formed during 3rd and higher order fluctuations in sea level (Fig. 4) following subaerial exposure and erosion of the Cabo

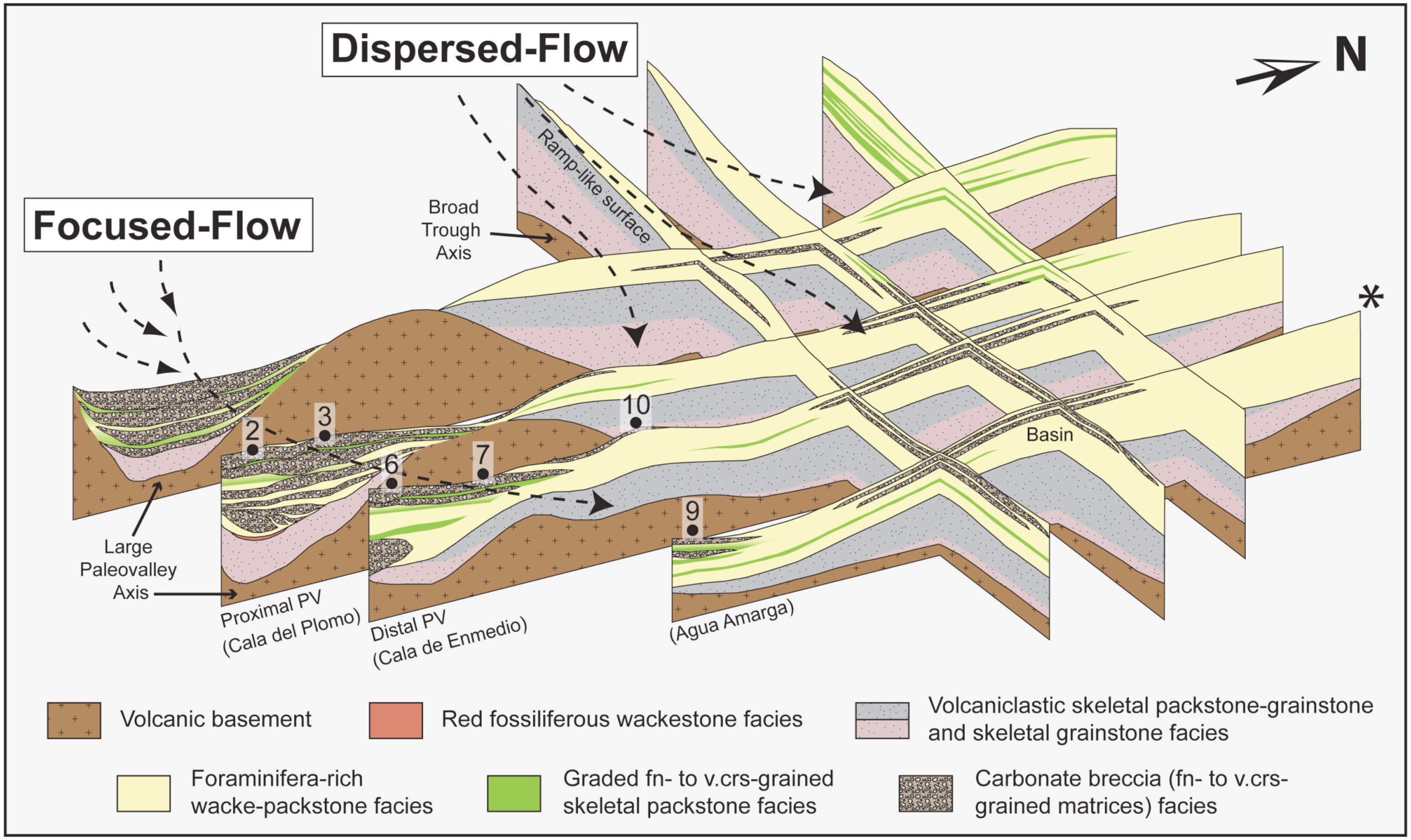

Fig. 8. – Fence diagram displaying the distribution of lithofacies within the Agua Amarga basin. Pink and grey represent *in situ* shallow-water Units 1 & 2. Green, yellow and light brown represent resedimented deep-water Units 3 – 7. The minor red fossiliferous wackestone facies (dark pink) crops out along the proximal paleovalley fence. Note the differences in geometries, distributions and volumes between the focused-flow deposits and the dispersed-flow deposits. Map view of this diagram is represented as a dashed polygon in Figure 2

de Gata Neogene volcanic complex (Goldstein and Franseen 1995; Betzler et al. 1997). The lateral distribution of the shallow-water deposits within the Agua Amarga basin was important in modifying paleotopography prior to deposition of the upper stratigraphic succession. Units 1 and 2 packstone-grainstone deposits filled a significant portion of the broad trough and ultimately resulted in a gently inclined ramp-like surface along which some later sediment-gravity flows were dispersed into the basin (Fig. 2B). Equivalent units are also found in the large paleovalley and in central basin locations. Units 1 and 2 are late Tortonian in age and are time-equivalent with the heterozoan depositional sequences DS1A and DS1B in the Las Negras area (Goldstein and Franseen 1995; Franseen and Goldstein 1996; Franseen et al. 1997a; Franseen et al. 1997b; Franseen et al. 1998; Johnson et al. 2005). Unit 1 is separated from Unit 2 by a sequence boundary (SB2, this study) and an interval of red fossiliferous wackestone (pre-Unit 2 interval).

Unit 1

Ample accommodation and gently sloping basement substrate allowed for deposition of Unit 1 in a high-energy subtidal environment. Deposits are thickest (up to 60 meters) and display the most cross stratification within the broad trough where they form meter-scale submarine bars and dunes (Fig. 2A). Previous work suggests that this broad gently sloped trough served as a high-energy shallow-water strait between the Agua Amarga basin and the adjacent Almeria basin (Betzler et al. 1997; Franseen and Goldstein 1997; Franseen and Goldstein 1999). Thick *in situ* packstone-grainstone deposits in this location are likely indicative of the prevailing currents and wind directions during the Late Tortonian. Betzler et al. (1997) document the presence of foreshore deposits in this area; however, this study maintains a shallow subtidal depositional environment interpretation for the entirety of the unit. Unit 1 deposits within the broad trough thin dramatically toward the center of the basin (approximately one meter thick at section 18). South of the broad trough, Unit 1 deposits form twenty to twenty-five meter-thick accumulations within proximal paleovalley locations at Cala del Plomo and become progressively thinner toward Cala de Enmedio. Unit 1 thicknesses within the paleovalley are largely controlled by the degree of erosional truncation. In general, however, Unit 1 deposits were thickest along the western/southwestern basin margin and thin toward the east/southeast. Distribution of these initial shallow-water carbonates indicates a wedge-like geometry that was dissected by syndepositional and/or post-depositional faulting. Faulting during this time is speculated to have contributed to basin paleotopography that affected distribution of later units. Additionally, tectonic activity following deposition of Unit 1 may have resulted in tilting that caused higher Unit 1 basal elevations within the broad trough than within the large paleovalley. Within the broad trough, Unit 1 deposits significantly modify volcanic basement paleotopography by creating a thick accumulation of sediment with a wide and gently sloped surface; topography within the large paleovalley was relatively unaffected by deposition of Unit 1 (Fig. 2B). Autoclastic brecciation, fissure-fills, local erosional truncation, and several tens of meters of erosional relief indicate that the top of Unit 1 is a subaerial exposure surface (SB2). Previous work on the shallow-water heterozoan carbonates in the Agua Amarga basin documents similar evidence for a subaerial exposure on top of Unit 1 deposits (Martin et al. 1996; Betzler et al. 1997; Brachert et al. 1998; Brachert et al. 2001).

Pre-Unit 2 Interval

The red fossiliferous wackestone facies likely represents an interval of deeper water sedimentation between deposition of Unit 2 and subaerial exposure of Unit 1. Red fossiliferous wackestone is found above the altered surface of subaerial exposure atop Unit 1 or on volcanic basement where Unit 1 has not been deposited. It is stratigraphically below Unit 2 skeletal grainstones and Unit 3 foraminifera-rich facies where Unit 2 has not been deposited. This facies fills fissures in the underlying substrate (SB 2, this study) and is abruptly overlain by overlying strata. Krautworst and Brachert (2003) assign an additional sequence boundary above the red fossiliferous wackestone deposits. Although this sequence boundary may exist, it is not recognized in this study due to lack of sufficient field evidence.

The red fossiliferous wackestone facies forms minor and laterally restricted deposits within proximal paleovalley locations and basinal locations. The fissure-filling subfacies is found in basinal locations (in the vicinity of location 18, see Fig. 2A) where it is overlain by Unit 2 deposits, and also below the massive subfacies in proximal paleovalley locations (locations 1 – 4, see Fig. 2A). The massive subfacies occurs as a localized wedge-like deposit within proximal paleovalley locations only.

An eight meter-thick deposit is present at location 1 and thins dramatically toward the distal paleovalley. A one to four meter-thick deposit is present at locations 2 and 3, but is no longer present at location 4 (see Fig. 2A). Interestingly, Unit 2 skeletal grainstones are not found in proximal paleovalley locations, where red fossiliferous wackestones are thickest.

Whereas the timing of deposition of the fissure-filling subfacies clearly pre-dates Unit 2, the timing of deposition of the massive subfacies is somewhat enigmatic relative to Unit 2. One hypothesis is that a thick accumulation of the massive subfacies in proximal paleovalley locations indicates that the massive subfacies is roughly coeval with Unit 2 deposits. This hypothesis is unlikely, however, considering the shallow-water character of Unit 2 relative to the deeper water environment interpreted for the red fossiliferous wackestone facies. Further, Unit 3 foraminifera-rich sediments abruptly, rather than gradationally overlie this facies, arguing against time equivalence. Thus, it is more likely that the red fossiliferous wackestone facies was deposited during an interval of deeper water in between two intervals of shallow-water deposition (Units 1 and 2).

Placing the red fossiliferous wackestone facies in a deeper water environment in between two phases of shallow-water sedimentation is, in part, speculation and raises questions about the causes for such a brief interval of inundation. It has been suggested that tectonic activity in this area prior to deposition of Unit 2 modified paleotopography and may have resulted in a deeper basin environment as a result of locally down faulted blocks (Brachert et al. 2001; Krautworst and Brachert 2003).

Brachert et al. (2001) and Krautworst and Brachert (2003) suggest that deposition of the massive subfacies occurred along the toes of steep slopes and emphasized the importance of faulting in creation of the paleotopography. Though compositionally and texturally unique from the other depositional units in the basin, the red fossiliferous wackestone facies comprises a volumetrically insignificant deposit. As a result, this study does not examine or speculate in further detail about this facies, or its implication for an additional small-scale relative sea-level cycle.

Unit 2

Unit 2 skeletal grainstone deposits are thickest in the center of the basin and thin up-dip toward basin margin locations. Southeast of section 24 (Fig. 2A), Unit 2 deposits onlap against underlying Unit 1 substrate and display high-energy subtidal sedimentary features similar to those seen elsewhere in the basin. The absence of beach and foreshore indicators at the up-dip extent of these deposits, as well as a gradational vertical transition into foraminifera-rich facies of Unit 3, suggest that a relative rise in sea level flooded the basin and shut off shallow-water carbonate production before deposits reached basin margin positions. Previous work in the basin on equivalent late Tortonian carbonates of the Azagador member (Martin et al. 1996) document the presence of foreshore deposits in the vicinity of La Gorra (location 23, Fig. 2A), and other locations such as Los Pacos (location 24). Examination of deposits at Location 23 refutes this claim for the following reasons: 1) vadose indicators are absent in the outcrop; 2) low-angle inclined bedding, which is characteristically interstratified with trough cross-bedding throughout Unit 2, does not exclusively indicate a beach environment; 3) measured sections throughout the basin document a gradational transition from Unit 2 skeletal grainstones into foraminifera-rich deposits of Unit 3, suggesting that water depth was never less than the shallow subtidal environment prior to deposition of Unit 3 hemipelagic-pelagic sediments.

Unit 2 skeletal grainstone deposits are conspicuously absent within proximal portions of the large paleovalley and, as a result, invoke questions about the factors controlling distribution of these sediments. One hypothesis is that submarine erosion from sediment gravity-flows evident in the overlying deep-water units removed Unit 2 deposits. Measured sections at Cala del Plomo (sections 1-3, see Figs. 2A and 10) effectively disprove this hypothesis. The bases of all three stratigraphic sections display the following depositional succession: Unit 1 capped by SB2; isolated and tightly cemented red fossiliferous wackestone deposits; and fine-grained foraminiferal- and volcanic foraminiferal wacke-packstones of Unit 3. Unit 2 deposits, which are stratigraphically older and more robust than Unit 3 fine-grained sediments, ought to be preserved in these sections if they were originally deposited in proximal paleovalley locations. A second, more likely hypothesis is that Unit 2 deposits were never deposited in proximal paleovalley locations. The paleotopography (Fig. 2B) shows that the proximal part of the paleovalley was a protected reentrant that could have lacked the energy necessary to deposit Unit 2. The preservation of Unit 1, but not Unit 2, deposits within proximal paleovalley locations supports this hypothesis.

Low-angle master bedding within Unit 2 skeletal grainstone deposits (Fig. 5D) indicates that subaerial exposure and erosion of Unit 1 resulted in a gently inclined surface that facilitated deposition of high-energy shallow-water deposits during the subsequent relative sea-level rise. Previous studies in the Cabo de Gata area have demonstrated that the interaction of base level and paleotopography plays an important role in the development and preservation of predictable depositional geometries within transgressive systems tracts. Deposition of heterozoan carbonates in basins with steep substrate slopes, as seen for DS1B strata in the Las Negras area, are dominated by bypass and re-sedimentation processes that result in accumulation of material at the toe of slope. These resedimented deposits display on-lapping and side-lapping geometries despite deposition during a relative rise in sea level (Franseen et al. 1998; Johnson et al. 2005). Gently sloped substrate paleotopography within the Agua Amarga basin, however, allows for the preservation of *in situ* shallow-subtidal deposits that display low-angle bedding with on-lapping geometries characteristic of transgressions.

Units 3 through 7

The text below, presents data on Units 3 through 7. In summary, Units 3 – 7 are composed of facies that were deposited as hemipelagic-pelagic sediments and fine- to coarse-grained sediment gravity flows (Fig. 8). These units are approximately coeval with depositional sequences DS2 and DS3 from the Las Negras area

(Goldstein and Franseen 1995; Franseen and Goldstein 1996; Franseen et al. 1997a; Franseen et al. 1998). An extensive reefal platform (La Rellena) bordering the southwestern basin margin (Fig. 2) developed following inundation of the basin, and served as the dominant sediment source for deep-water sediment gravity flow deposits within Units 3 through 7 (Franseen and Goldstein 1997). Sediment gravity-flows followed two main pathways into the basin: 1) material was funneled into and along the large paleovalley and point-sourced into the basin (focused-flow deposits), or 2) dispersed along the ramp-like surface produced from earlier accumulation of Units 1 and 2 packstone-grainstones (dispersed-flow deposits) (Fig. 2B).

The modern day coastal section from Cala del Plomo to Agua Amarga preserves a detailed record of Units 3 – 6 focused-flow deposits. The coastal section lies along the axis of the paleovalley (along depositional dip), and thus offers documentation of proximal to distal lithofacies architectures (Fig. 9). Numerous outcrops that are oriented perpendicular to the axis of the paleovalley document axial to marginal lithofacies architectures (Figs. 10 and 11). Dispersed-flow deposits that were transported along the ramp-like surface (Fig. 2B) document the lithofacies architecture of contemporaneous deep-water strata, including that of Unit 7. Within both focused-flow and dispersed-flow systems, Units 3 – 7 are defined by episodes of high-density gravity-flow deposition in the basin (dominantly debrites and high-density turbidites) and periods of relative quiescence (dominantly pelagic-hemipelagic sediments and low-density turbidites).

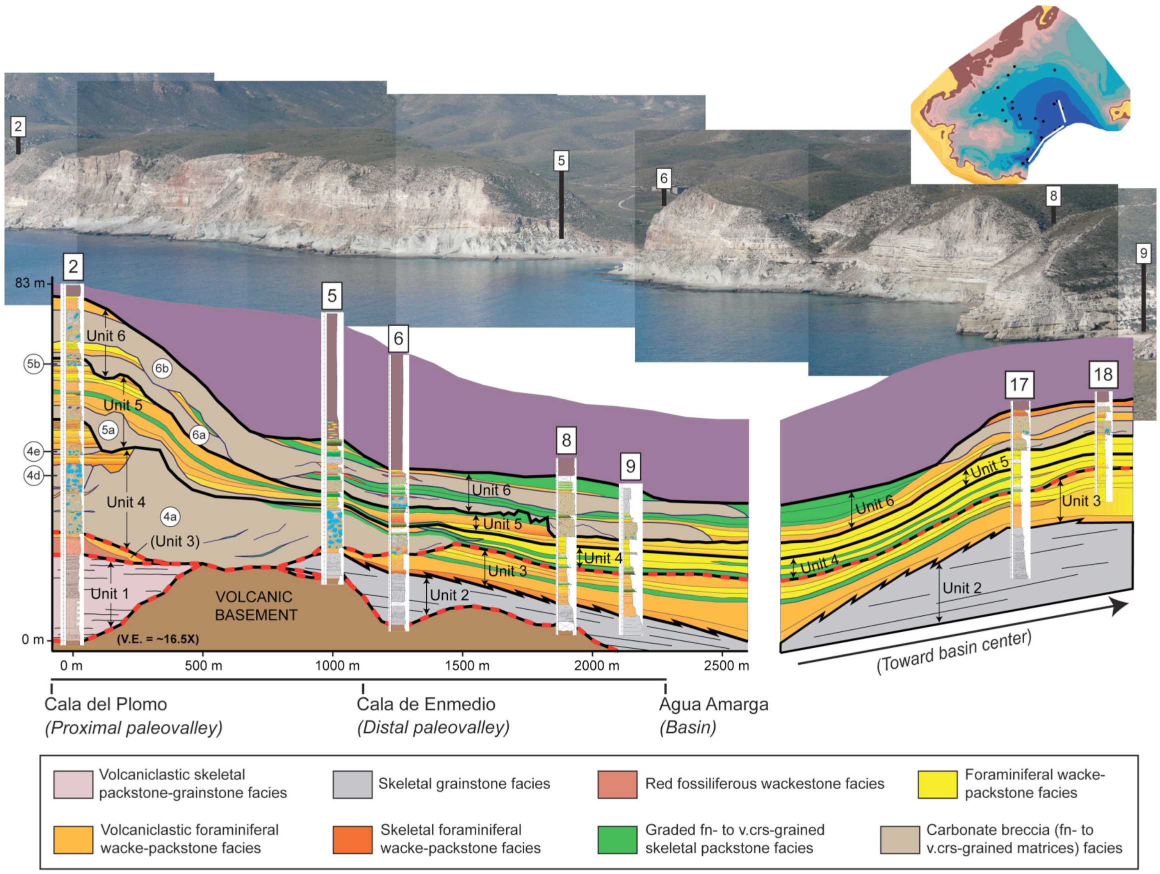

Fig. 9. – A proximal to distal schematic cross-section of depositional units along the axis of the paleovalley, as well as an oblique transect toward the ramp (white lines on map). This cross section documents the complex lithofacies architecture of deep-water units within the paleovalley and reveals that the sediment gravity flow deposits focused into the paleovalley are laterally discontinuous from those dispersed along the ramp (see Unit 6 breccia facies). Focused-flow debrite subunits traceable along depositional dip are labeled (white circles). Unit 7 is not exposed in this cross-section. Black lines represent unit boundaries; dashed red-black lines represent unit boundaries that are also sequence boundaries.

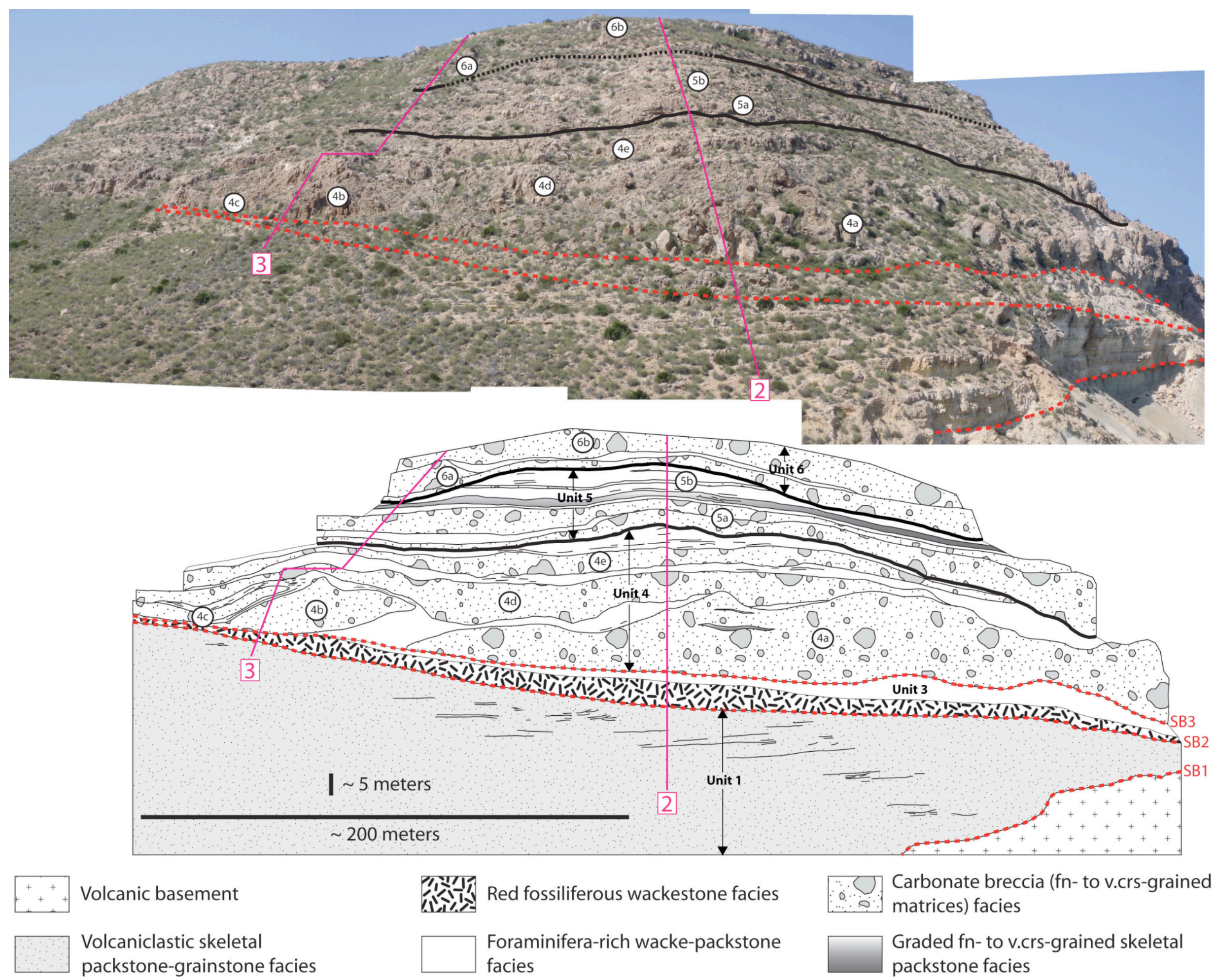

Fig. 10. – Outcrop photomosaic and schematic cross section of an axial to marginal transect within the proximal paleovalley at Cala del Plomo. View toward the northeast. Black lines represent unit boundaries. Dashed red lines represent unit boundaries that are also sequence boundaries (SB1, SB2, SB3).

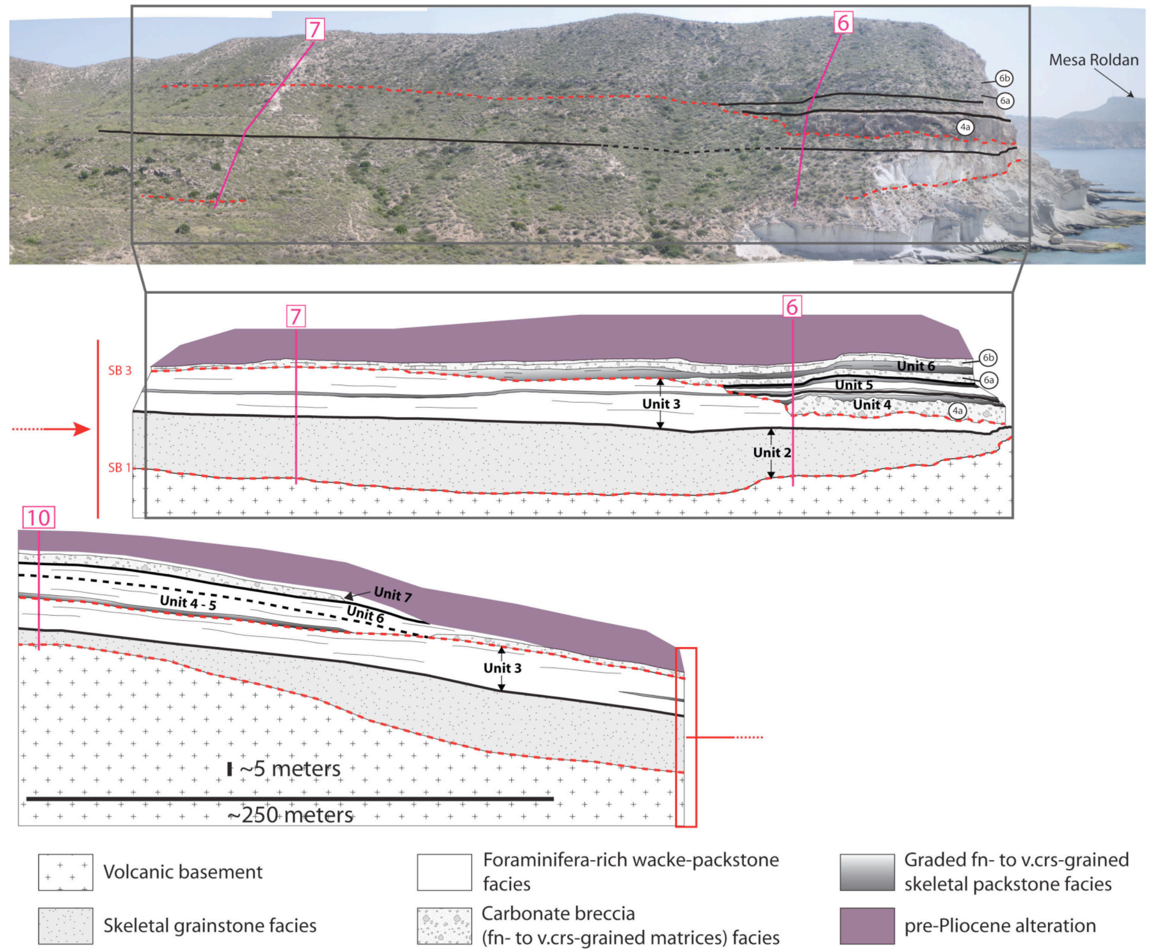

Fig. 11. – Outcrop photomosaic and schematic cross section of an axial to marginal transect within the distal paleovalley at Cala de Enmedio (sections 6 to 7). View toward the northeast (note Mesa Roldan in the background). In this location, Unit 7 sediment gravity flow deposits dispersed along the ramp-like surface (left of outcrop photomosaic) downlap against deposits within the distal paleovalley (sections 10 to 7). Black lines represent unit boundaries. Dashed red lines represent unit boundaries that are also sequence boundaries (SB1 and SB3).

Unit 3

Unit 3 deposits within the large paleovalley are dominantly composed of foraminiferal wacke-packstone and volcaniclastic foraminiferal wacke-packstone facies, interpreted as hemipelagic-pelagic sediments and low-density turbidites. These fine-grained beds tend to drape substrate paleotopography, displaying uniform thickness for significant distances (Fig. 9) Less common interstratified high-density turbidites (graded skeletal packstone facies) also occur and display truncation of underlying sediment at their bases. Dm-scale channel-scour features truncate high- and low-density turbidites within and just outside of the paleovalley at Agua Amarga and are filled with finer-grained foraminifera-rich deposits. These truncation features are interpreted as bypass erosional scours from high-density turbidity currents that moved farther out into the basin (Fig. 12). Unit 3 deposits are variably preserved in proximal paleovalley locations (Cala del Plomo) because of erosional truncation at the base of Unit 4 (Figs. 9 and 10).

Hemipelagic-pelagic sediments and low-density turbidites are also the dominant deposits that occur along the ramp-like surface, and within central and basin margin locations. Deposits are generally thicker (up to 20 meters) in these areas than within the paleovalley due to less erosional truncation at the base of Unit 4. Hemipelagic-pelagic and low-density turbidite deposits tend to drape substrate topography, except for locations near the steeper basin margins where flanking sediments were likely remobilized into low-density turbidites and there is some truncation of the underlying sediment. Interstratified high-density turbidites (graded

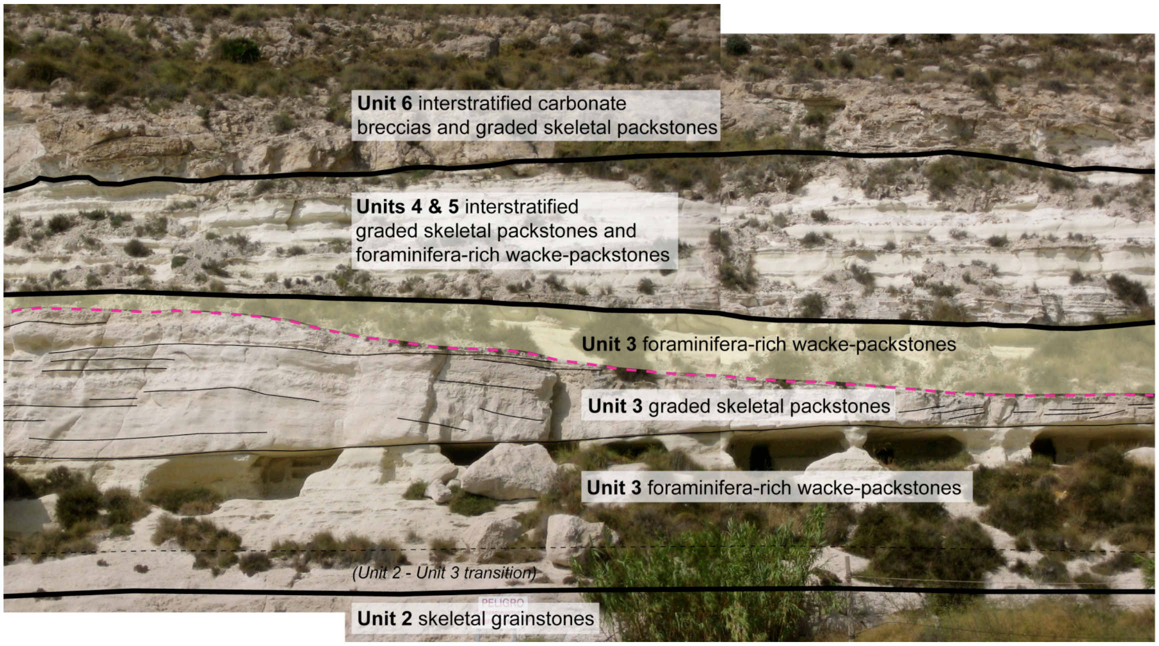

Fig. 12. – Erosional bypass surface at section 9 (pink dashed line, view to the SW) likely from high-density turbidity currents that moved farther into the basin. The surface truncates previously deposited high-density turbidites (graded skeletal packstone facies) and is filled by hemipelagic-pelagic sediments and low-density turbidites (foraminifera-rich wacke-packstone facies).

skeletal packstone facies) occur along the northern margin of the basin at section 25 (Fig. 2A) and display truncation of underlying sediment at their bases.

Unit 4

Unit 4 deposits within the paleovalley are dominantly composed of carbonate breccia facies interpreted as debrites. Within proximal paleovalley locations, five distinct debrite subunits (4a through 4e) are identified from an axial to marginal cross section at Cala del Plomo (Fig. 10). Debrites form thick (up to 20 meters), stacked accumulations that display compensatory geometries between successive subunits 4a through 4c. Subunits 4d and 4e drape the substrate topography created from previous debrite subunits and creates a relatively flat surface for Unit 5 deposits. The base of Unit 4 in this location is defined by several meters of erosional truncation of underlying Unit 3 deposits. Debrite subunits are interstratified with foraminifera-rich wacke-packstone and graded skeletal packstone facies interpreted as hemipelagic-pelagic sediments and low- and high-density turbidites. Interstratified facies relationships display truncation, drape and local onlap against pre-existing topography (Fig. 10). Several meters of hemipelagic-pelagic sediments and low-density turbidites characterize the top of Unit 4 in the most proximal locations. Along depositional dip (Cala del Plomo to Cala de Enmedio, Fig. 9), the only traceable debrites are those within subunit 4a; subunits 4b-e cannot be traced along depositional dip and are hypothesized to be more proximal deposits that have significantly less volume than 4a. Subunit 4a displays multiple back-stepping debrites and truncated high-density turbidites. The base of debrite subunit 4a is defined by several meters of erosional truncation of underlying Unit 3 and Unit 2 sediments, and displays common soft-sediment deformation structures and clasts of Unit 3 foraminifera-rich wacke-packstone deposits. Down depositional dip, subunit 4a becomes thinner and is overlain by a single high-density turbidite that continues for hundreds of meters into the basin (Fig. 9). Within distal paleovalley locations, an axial to marginal cross section at Cala de Enmedio displays approximately 20 meters of incision into underlying Unit 3 deposits at the base of subunit 4a (Fig. 11). Debrites at Cala de Enmedio are thinner (5 meters) and more tabular than they are proximally, and are capped by high- and low-density turbidites that lapout against incised Unit 3 deposits (Fig. 11). Several meters down-dip from Cala de Enmedio, debrite subunit 4a pinches out and the base of Unit 4 is defined by the overlying high-density turbidite that continues into the basin. Several meters of interstratified low-density turbidites and hemipelagic-pelagic sediments overlie this high-density turbidite and characterize the upper portions of Unit 4 deposits immediately outside of the paleovalley (Fig. 9).

Low-density turbidites and hemipelagic-pelagic sediments are the dominant deposits along the ramp-like surface and within central and basin margin locations. The coarse-grained component of Unit 4 is characterized by a single debrite capped by low-density turbidites and hemipelagic-pelagic sediments along a narrow transect from sections 21/22 to sections 13/14 (Fig. 2A). This debrite forms an isolated 1 to 3 meter-thick tabular deposit that scours underlying Unit 3 sediments and transitions into a high-density turbidite that downlaps against the top of Unit 3 at Cala de

Enmedio (Fig. 11). Along the northern margin of the basin Unit 4 dominantly consists of interbedded low-density turbidites and hemipelagic-pelagic sediments, with the exception of high-density turbidites at sections 24 and 25.

Unit 4 sediment-gravity flows are compositionally unique from later deposits in that they contain a greater relative abundance of *Tarbellastreae* reef clasts and fragments. Decreasing *Tarbellastreae* abundance within progressively younger depositional units in the basin is reflective of the La Rellena platform stratigraphy and coincides with the early to late Messinian trend of decreasing coral diversity throughout the Mediterranean region (Esteban 1996; Esteban et al. 1996).

Unit 5

Deposits within the paleovalley are composed of interstratified foraminifera-rich wacke-packstones, graded skeletal packstones and carbonate breccia facies interpreted as hemipelagic-pelagic sediments, low- and high-density turbidites and debrites. In proximal paleovalley locations, Unit 5 is approximately 16 meters thick and is dominantly composed of hemipelagic-pelagic sediments and low-density turbidites that overlie the basal debrite subunit 5a (Fig. 10). Unit 5 debrite subunits 5a and 5b form more tabular deposits than Unit 4 debrite subunits in this area. Lateral continuity of fine- and coarse-grained deposits along an axial to marginal transect is fairly high as a result of relatively flat substrate topography. Lateral continuity down dip, however, is relatively poor as a result of intra-unit erosional truncation by debrite subunit 5b, as well as truncation of upper Unit 5 deposits by Unit 6 debrite subunit 6a

(Fig. 9). Additionally, debrite subunit 5a evolves into a high-density turbidite approximately 800 meters down dip (Fig. 9). This transition likely occurs where substrate slope and lateral confinement decreases enough to trigger a change in flow conditions (Kneller 1995; Mulder and Alexander 2001). In distal paleovalley locations, Unit 5 is approximately 5 meters thick and consists of low- and high-density turbidites that display minor truncation and lap out against incised Unit 3 deposits (Fig. 11). Further into the basin, Unit 5 consists entirely of low-density turbidites and hemipelagic-pelagic sediments that drape substrate topography.

Hemipelagic-pelagic sediments and low-density turbidites are the dominant deposits along the ramp-like surface and within central and basin margin locations. These deposits form several meters of laterally continuous beds that drape substrate paleotopography. A single high-density turbidite occurs along the margin of the basin at sections 24 and 25. The base of it shows erosional truncation of underlying deposits.

Unit 6

Carbonate breccias and graded skeletal packstones are the dominant deposits within the paleovalley and are interpreted as debrites and high-density turbidites. In proximal paleovalley locations, debrite subunits 6a and 6b form tabular deposits along an axial to marginal transect that display truncation of underlying Unit 5 deposits at their bases (Fig. 10). Debrite subunits also display internal scouring indicating flow surging or multiple amalgamated events (Mulder and Alexander

2001). In distal paleovalley locations, debrite subunits maintain their tabular geometries and are thinner and display less truncation of underlying sediment than in proximal locations (Fig. 11). Along depositional dip, debrite subunits are laterally continuous for thousands of meters into the basin, pinching out just southwest of Agua Amarga (Fig. 9). Vertically, debrite subunits 6a and 6b fine and thin upward into high- and low-density turbidites. Overall character relationships between Unit 6 debrites and Units 4 and 5 debrites within the paleovalley reveals that Unit 6 debrites travel several hundreds of meters farther into the basin than debrites within earlier units (Fig. 9). The top of Unit 6 within the paleovalley is defined by an irregular surface of pre-Pliocene alteration, and thus Unit 7 deposits are not documented.

Debrites and high-density turbidites are also the dominant deposits along the packstone-grainstone ramp-like surface and within central basin locations. Two distinct debrite subunits, approximately coeval with subunits 6a and 6b within the paleovalley, form tabular laterally extensive deposits that bypass locations proximal to the shelf margin and pinchout distally around sections 17 – 19 (Fig. 2A). Debrites dispersed along the ramp-like surface form more laterally continuous deposits and display less truncation of underlying Unit 5 sediments than contemporaneous debrites focused along the paleovalley. Additionally, facies relationships within Unit 6 in these areas reveal that the second episode of breccia sedimentation travels several tens of meters farther into the basin than the first episode. In bypass locations along the ramp-like surface, high-density turbidite deposits characterize the base of Unit 6. Vertically, both debrites and high-density turbidites pass upward into low-density turbidites and hemipelagic-pelagic sediments. Within the center of the basin, the top of Unit 6 is defined by an irregular surface of pre-Pliocene alteration. In most locations along the ramp-like surface and the northern basin margin, however, Unit 7 deposits are preserved and cap Unit 6.

Unit 7

Unit 7 deposits are not preserved within the paleovalley or within central basin locations as a result of pre-Pliocene alteration and modern erosion. Along the ramp-like surface, Unit 7 ranges from 2 to 5 meters-thick and is defined by carbonate breccia facies interpreted as a single debrite that is capped by foraminifera-rich wacke-packstone deposits (interpreted as low-density turbidites and hemipelagic-pelagic sediments). The debrite is a narrow tabular 1 to 2 meter-thick deposit that crops out at sections 10 and 14 (Fig. 2A). The base of Unit 7 in this location is defined by deformation of underlying Unit 6 sediment. Down dip (southeast) of section 10, the debrite downlaps against the top of Unit 6 deposits near Cala de Enmedio (Fig. 11), thereby establishing a clear stratigraphic relationship as the uppermost preserved unit within the basin. Along the northern margin of the basin at sections 24 and 26 (Fig. 2A), Unit 7 is defined by a graded skeletal packstone deposit interpreted as a high-density turbidite that fines upward into foraminiferal-rich wacke-packstone deposits interpreted as low-density turbidites and hemipelagic-pelagic sediments. The high-density turbidite displays minor truncation of underlying

Unit 6 sediments; low-density turbidites and hemipelagic-pelagic sediments in these areas tend to drape substrate topography.

DISCUSSION

Climate Control on Development of Miocene Carbonates

Heterozoan Carbonates

The relative absence of light-dependent organisms such as hermatypic corals, green algae, and large benthic forams (as well as non-skeletal grains such as peloids and ooids) within Units 1 and 2 indicate that these deposits are part of the heterozoan association (Franseen et al. 1997b; James 1997; Randazzo et al. 1999; John and Mutti 2005). James (1997) and other workers have attributed various factors such as water depth, salinity, temperature, and clarity to the paucity of photozoan skeletal and non-skeletal grains in heterozoan systems. Deposition of heterozoan carbonates in the Agua Amarga basin was influenced primarily by temperature and clarity of the water. Sedimentary features within Units 1 and 2 packstone-grainstone deposits indicate that these sediments accumulated within the depth of possible light-penetration, thereby eliminating water depth as a probable control. Another potential controlling factor is water salinity, however, communication of basin waters with the Atlantic ocean via the Betic and Rif straits during the Tortonian (Esteban 1996) suggests that aberrant salinities were not a limiting factor. Regionally, age-equivalent carbonates of the

Cabo de Gata area also contain heterozoan skeletal assemblages and suggest that a temperate climate during the Tortonian resulted in ocean waters that were too cool for photosynthetic communities. This is a reasonable hypothesis considering paleo-latitude and the transition to an icehouse climate during the middle-late Miocene (Randazzo et al. 1999; John and Mutti 2005). Further, previous work in the basin by Brachert et al. (1998) suggest warm-temperate climate conditions based on the presence of large foraminifera that imply water temperatures above 17 degrees Celsius. Possible temperate water conditions, however, may not be the only limiting factor; age-equivalent upper Tortonian coral reef assemblages have been found in a variety of other locations throughout the Mediterranean including Fortuna, Mallorca, and Tuscany (Esteban 1996; Esteban et al. 1996). Water clarity is the other likely control on deposition of heterozoan carbonates in the Cabo de Gata area. Exposed Neogene volcanic rocks formed an archipelago during the Tortonian, making it probable that terrigenous influx into shallow marine basins caused a reduction in water transparency that inhibited deposition of photozoan deposits (Hallock and Schlager 1986). Nutrient-rich waters from runoff, however, tend to display a more local effect on prevalence of heterozoan carbonate patterns. The widespread distribution of heterozoan carbonate deposits in the western Mediterranean points to a regional control, such as a temperate climate and/or regional upwelling of cool nutrient-rich waters (Franseen et al. 1997b).

Photozoan Carbonates

The transition from shallow-water heterozoan deposits into deep-water resedimented deposits containing abundant photozoan constituents (*Porites, Tarbellastreae,* and *Halimeda*) suggests a shift from a temperate climate during the late Tortonian, to subtropical-tropical climate during the Messinian (Franseen and Goldstein 1996; Franseen et al. 1997a; Brachert et al. 1998; Franseen et al. 1998; Brachert et al. 2001). Evidence for a warming climate in the Agua Amarga basin coincides with the development of shallow-water carbonate factories on surrounding paleohighs and subsequent deposition of deep-water sediment-gravity flows. High-density turbidites containing abundant shallow-water bioclasts are sparsely intercalated within early Messinian Unit 3 deposits and have a distinct shallow-water provenance indicative of carbonate production on the shelf. The absence of photozoan grains within Unit 3 high-density turbidites, however, suggests that subtropical-tropical climate conditions had not yet developed. Deposition of overlying Unit 4 breccias consisting of meter-scale *Porites* and *Tarbellastreae* reef clasts, as well as *Halimeda*, *Porites*, and *Tarbellastreae* fragments within breccia matrices, are unequivocal evidence of photozoan proliferation on the platform and suggests initiation of a subtropical-tropical climate by the early-middle Messinian. Development of a photozoan association on surrounding paleohighs may also indicate less turbid waters as a result of regional inundation and development of reef complexes on top of previously exposed volcanic basement, or changes in upwelling patterns.

Controls on Deep-water Lithofacies Architecture

The internal lithofacies architecture of resedimented deep-water deposits in the Agua Amarga basin is dominantly controlled by paleotopography and fluctuations in sea level. Other possible autogenic controls, such as variations in rates of sediment accumulation and transport as a result of carbonate productivity on the shelf and/or earthquake-induced sedimentation, may play an additional role.

Paleotopography

Paleotopography was a major control on the lateral distribution and facies geometries of deep-water depositional units within the Agua Amarga basin. The original basement and modified paleotopography displayed in Figure 2 represents Miocene topography. Subaerial exposure and erosion of volcanic substrate prior to deposition of any carbonate strata contributed to the evolution of the basement paleotopography, particularly the large margin-parallel paleovalley in the southwest corner of the basin (Franseen et al. 1993; Franseen and Goldstein 1997b). In addition to subaerial processes, variable amounts of faulting of the area directly north of the large paleovalley during or immediately following deposition of Unit 1 may have accentuated major topographic features in the basin. Basement topography was further modified by deposition of Units 1 and 2 packstone-grainstones, which formed a thick and gently dipping ramp-like surface in the northwest portion of the basin (Fig. 2B). The paleovalley to the south, however, was largely unfilled and served as the dominant pathway for later resedimented material into the basin.

Deep-water units within the paleovalley form a complex and channelized accumulation of proximal coarse-grained gravity flow deposits that become increasingly tabular and finer-grained down depositional dip. A fairly uniform and low substrate slope along the paleovalley floor indicates that proximity to steeply dipping valley walls and lateral confinement are the dominant paleotopographic controls on focused-flow lithofacies architectures. Sediment-gravity flows along the ramp-like surface form thinner sheet-like deposits that responded primarily to subtle changes in substrate slope.

Lateral confinement within paleovalley walls is a major control on geometries within the proximal paleovalley at Cala del Plomo (Figs. 8 and 10). Early phases of debrite accumulation display mounded depositional topographies that form in response to lateral confinement and averted flow around previous deposits. This type of compensation geometry results in lateral accretion of successive flows and is similar to calciclastic fan deposits of the Eocene Anotz Formation, western Pyrenees (Payros et al. 2007) and Miocene carbonate-siliciclastic gravity flows of the Porto Torres basin in Sardinia, Italy (Vigorito et al. 2006). Mounded debrite geometries may also be a result of the low transport efficiency of carbonate debris flows due to high internal friction resulting from the absence of abundant lubricating clay particles (Payros and Pujalte 2008). Additionally, lateral confinement within proximal paleovalley locations results in lapout of sediment-gravity flows against valley walls. Later phases of debrite accumulation that fill in and flatten depositional topography display more lenticular and tabular geometries than earlier deposits, largely in response to progressively less lateral confinement as the paleovalley is filled and confining walls become broader (Kneller 1995; Haughton 2000; Vigorito et al. 2006). A similar vertical evolution from channelized to sheet-like turbidites is documented within late Miocene strata of the Tabernas-Sorbas basin, southeast Spain (Haughton 2000). In addition to irregular geometries, high-density turbidity currents and debris flows have significant erosive tendencies within proximal paleovalley locations interbedded low-density turbidites and pelagic-hemipelagic sediments are commonly truncated. Where preserved, finer-grained deposits tend to drape the irregular topography created by earlier high-density events. Coarse- to fine-grained sediment ratios are commonly high in proximal locations adjacent to steeply sloping substrate and tend to decrease away from the sediment source where substrate slopes are commonly less (Wynn et al. 2000).

The paleovalley is broader and exhibits less of a confining effect on sediment gravity-flows in distal paleovalley locations at Cala de Enmedio (Figs. 8 and 11). Incision of a large channel feature into Unit 3 foraminifera-rich deposits in this area, however, resulted in confinement of Unit 4 and 5 sediment-gravity flows. These deposits lapout against channel walls and almost completely fill the channel prior to deposition of Unit 6. As a result of this near filling, Unit 6 sediment gravity flow deposits display thinner sheet-like geometries with less truncation of underlying sediment at their bases. Sheet-like debrites and turbidites are largely indicative of deposition in more distal locations where lateral confinement is less and substrate slopes are commonly more gently dipping (Mullins and Cook 1986; Bouma 2000; Haughton 2000; Vigorito et al. 2006; Payros and Pujalte 2008).

The topography on the ramp-like surface served as an additional pathway for resedimented material into the basin. The absence of a funneling mechanism in this location resulted in sediment-gravity flows that were dispersed into the basin, and thus form depositional geometries that are more consistent with slope-apron deposits. However, unlike most line-sourced accumulations, where debrites and turbidites commonly form stacked accumulations at the base of a steep slope (Cook and Mullins 1983; Mullins and Cook 1986), dispersed-flow deposits in the Agua Amarga basin bypassed the upper portions of the ramp-like surface and were transported farther into the basin, forming isolated and thin sheet-like bodies interstratified with hemipelagic-pelagic sediments and low-density turbidites. These base of these debrites display little truncation of underlying material as a result of increasing sediment dispersal and decreasing internal energy (Kneller 1995; Mulder and Alexander 2001; Vigorito et al. 2006). Debrite deposits are located in basinal areas where substrate slopes are lowest.

Relative sea level

The quantitative relative sea-level curve (Fig. 4) generated by Goldstein and Franseen (1995) and Franseen et al. (1998) from “pinning points” within the Las Negras strata can be used as a guideline to discuss controls on lithofacies architecture in the Agua Amarga basin and offer insight into the history of adjacent platform development. Depositional sequences similar to those within the Agua Amarga basin are recognized within temperate and subtropical carbonate deposits throughout the Mediterranean region, strongly supporting a regional Mediterranean sea level control on stratigraphy and depositional architectures (Franseen and Mankiewicz 1991).

Correlation of the lower stratigraphic Units 1 and 2 in the Agua Amarga basin to an interval encompassing pinning points 1 – 5 on the relative sea-level curve (Fig. 4) is based on similar DS1A and DS1B heterozoan packstone-grainstone deposits in the Las Negras area that are separated by a distinct subaerial exposure surface, as well as age data control from an interbedded volcanic unit in the Las Negras area (Goldstein and Franseen 1995; Franseen and Goldstein 1996; Franseen et al. 1997a; Franseen et al. 1997b; Franseen et al. 1998; Johnson et al. 2005), and Cala del Plomo area in the Agua Amarga basin (Fig. 2). Unit 1 volcaniclastic skeletal packstone-grainstones were deposited on top of subaerially exposed and eroded volcanic basement. It is hypothesized that deposition and subaerial exposure of Unit 1 may have taken place during the same time interval as pinning points 1 through 3 (Figs. 4 and 13). Unit 2 and the underlying red fossiliferous wackestone was likely deposited during one or more relative sea level changes between pinning points 4 and 5 (Fig. 13). Inundation of the basin as a result of the sea-level rise leading up to pinning point 5 (Fig. 4) represents the gradational facies transition from Unit 2 shallow-water packstone-grainstones into deep-water hemipelagic-pelagic deposits, low-density turbidites and uncommon high-density turbidites of Unit 3.

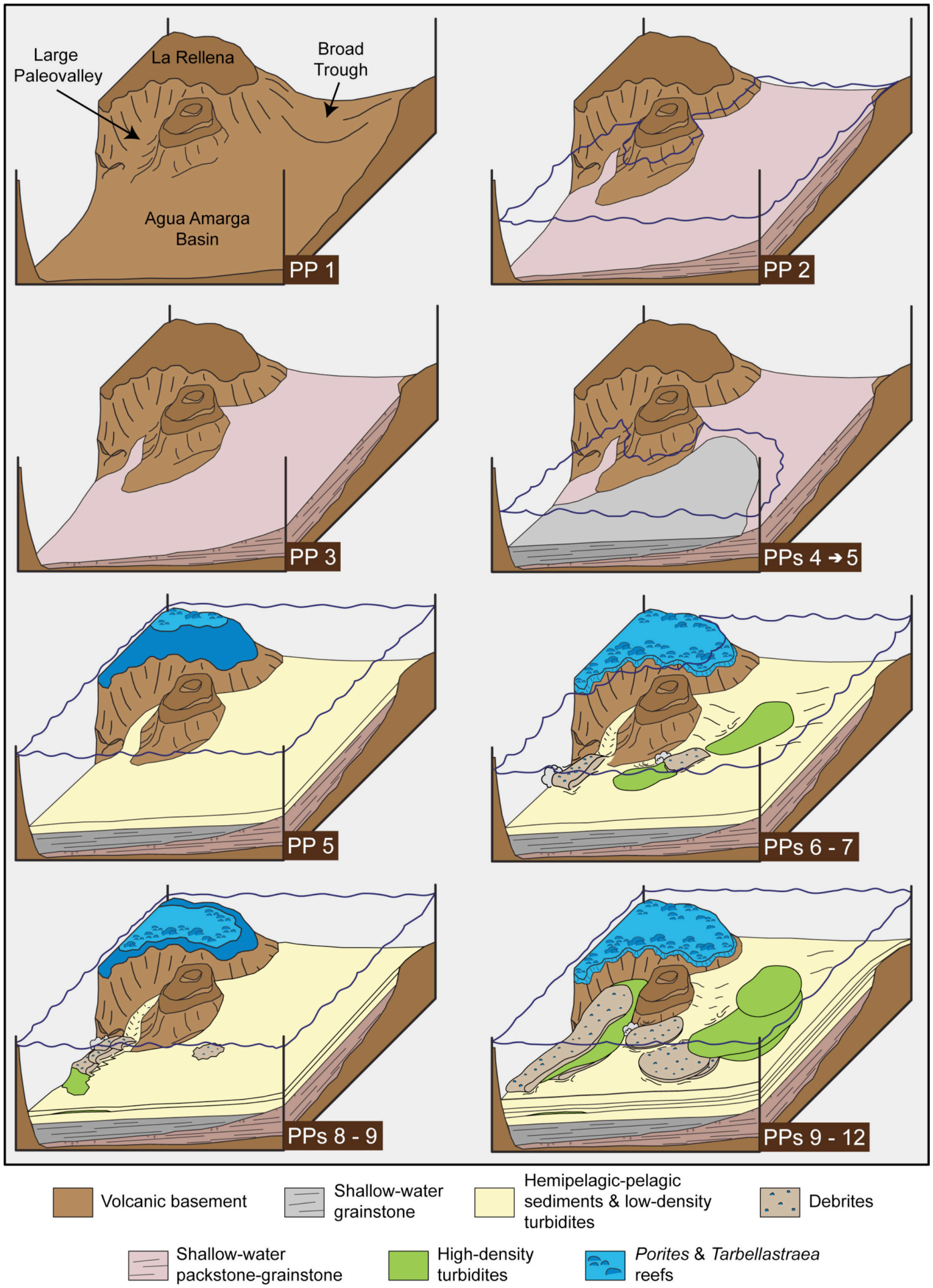

Fig. 13. – Schematic block diagrams representing deposition in the Agua Amarga basin during various positions of relative sea level (pinning points on the relative sea-level curve in Figure 4). Geometries, distributions and volumes of deposits are not to scale.

The time interval of point 5 (Fig. 4) approximately coincides with a transition to subtropical-tropical climate and development of photozoan reefs on paleohighs throughout the region. In the Agua Amarga basin, pinning point 5 (Figs. 4 and 13) is likely represented by hemipelagic-pelagic sediments, low-density turbidites and uncommon high-density turbidites of Unit 3. After such a major relative rise in sea level, the shallow-water sediment source would be far up on the La Rellana platform, and little sediment would make it out into the basin. The overall transgressive nature of Unit 3 deposits is consistent with this correlation.

The period between pinning points 5 and 6 likely represents a time when reefs rich in both *Tarbellastreae* and *Porites* were growing on the La Rellena Platform (Fig. 4). As they would be distal from the basin margin, it is likely that only fine-grained sediments of the upper part of Unit 3 would be their lateral equivalent in the basin.

The period between pinning points 6 – 7 (Figs. 4 and 13) represent a subsequent major relative fall in sea level. A persistent relative fall in sea level may have shifted factory production closer to the platform margin and eventually destabilized internal pore pressures, thereby promoting significant shedding of platform debris into the basin (Crevello and Schlager 1980; Payros et al. 2007; Payros and Pujalte 2008). Debrites and high-density turbidites within the paleovalley and along the ramp-like surface were likely deposited in response to this significant fall in sea level (Fig. 13). There is significant truncation of underlying sediment at the base of breccia subunit 4a, traceable from Cala del Plomo to just past Cala de Enmedio

(Fig. 9). The possibility for submarine currents or subaerial exposure as the cause of this erosional surface is unlikely: there are no indicators for subaerial exposure anywhere along this surface, and the overlying breccia subunit 4a contains clasts of underlying foraminifera-rich material and displays common soft sediment deformation structures at its base. Furthermore, distal from the location of breccia 4a, significant erosion on this surface is not apparent. Evidence for subaerial exposure of coeval carbonate strata on the La Rellena platform (Toomey 2002), as well as above DS2 deposits in the Las Negras area (Franseen et al. 1998), offers support for a large-scale relative fall in sea level as the dominant triggering mechanism of these initial sediment-gravity flow deposits in the basin. In addition to relative sea-level fluctuations, earthquakes induced from nearby tectonic activity cannot be ruled out as a possible triggering mechanism. Within the Nijar basin directly north of the Carboneras fault (Fig. 1), seismites have been documented within late Messinian alluvial and lacustrine sediments (Fortuin and Dabrio 2008). Deformed strata indicative of various levels of seismic intensity in the Nijar basin suggest that high magnitude earthquakes may have induced some sediment-gravity flows in the Agua Amarga basin during the early to middle Miocene as well.

Multiple backstepping Unit 4 debrites within the paleovalley are capped by several meters of high- and then low-density turbidites in proximal parts of the paleovalley (Figure 9). Along the ramp-like surface and within central and basin margin locations, this interval is characterized by deposition of low-density turbidites and hemipelagic-pelagic sediments (Fig. 13). The most reasonable explanation for the backstepping geometries and upward fining is a relative sea-level rise, which would have shifted carbonate production away from the platform margin. This rise could correspond to the time interval between pinning points 8 and 9.

The period between pinning points 9 – 12 (Fig. 4) represent minor transgression and subsequent highstand conditions, which would have resulted in progradation of a reefal margin on the platform (Fig. 13). Unit 5 is marked by a basal erosion surface followed by a thick basal debrite of limited extent into the basin, and an overlying section of mostly fine high- and low-density turbidites, and hemipelagic-pelagic sediments. The overall fine-grained nature of the unit is consistent with deposition during the time interval represented by pinning points 9 – 12, associated with late transgression and early highstand. Dominant low-density turbidites and hemipelagic-pelagic deposits within the paleovalley, along the packstone-grainstone ramp-like surface, and within central and basin margin locations during this interval indicate reduced shedding of platform debris into the basin as a result of renewed platform sedimentation within platform interior locations away from the margin. Laterally restricted debrite subunits 5a and 5b within the proximal paleovalley (Figs. 9 and 10), however, indicate some shedding into the basin during this interval that may have resulted from a shifting depocenter on the platform due to small-scale relative fluctuations in sea level, or earthquake-induced platform shedding.

Unit 6 debrite subunits are transported farther into the basin than debrites of previous units. These progradational geometries suggest proliferation and progradation of the carbonate factory toward the platform margin. Internally, Unit 6 deposits display two thinning and fining upward cycles; debrite subunits pass vertically into high- and low-density turbidites. Finer-grained deposits within these cycles suggest intervals of stopped resedimentation processes that may be due to periods of small-scale sea-level rise and backstepping of the platform margin. The high-density gravity flow deposits of Unit 6 are volumetrically the most significant in the basin. They could represent shedding of debris during the late highstand (Crevello and Schlager 1980; Schlager et al. 1994) or during falling sea level (see pinning point 13). Dominant triggering mechanisms for these deposits may have included small-scale relative falls in sea level that caused platform instability, and/or platform oversteepening due to high rates of sediment accumulation (Drzewiecki and Simo 2002; Payros and Pujalte 2008). Considering Unit 6 deposition likely occurred during the late Miocene, and are approximately coeval with reported seismites in the Nijar basin (Fortuin and Dabrio 2008), earthquake-induced sediment gravity flow deposition cannot be ruled out as a possible triggering mechanism. Finally, though Unit 7 deposits are limited in thickness and lateral extent as a result of modern erosion and pre-Pliocene alteration, these deposits likely represent a continuation of resedimentation into the basin during a period of relative sea-level fall. In the Las Negras area, this period of continued sea-level fall resulted in progradational and down-stepping reef geometries (Franseen et al. 1998). The overall progradational character of Unit 6 (and to some extent, Unit 7) debrites and high-density turbidites likely represent the deep-water-equivalent to prograding and down-stepping reef and fore-reef deposits along the La Rellena platform margin.

CONCLUSIONS

(1) Two major depositional successions characterize the stratigraphy of the Agua Amarga basin: dominant shallow-water high-energy deposits of Units 1 and 2; and deep-water interstratified hemipelagic-pelagic and sediment gravity flow deposits of Units 3 – 7. The late Tortonian shallow-water succession formed following subaerial exposure and erosion of volcanic basement. The early Messinian deep-water succession formed after continued inundation of the basin and subsequent shallow-water production on surrounding paleohighs. Deep-water units are defined by intervals of relatively low platform shedding (dominantly hemipelagic-pelagic sediments and fine-grained turbidites), and intervals of relatively high platform shedding (dominantly coarse-grained turbidites and debrites).

(2) The shallow-water units consist of heterozoan fauna that suggests a temperate climate during the late Tortonian. Other factors related to water clarity, however, may have been the primary control. Surrounding volcanic basement paleohighs were largely exposed during this time and likely provided a significant source of volcaniclastic detritus that would have caused turbid water conditions. Additionally, upwelling may have triggered phytoplankton blooms and impeded light requirements necessary for photozoan development. Resedimented deposits of the overlying deep-water units contain photozoan constituents that were sourced from an

extensive reefal platform, suggesting a shift to a more subtropical-tropical climate during the Messinian.

(3) Paleotopography plays a key role in predicting the development of focused-flow versus dispersed-flow deep-water carbonate systems. The deep-water succession in the Agua Amarga basin contains both systems. In the southwest portion of the basin, a large paleovalley focused the majority of resedimented platform material into and along its axis and then out into the basin. These deposits provide an analogue for focused-flow deep-water carbonate systems that display aspects of point-sourced deep-water siliciclastic systems. Directly north of the paleovalley, a gently dipping ramp-like surface abutted the remaining portion of the platform margin, and dispersed resedimented material into the basin directly from its original line source.

Paleotopographic features that serve as funneling mechanisms have a significant effect on the location, lithofacies architecture and lateral distributions of coarse-grained deep-water carbonate deposits. Proximal exposures within the paleovalley at Cala del Plomo reveal thick accumulations of channelized and complexly interstratified debrites and turbidites that become thinner and more tabular as the paleovalley broadens and lateral confinement decreases. The most important factors controlling the architectures of focused-flow accumulations include the degree of lateral confinement within valley walls, and proximity to the sediment source and steeply dipping platform slopes. In this study, the large paleovalley is parallel to the platform margin (sediment source) and thus serves as a focus for a significant volume of resedimented material into the basin. Dispersed-flow deposits along the ramp-like surface display thinner sheet-like geometries with less pronounced truncation of underlying facies at their bases. Debrites and high-density turbidites in these locations are not influenced by lateral confinement and deposition is most significantly controlled by substrate slope and distance from the platform margin.

(4) The internal lithofacies architecture of the deep-water succession in the Agua Amarga basin displays a predictable response to fluctuations in relative sea level. Progradational packages of sediment are deposited in the basin during periods of relative sea level fall and after highstand progradation when carbonate production is closest to the shelf margin, and debris flows and coarse-grained turbidity currents are readily triggered. The sediment-gravity flows of Unit 6 display progradation of coarse-grained material into the basin within the paleovalley and along the ramp-like surface. Relative rises in sea level cause backstepping of debrite material, ultimately decreasing the amount of coarse sediment transported into the basin. Backstepping geometries within Unit 4 debrites and capping hemipelagic-pelagic sediments and low-density turbidites are indicative of a retrogradational carbonate factory on the platform. The dominant basinal deposits at the time of maximum flooding are fine-grained deposits, as is evident in the abundance of hemipelagic-pelagic sediments and low-density turbidites (and relative paucity of coarse-grained sediment gravity flow deposits) in the upper part of Unit 4 and throughout Unit 5.

References Cited

BETZLER, C., BRACHERT, T.C., BRAGA, J.C., AND MARTIN, J.M., 1997, Nearshore, temperate, carbonate depositional systems (lower Tortonian, Agua Amarga Basin, southern Spain): implications for carbonate sequence stratigraphy: Sedimentary Geology, v. 113, p. 27-53.

BOUMA, A.H., 2000, Fine-Grained, Mud-Rich Turbidite Systems: Model and Comparison with Coarse-Grained, Sand-Rich Systems, *in* Bouma, A.H., and Stone, C.G., eds., Fine-Grained Turbidite Systems, AAPG Memoir 72 / SEPM Special Publication No. 68. P. 9-19.

BOUMA, A.H., DEVRIES, M.B., AND STONE, C.G., 1997, Reinterpretation of Depositional Processes in a Classic Flysch Sequence (Pennsylvanian Jackfork Group), Ouachita Mountains, Arkansas and Oklahoma: Discussion: AAPG Bulletin, v. 81, p. 470-472.

BRACHERT, T.C., BETZLER, C., BRAGA, J.C., AND MARTIN, J.M., 1998, Microtaphofacies of a Warm-Temperate Carbonate Ramp (Uppermost Tortonian/Lowermost Messinian, Southern Spain): Palaios, v. 13, p. 459-475.

BRACHERT, T.C., HULTZSCH, N., KNOERICH, A.C., KRAUTWORST, U., AND STUCKRAD, O.M., 2001, Climatic signatures in shallow-water carbonates: high-resolution stratigraphic markers in structurally controlled carbonate buildups (Late Miocene, southern Spain): Palaeogeography, Palaeoclimatology, Palaeoecology, v. 175, p. 211-237.

BRACHERT, T.C., KRAUTWORST, U.M.R., AND STUECKRAD, O.M., 2002, Tectono-climatic evolution of a Neogene intramontane basin (Late Miocene Carboneras subbasin, southeast Spain): revelations from basin mapping and biofacies analysis: Basin Research, v. 14, p. 503-521.

COOK, H.E., AND ENOS, P., 1977, Deep-water Carbonate Environments, SEPM Special Publication 25, p. 336.

COOK, H.E., AND MULLINS, H.T., 1983, Ch. 11: Basin Margin Environments, *in* Scholle, P.A., Bebout, D.G., and Moore, C.H., eds., Carbonate Depositional Environments, AAPG Memoir 33, p. 540-617.

CREVELLO, P., AND SCHLAGER, W., 1980, Carbonate Debris Sheets and Turbidites, Exuma Sound, Bahamas: Journal of Sedimentary Petrology, v. 50, p. 1121-1148.

DABRIO, C.J., ESTEBAN, M., AND MARTIN, J.M., 1981, The Coral Reef of Nijar, Messinian (Uppermost Miocene), Almeria Province, SE Spain: Journal of Sedimentary Petrology, v. 51, p. 521-439.

DAVIES, D., 1968, Carbonate Turbidites, Gulf of Mexico: Journal of Sedimentary Petrology, v. 38, p. 1100-1109.

DILLETT, P.M., 2004, Paleotopographic and sea-level controls on the sequence stratigraphic character of a heterozoan carbonate succession: Pliocene, Carboneras basin, southeast Spain [unpublished Unpublished M.S. thesis]: University of Kansas, Lawrence, KS, 116 p.

DRZEWIECKI, P.A., AND SIMO, J.A., 2002, Depositional processes, triggering mechanisms and sediment composition of carbonate gravity flow deposits: examples from the Late Cretaceous of the south-central Pyrenees, Spain: Sedimentary Geology, v. 146, p. 155-189.

DUNHAM, R.J., 1962, Classification of carbonate rocks according to depositional texture, *in* Ham, W.E., ed., Classifications of carbonate rocks - a symposium, AAPG Memoir, p. 108-121.

ESTEBAN, M., 1996, An Overview of Miocene Reefs from Mediterranean Areas: General Trends and Facies Models, *in* Franseen, E.K., Esteban, M., Ward, W.C., and Rouchy, J.-M., eds., Models for Carbonate Stratigraphy from Miocene Reef Complexes of the Mediterranean Regions, SEPM Concepts in Sedimentology and Paleontology Series No. 5, p. 3-54.

ESTEBAN, M., BRAGA, J.C., MARTIN, J., AND SANTISTEBAN, C., 1996, Western Mediterranean Reef Complexes, *in* Franseen, E.K., Esteban, M., Ward, W.C., and Rouchy, J.-M., eds., Models for Carbonates Stratigraphy from Miocene Reef Complexes of Mediterranean Regions, SEPM Concept in Sedimentology and Paleontology, p. 55-72.

FERNANDEZ-SOLER, J.M., 2001, Volcanics of the Almeria Province, *in* Mather, A.E., Martin, J.M., Harvey, A.M., and Braga, J.C., eds., A Field Guide to the Geology and Geomorphology of the

Neogene Sedimentary Basins of the Almeria Province, SE Spain: Oxford, Blackwell, p. 58-88.
FORTUIN, A.R., AND DABRIO, C.J., 2008, Evidence for Late Messinian seismites, Nijar Basin, south-east Spain: Sedimentology, v. 55, p. 1595-1623.
FRANSEEN, E.K., AND GOLDSTEIN, R.H., 1996, Paleoslope, Sea-level and Climate Controls on Upper Miocene Platform Evolution, Las Negras Area, Southeastern Spain, *in* Franseen, E.K., Esteban, M., Ward, W. C., and Rouchy, J.-M., eds., Models for Carbonates Stratigraphy from Miocene Reef Complexes of Mediterranean Regions, SEPM Concept in Sedimentology and Paleontology, p. 159-176.
FRANSEEN, E.K., AND GOLDSTEIN, R.H., 1997, Controls on Sequence Stratigraphy in the Agua Amarga Basin Area, *in* Franseen, E.K., Goldstein, R.H., and Esteban, M., eds., Controls on Porosity Types and Distribution in Carbonate Reservoirs: A Guidebook for Miocene Carbonate Complexes of the Cabo de Gata Area, SE Spain: American Association of Petroleum Geologists Education Program, p. 91-100.
FRANSEEN, E.K., AND GOLDSTEIN, R.H., 1999, Paleovalley Morphology: A Controlling Factor on Carbonate Sequence Location, Architecture and Sediment Dispersal, 1999 AAPG Annual Convention Official Program: San Antonio, Texas, p. A43.
FRANSEEN, E.K., AND MANKIEWICZ, C., 1991, Depositional sequences and correlation of middle(?) to late Miocene carbonate complexes, Las Negras and Nijar areas, southeastern Spain.: Sedimentology, v. 38, p. 871-898.
FRANSEEN, E.K., GOLDSTEIN, R.H., AND ESTEBAN, M., 1997a, Controls on Porosity Types and Distribution in Carbonate Reservoirs: A Guidebook for Miocene Carbonate Complexes of the Cabo de Gata Area, SE Spain: American Association of Petroleum Geologists Education Program, p. 1-150.
FRANSEEN, E.K., GOLDSTEIN, R.H., AND FARR, M.R., 1997b, Substrate-Slope and Temperature Controls on Carbonate Ramps: Revelations from Upper Miocene Outcrops, SE Spain, *in* James, N.P., and Clarke, A.D., eds., Cool-Water Carbonates, SEPM Special Publication, p. 271-290.
FRANSEEN, E.K., GOLDSTEIN, R.H., AND FARR, M.R., 1998, Quantitative Controls on Location and Architecture of Carbonate Depositional Sequences: Upper Miocene, Cabo de Gata Region, SE Spain: Journal of Sedimentary Research, v. 68, p. 283-298.
FRANSEEN, E.K., GOLDSTEIN, R.H., AND WHITESELL, T.E., 1993, Sequence stratigraphy of Miocene carbonate complexes, Las Negras area, southeastern Spain: implications for quantification of changes in relative sea-level, *in* Loucks, R.G., and Sarg, J.F., eds., Carbonate Sequence Stratigraphy: Recent Developments and Applications, AAPG Memoir 57, p. 409-434.
GANI, M.R., 2004, From Turbid to Lucid: A straightforward Approach to Sediment Gravity Flows and Their Deposits: The Sedimentary Record, v. 2, p. 4-8.
GIBBONS, W., AND MORENO, M.T., eds., 2003, The Geology of Spain: Geological Society of London, p. 649.
GOLDSTEIN, R.H., AND FRANSEEN, E.K., 1995, Pinning points: a method providing quantitative constraints on relative sea-level history: Sedimentary Geology, v. 95, p. 1-10.
HALLOCK, P., AND SCHLAGER, W., 1986, Nutrient Excess and the Demise of Coral Reefs and Carbonate Platforms: Palaios, v. 1, p. 389-398.
HARDENBOL, J., THIERRY, J., FARLEY, M.B., JACQUIN, T., DE GRACIANSKY, P.C., AND VAIL, P.R., 1998, Mesozoic and Cenozoic sequence chronostratigraphic framework of European Basins, *in* de Graciansky, P.C., Hardenbol, J, Jacquin, T., and Vail, P.R., eds., Mesozoic and Cenozoic Sequence Stratigraphy of European Basins. Soc. Sediment. Geol. Spec. Publ., v. 60. SEPM, Tulsa, OK, p. 3-13.
HAUGHTON, P.D.W., 2000, Evolving turbidites systems on a deforming basin floor, Tabernas, SE Spain: Sedimentology, v. 47, p. 497-518.
JAMES, N.P., 1997, The Cool-Water Carbonate Depositional Realm, *in* James, N.P., and Clarke, J., eds., Cool-Water Carbonates, SEPM Special Publications, p. 1-20.

JOHN, C., AND MUTTI, M., 2005, Relative Control of Paleoceanography, Climate, and Eustasy over Heterozoan Carbonates: A Perspective from Slope Sediments of the Marion Plateau (ODP LEG 194): Journal of Sedimentary Research, v. 75, p. 216-230.

JOHNSON, C.L., FRANSEEN, E.K., AND GOLDSTEIN, R.H., 2005, The effects of sea level and paleotopography on lithofacies distribution and geometries in heterozoan carbonates, south-eastern Spain: Sedimentology, v. 52, p. 513-536.

KNELLER, B.C., 1995, Beyond the turbidite paradigm: physical models for deposition of turbidites and their implications for reservoir prediction, *in* Hartley, A.J., and Prosser, D.J., eds., Characterization of Deep Marine Clastic Systems, Geological Society, London, Special Publications 94, p. 31-49.

KRAUTWORST, U.M.R., AND BRACHERT, T.C., 2003, Sedimentary facies during early stages of flooding in an extensional basin: the Breche Rouge de Carboneras (Late Miocene, Almeria/SE Spain): International Journal of Earth Science, v. 92, p. 610-623.

LOWE, D.R., 1982, Sediment gravity flows: II. Depositional models with special reference to the deposits of high-density turbidity currents: Journal of Sedimentary Petrology, v. 52, p. 279-297.

LOWE, D.R., 1997, Reinterpretation of Depositional Processes in a Classic Flysch Sequence (Pennsylvanian Jackfork Group), Ouachita Mountains, Arkansas and Oklahoma: Discussion: AAPG Bulletin, v. 81, p. 460-465.

MANKIEWICZ, C., 1996, The Middle to Upper Miocene carbonate complex of Nijar, Almeria Province, southeastern Spain, *in* Franseen, E.K., Esteban, M., Ward, W.C., and Rouchy, J.-M., eds., Models for Carbonates Stratigraphy from Miocene Reef Complexes of Mediterranean Regions, SEPM Concept in Sedimentology and Paleontology.

Mapa Geologico de Espana: Instituto Geologico y Minero de Espana. 1981.

MARTIN, J.M., BRAGA, J.C., AGUIRRE, J., AND BETZLER, C., 2004, Contrasting models of temperate carbonate sedimentation in a small Mediterranean embayment: the Pliocene Carboneras Basin, SE Spain: Journal of the Geological Society, London, v. 161, p. 387-399.

MARTIN, J.M., BRAGA, J.C., AND BETZLER, C., 2003, Late Neogene - Recent uplift of the Cabo de Gata volcanic province, Almeria, SE Spain: Geomorphology, v. 50, p. 27-42.

MARTIN, J.M., BRAGA, J.C., BETZLER, C., AND BRACHERT, T., 1996, Sedimentary model and high-frequency cyclicity in a Mediterranean, shallow-shelf, temperate-carbonate environment (uppermost Miocene, Agua Amarga Basin, Southern Spain): Sedimentology, v. 43, p. 263-277.

MILLER, K.G., KOMINZ, M.A., BROWNING, J.V., WRIGHT, J.D., MOUNTAIN, G.S., KATZ, M.E., SUGARMAN, P.J., CRAMER, B.S., CHRISTIE-BLICK, N., AND PEKAR, S.F., 2005, The Phanerozoic Record of Global Sea-Level Change: Science, v. 310, p. 1293-1298.

MONTENANT, C., AND OTT D'ESTEVOU, P. , 1990, Le bassin de Nijar-Carboneras et le couloir de Bas-Andarax, *in* Montenant, C., ed., Les Bassins Neogenes Du Domaine Betique Oriental (Espagne): Institut Geologique Albert-de-Lapparent, Paris, Documents et Travaux Institut Geologique Albert-de-Lapparent, p. 129-164.

MULDER, T., AND ALEXANDER, J., 2001, The physical character of subaqueous density flows and their deposits: Sedimentology, v. 48, p. 269-299.

MULLINS, H.T., AND COOK, H.E., 1986, Carbonate Apron Models: Alternatives to the Submarine Fan Model for Paleoenvironmental Analysis and Hydrocarbon Exploration: Sedimentary Geology, v. 48, p. 37-79.

PAYROS, A., AND PUJALTE, V., 2008, Calciclastic submarine fans: An integrated overview: Earth-Science Reviews, v. 86, p. 203-246.

PAYROS, A., PUJALTE, V., AND ORUE-ETXEBARRIA, X., 2007, A point-sourced calciclastic submarine fan complex (Eocene Anotz Formation, western Pyrenees): facies architecture, evolution and controlling factors: Sedimentology, v. 54, p. 137-168.

PLATT, J.P., AND VISSERS, R.L.M., 1989, Extensional collapse of thickened continental lithosphere: a working hypothesis for the Alboran sea and Gibraltar arc: Geology, v. 17, p. 540-543.

POSAMENTIER, H.W., AND WALKER, R.G., 2006, Deep-water turbidites and submarine fans, *in* Posamentier, H.W., and Walker, R.G., eds., Facies Models Revisited, SEPM Special Publication 84, p. 399-520.

RANDAZZO, A.F., MULLER, P., LELKES, G., JUHASZ, E., AND HAMOR, T., 1999, Cool-water Limestones of the Pannonian Basinal System, Middle Miocene, Hungary: Journal of Sedimentary Research, v. 69, p. 283-293.

RUIZ-ORTIZ, P.A., 1983, A carbonate submarine fan in a fault-controlled basin of the Upper Jurassic, Betic Cordillera, southern Spain: Sedimentology, v. 30, p. 33-48.

SCHLAGER, W., REIJMER, J.J.G., AND DROXLER, A., 1994, Highstand Shedding of Carbonate Platforms: Journal of Sedimentary Research, v. B64, p. 270-281.

SCHOLLE, P.A., ARTHUR, M.A., AND EKDALE, A.A., 1983, Ch. 12: Pelagic Environment, *in* Scholle, P.A., Bebout, D.G., and Moore, C.H., eds., Carbonate Depositional Environments, AAPG Memoirs 33, p. 620-691.

SHANMUGAM, G., 1996, High-density turbidity currents: Are they sandy debris flows?: Journal of Sedimentary Research, v. 66, p. 2-10.

SHANMUGAM, G., AND MOIOLA, R.J., 1995, Reinterpretation of Depositional Processes in a Classic Flysch Sequence (Pennsylvanian Jackfork Group), Ouachita Mountains, Arkansas and Oklahoma: AAPG Bulletin, v. 79, p. 672-695.

STELTING, C.E., BOUMA, A.H., AND STONE, C.G., 2000, Fine-Grained Turbidite Systems: Overview, *in* Bouma, A.H., and Stone, C.G., eds., Fine-Grained Turbidite Systems, AAPG Memoir 72 / SEPM Special Publication No. 68.

TOOMEY, N., 2002, Controls on sequence stratigraphy in upper Miocene carbonates of Cerro de Ricardillo, southeastern Spain [unpublished Unpublished M.S. thesis]: University of Kansas, Lawrence, KS, 145 p.

VIGORITO, M., MURRU, M., AND SIMONE, L., 2006, Architectural patterns in a multistorey mixed carbonate-siliciclastic submarine channel, Porto Torres Basin, Miocene, Sardinia, Italy: Sedimentary Geology, v. 186, p. 213-236.

WYNN, R., B., MASSON, D.G., STOW, D.A., AND WEAVER, P.P., 2000, The Northwest African slope apron: a modern analogue for deep-water systems with complex seafloor topography: Marine and Petroleum Geology, v. 17, p. 253-265.

Chapter 3:
Reservoir Characterization and 3-D Static Modeling of *In Situ* Shallow-water and Resedimented Deep-water Carbonate Deposits: Agua Amarga Basin, Southeast Spain

Rachel A. Dvoretsky[1)], Robert H. Goldstein[2)] and Evan K. Franseen[3)]

1) Department of Geology, University of Kansas, Lindley Hall, 1475 Jayhawk Blvd., Lawrence, KS, 66044, Ph. # (785) 766-6995, e-mail: rdvorets@ku.edu

2) Department of Geology, University of Kansas, Lindley Hall, 1475 Jayhawk Blvd., Lawrence, KS, 66044, Ph. # (785) 864-2738, e-mail: gold@ku.edu

3) Department of Geology, University of Kansas, Lindley Hall, 1475 Jayhawk Blvd., Lawrence, KS, 66044, Ph. # (785) 864-2723, e-mail: evanf@kgs.ku.edu

CHAPTER SUMMARY

Reservoir-analog characterization of upper Miocene carbonate deposits within the Agua Amarga basin, southeast Spain documents an important outcrop analog for assessing reservoir potential of subsurface *in situ* shallow-water and resedimented deep-water carbonate systems. 3-D outcrop exposures in the basin allow for extensive characterization of lithofacies and lithofacies architecture through measured sections, photomosaics, and collection of core plug petrophysical data. Integration of field and lab data into 2-D and 3-D cellular models facilitated the creation of a whole-field reservoir model that is largely constrained by geological observations. Initial pore volumes calculated from the 3-D model reveal three potential reservoir targets: 1) *in situ* skeletal packstone-grainstones (shallow-water play); 2) focused-flow sediment-gravity flows (deep-water play); and 3) dispersed-flow sediment-gravity flows (deep-water play). Within the shallow-water play, reservoir units are composed of volcaniclastic skeletal packstone-grainstone and skeletal grainstone facies. Combined mean porosity and corresponding permeability for these shallow-water deposits is 26.3% and 81.1md. Within the deep-water plays, reservoir units are composed of graded fine- to very coarse-grained skeletal packstone facies with a combined mean porosity and corresponding permeability of 30.5% and 136.1md, as well as breccia (fine- to very coarse-grained matrices) facies with a combined mean porosity and corresponding permeability of 30.1% and 64.6md. Baffle units within the deep-water plays are composed of foraminiferal-, volcaniclastic foraminiferal-, and skeletal foraminiferal wacke-packstone facies. Combined mean porosity and corresponding permeability for these fine-grained deposits is 35.9% and 12.3md.

Paleotopography, in conjunction with sea-level history, largely controls the geometry, lateral continuity and volume of a given reservoir body. The effect of paleotopography on the accumulation of volumetrically significant reservoir bodies is particularly relevant for the sediment gravity flow deposits within the deep-water plays. Modeled results suggest that focused-flow deposits have greater coarse- to fine-grained sediment ratios (0.70 compared to 0.09) and greater total reservoir bulk volumes (46.5 million m^3 compared to 18.6 million m^3) than dispersed-flow deposits. Ratio of reservoir bulk volume-to-linear dimension of shelf margin is similar for both focused-flow and dispersed-flow systems, suggesting that deep-water reservoir volume may be predictable on the basis of the linear dimension of shelf margin. Further, this study predicts that where funneling topographic features are located in close proximity and oriented approximately parallel to carbonate platform margins, high-volume focused-flow deep-water carbonate systems will occur.

INTRODUCTION

This paper documents a comprehensive outcrop-to-model study that includes collection of field and lab data, processing and interpretation of the data, and construction of a static 3-D reservoir-analog model from upper Miocene carbonate deposits within the Agua Amarga basin, southeast Spain. Reservoir-analog models are important tools that can better define the input parameters in dynamic subsurface reservoir simulations (Borgomano et al., 2002; Adams et al., 2005; Dutton et al., 2005; Enge et al., 2007; Pranter et al., 2007; Borgomano et al., 2008). The whole-field reservoir-analog model constructed for the carbonates in this study documents analogs for shallow-water and deep-water plays. The deep-water plays are particularly important because they challenge paradigms about deep-water carbonate deposition and document the effects of paleotopography on the architectures and lateral distributions of sediment gravity flow deposits. The majority of sediment gravity flow deposits within the Agua Amarga basin were focused into and along a large submarine and margin-parallel paleovalley, and ultimately point-sourced into the basin. These resedimented materials are referred to as focused-flow deposits and display geometries similar to point-sourced deep-water siliciclastic fan deposits. Sediment-gravity flows were also dispersed into the basin (dispersed-flow deposits) along a gently dipping ramp-like surface produced from deposition of older shallow-water carbonates.

Relatively little is known about the reservoir potential of focused-flow deep-water carbonate systems. Examples of producing deep-water carbonates in the subsurface are predominantly carbonate slope and slope-apron deposits such as the Cretaceous Poza Rica Field in Mexico (Enos, 1977) and the Carboniferous Tengiz and Korolev Fields in Kazakhstan (Harris et al., 2000; Weber et al., 2003; Francis et al., 2004), as well as the Wolfcampian slope and basinal carbonates within the Permian Basin of west Texas and New Mexico (Dutton et al., 2005). Focused-flow deep-water carbonate systems are mostly documented as outcrop analogs. Payros and Pujalte (2008) reviewed various examples of deep-water carbonate deposits that formed in response to a “funneling mechanism” on the shelf and were point-sourced into the basin. One system in particular, the Eocene Anotz Formation, western Pyrenees (Payros et al., 2007; Payros and Pujalte, 2008), has depositional geometries and potential reservoir bodies similar to those found in this study. Increasing recognition of focused-flow deep-water carbonate outcrops suggests that similar systems should be present in the subsurface where topographic controls are known and funneling mechanisms occur in close proximity to carbonate-producing margins.

This study also demonstrates that the volume and distribution of deep-water reservoir facies may be predictable given a record of the paleotopography that controlled dispersal of sediment-gravity flows. We hypothesize that dispersal patterns are important controls on reservoir heterogeneity, and the linear dimension of shelf margin sourcing the reservoir is a predictor of reservoir volume. Observations suggest that the largest deep-water carbonate reservoir systems with the highest ratio of reservoir to non-reservoir facies are those in which a long linear dimension of shelf margin debris is focused into a small area by substrate paleotopography. Deep-water systems that are sourced from a short linear dimension of shelf margin and contain deposits that are dispersed broadly across substrate paleotopography (due to the absence of a paleotopographic focus) would be expected to have more heterogeneous reservoir properties and lower volumes of reservoir facies.

Detailed characterization and mapping of the deep-water deposits in the Agua Amarga basin reveal that the focused-flow and dispersed-flow systems are laterally isolated from one another and display unique depositional geometries and distributions (Chapter 2, this thesis). As a result, the focused-flow and dispersed-flow systems represent two separate reservoir play-analogs and subsurface exploitation strategies for each play would be different. The goal of this study is to construct a 3-D model of reservoir analogs at the scale of the correlated deposits in the field (the major debrites and high-density turbidites), and populate each with measurements made on a smaller scale (core-plug porosity and permeability data). Initial whole-field characterization facilitates predictions about the potential volume of hydrocarbons within each play-analog and documents the controls on geometries and reservoir volumes within deep-water carbonate systems.

LOCATION AND GEOLOGIC BACKGROUND

The Agua Amarga basin is located in the northeastern portion of the Cabo de Gata volcanic province, roughly 35 km east of Almeria, SE Spain (Figure 1). Extrusion of volcanic rocks in the region was initiated in the early-middle Miocene from post Alpine-orogenic extension and strike-slip faulting (Sanz de Galdeano and Vera, 1992; Esteban, 1996; Esteban et al., 1996) and continued until the late Miocene, dominantly predating deposition of carbonate sediments (Franseen and Goldstein, 1996; Martin et al., 2003). Volcanic rocks were deposited as dome complexes and

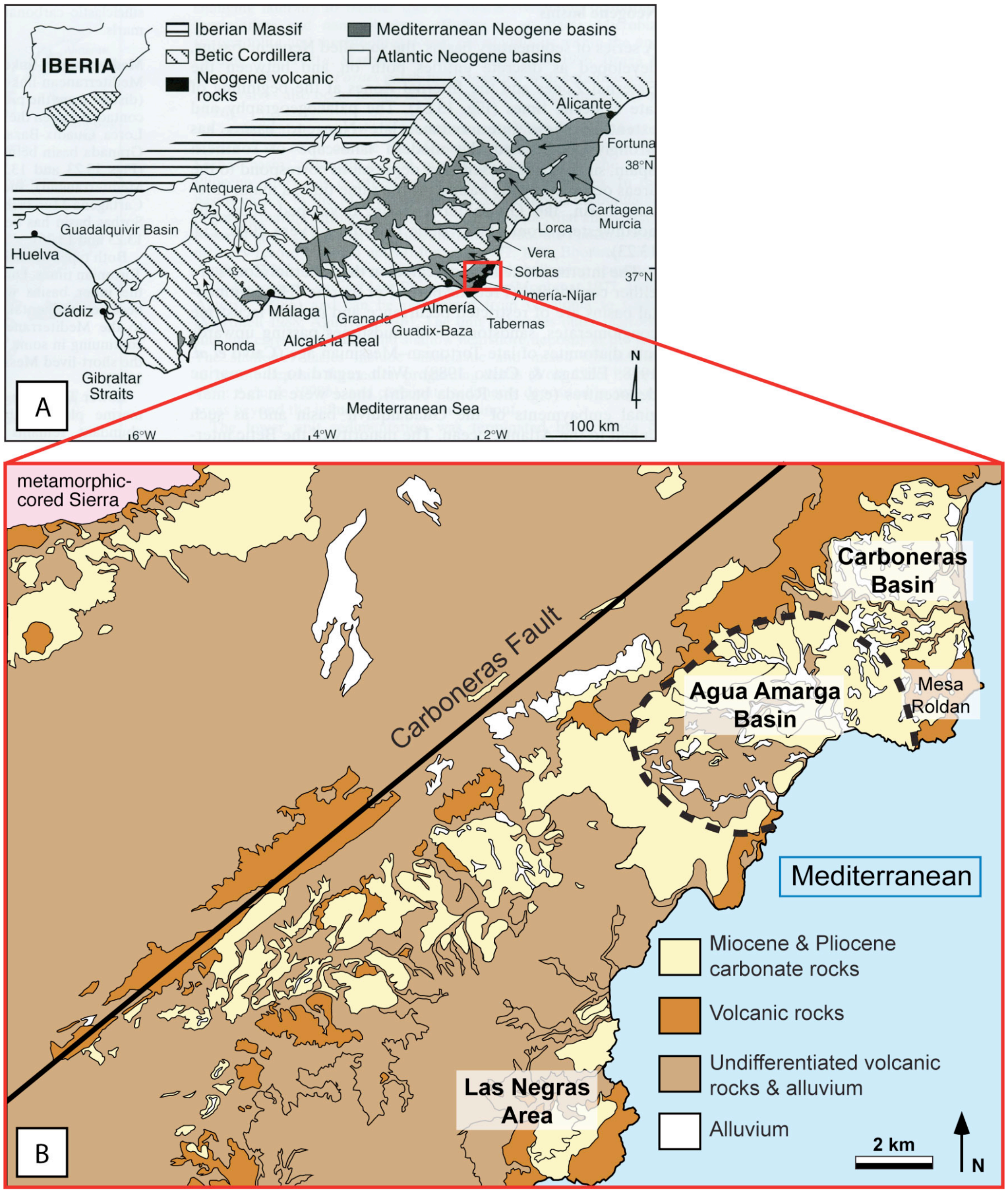

Figure 1. (A) Location map of Neogene basins within the Betic Cordillera of southeastern Spain. Red box outlines the Cabo de Gata volcanic province. *After: Gibbons and Moreno, 2003.* (B) Generalized geologic map of the Cabo de Gata region and location of the Agua Amarga basin (dashed black line), the Carboneras and Las Negras basins, and the Carboneras fault. *Modified from Mapa Geologico de Espana (1981)*

pyroclastic flow deposits (Martin et al., 2003), forming an archipelago of emergent highs and small submarine basins with interconnected straits and passageways onto which upper Miocene carbonate strata were deposited (Franseen and Goldstein, 1996; Franseen et al., 1998).

Tortonian and Messinian carbonate deposits within the Agua Amarga basin unconformably overlie volcanic basement and are the focus of this study. Present-day outcrop exposures in the basin occur as a result of regional uplift (Martin et al., 2003) and sea-level drop since the Pliocene (Franseen and Goldstein, 1996). Despite the presence of a major sinistral strike-slip fault located on the northwestern margin of the Cabo de Gata volcanic province (the Carboneras fault, Figure 1), basement topography in the Agua Amarga basin has been largely preserved since the late Miocene (Figure 2A). Studies within the Agua Amarga basin (Chapter 2, this thesis), the Las Negras area (Franseen and Goldstein, 1996; Franseen et al., 1997; Franseen et al., 1998), the Carboneras basin (Dillett, 2004), and the Nijar basin (Mankiewicz, 1996) all contain evidence for minimal deformation or tilting of upper Miocene-Pliocene carbonate strata. Some major faults, however, do cut through the lowermost stratigraphic unit and this may have had an effect on paleotopography and affected later deposition. Important paleotopographic features such as a large paleovalley and a broad submarine trough in the Agua Amarga basin resulted, at least in part, from subaerial exposure and erosion of volcanic basement prior to carbonate deposition (Franseen et al., 1993).

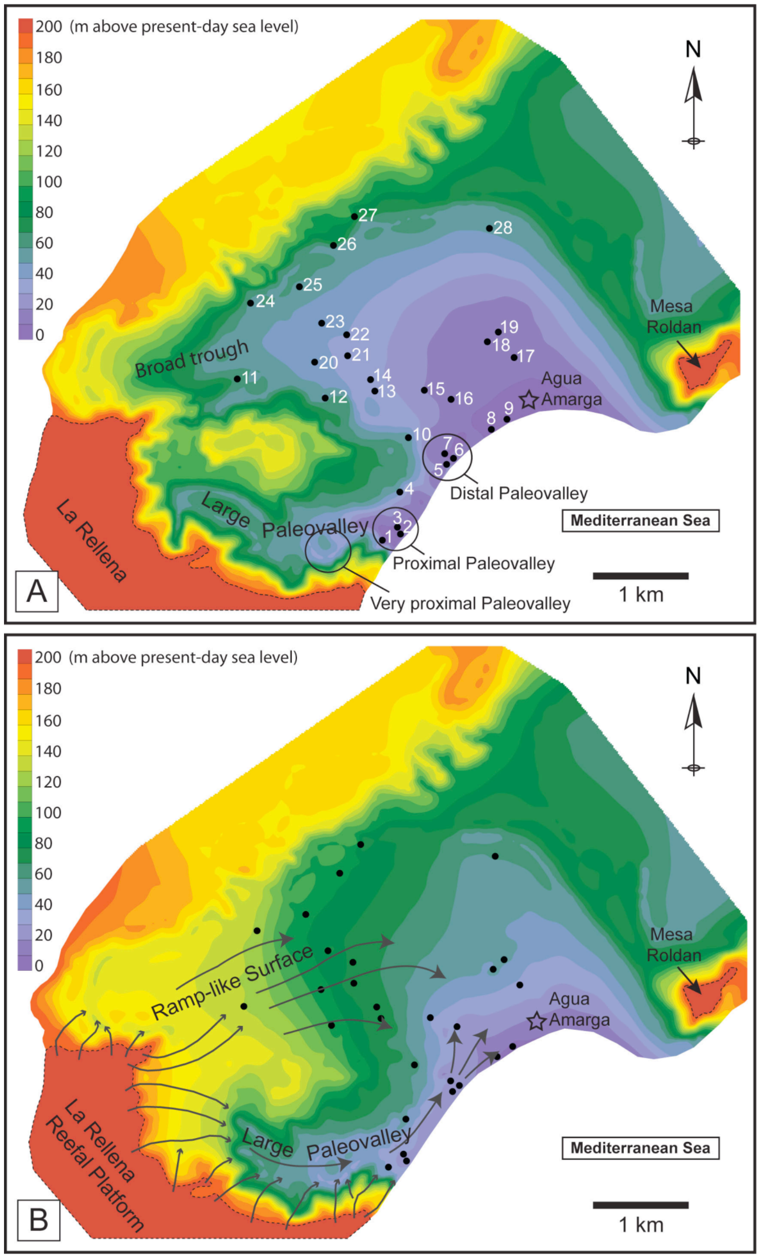

Figure 2. (A) Neogene volcanic basement paleotopography in the Agua Amarga basin. Topographic features have been largely preserved since the late Miocene and play an important role in the distribution of both the shallow-water and deep-water carbonate deposits. Numbered black dots represent locations of measured stratigraphic sections. (B) Modified paleotopography after deposition of Units 1 and 2 shallow-water packstone-grainstone deposits. Notice the broad trough has largely been filled, whereas the large paleovalley remained relatively unfilled. The La Rellena reefal platform served as the main source of resedimented material into the basin. The majority of sediment-gravity flows were focused into the paleovalley (focused-flow deposits), but some were dispersed across the ramp-like surface created by deposition of Units 1 and 2 (dispersed-flow deposits). Transport direction shown with grey arrows.

LITHOFACIES AND STRATIGRAPHIC UNITS

Lower Stratigraphic Succession

Upper Tortonian and lower Messinian carbonate deposits in the Agua Amarga basin are divided into a lower stratigraphic succession and an upper stratigraphic succession (Figure 3) on the basis of major changes in facies. Units 1 and 2 make up the lower succession and are composed of trough-cross bedded volcaniclastic skeletal packstone-grainstone and skeletal grainstone facies, respectively (Figure 4A). Unit 1 volcaniclastic skeletal packstone-grainstone deposits onlap against volcanic basement and are thickest in the northwest portion of the basin where they were deposited within a broad submarine trough (Figure 2A), and thin toward the modern Mediterranean. The top of Unit 1 is characterized by autoclastic breccia and fissure fill. Unit 2 skeletal grainstone deposits onlap against underlying Unit 1 substrate (or volcanic substrate in locations where Unit 1 was not deposited), are thinnest at their up-dip extent (between sections 23 and 24, Figure 2A), and thicken toward the modern Mediterranean. Unit 2 displays a gradational vertical transition into overlying Unit 3 deposits of the upper stratigraphic succession. Unit 2 deposits are absent along the northern margin of the basin and within proximal paleovalley locations; in these locations Unit 3 deposits abruptly overlie Unit 1 deposits. Combined deposition of Units 1 and 2 packstone-grainstones within the basin forms a ramp-like surface that dips gently to the east/southeast toward the modern Mediterranean (Figure 2B). With

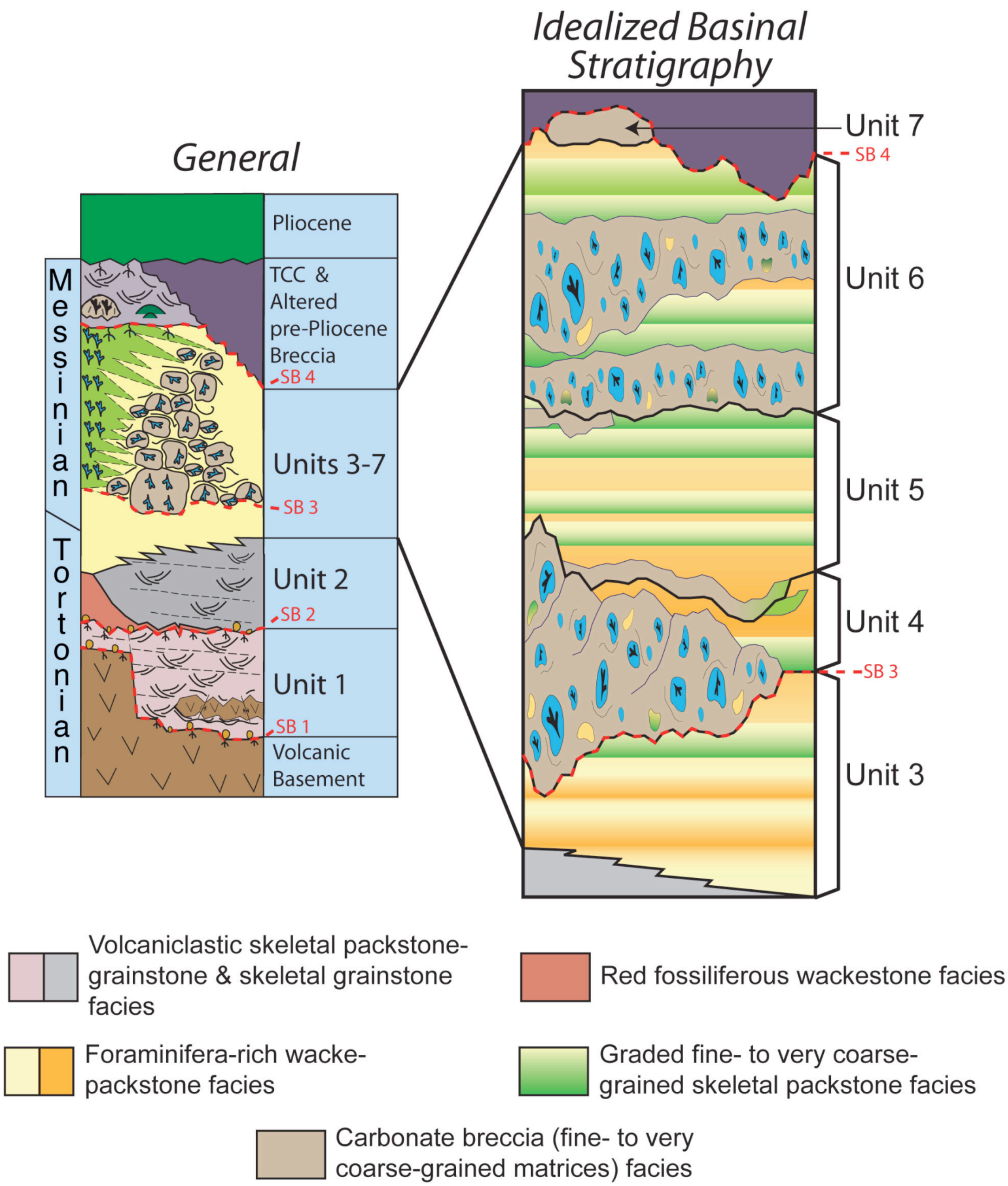

Figure 3. General and idealized stratigraphy in the Agua Amarga basin. The lower stratigraphic succession is composed of Units 1 and 2 volcaniclastic skeletal packstone-grainstones and skeletal grainstones. The upper stratigraphic succession is composed of Units 3 – 7 interstratified foraminifera-rich wacke-packstones, graded skeletal packstones and carbonate breccias. The red fossiliferous facies is volumetrically minor and is not included in this study. SB = sequence boundary. *Modified from Franseen et al. (1997).*

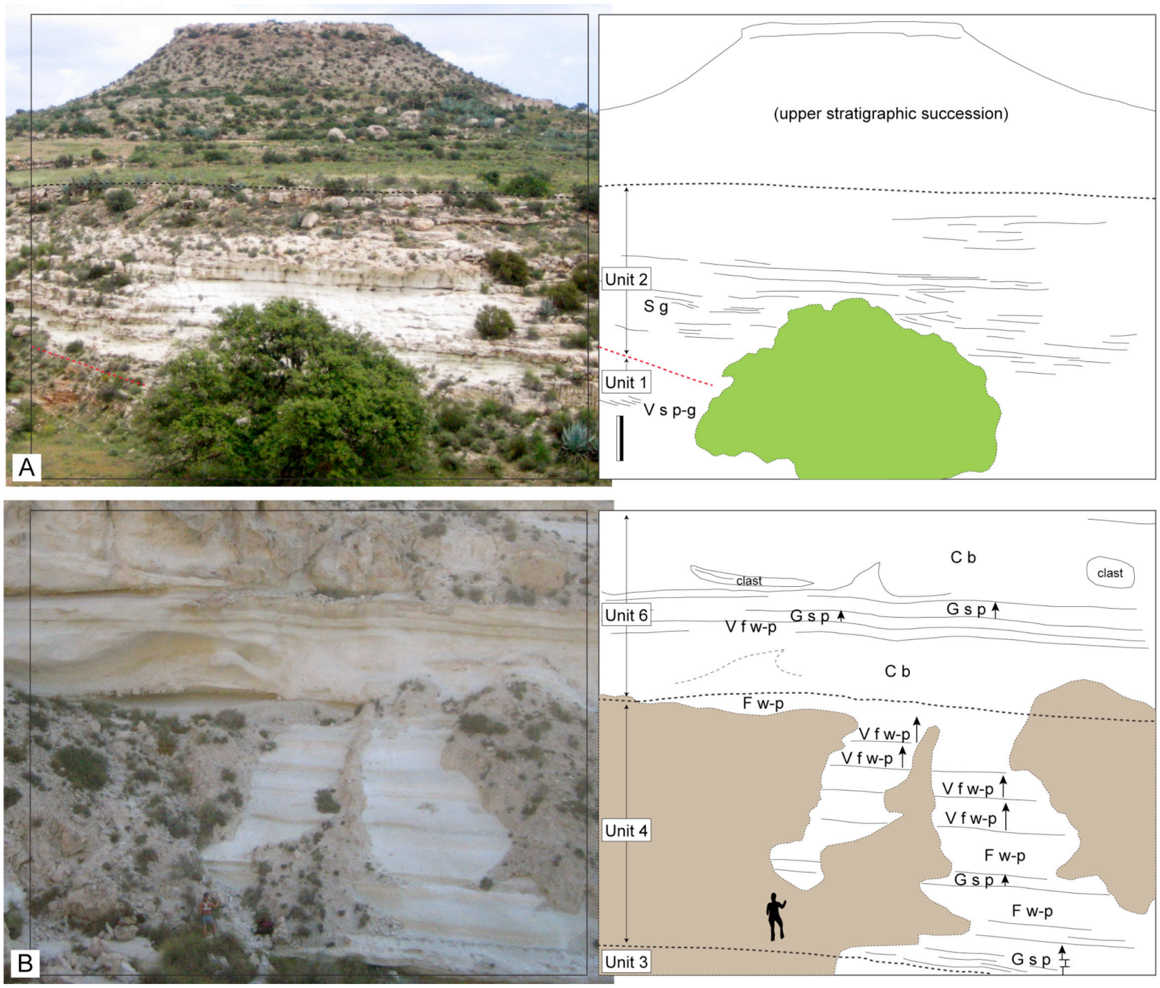

Figure 4. (A) Outcrop photograph and corresponding line drawing focusing on the lower stratigraphic succession at section 23. Unit 1 is composed of volcaniclastic skeletal packstone-grainstone (V s p-g) facies; Unit 2 is composed of skeletal grainstone (S g). The dashed red line represents the unconformity between these shallow-water units. The scale bar is 4 meters. Green area is the large tree in the foreground. (B) Outcrop photograph and corresponding line drawing of the upper stratigraphic succession at section 8. Units 3 through 7 (Units 5 and 7 not represented in this photograph) are composed of interstratified foraminiferal wacke-packstone (F w-p), volcaniclastic foraminiferal wacke-packstone (V f w-p), graded skeletal packstone (G s p), and carbonate breccia (C b) facies that are interpreted as hemipelagic-pelagic sediments, low-density turbidites, high-density turbidites, and debrites, respectively. The skeletal foraminiferal wacke-packstone facies interpreted as low-density turbidites (not shown here) is also present within the upper stratigraphic succession. Black arrows indicate normal gradation. Geologist is 1.7 meters tall. Brown area is covered outcrop.

the exception of minor changes in grain size, sorting and abrasion, overall vertical and lateral facies variability within these units is low.

Units 1 and 2 are interpreted as high-energy shallow-subtidal deposits. Unit 1 represents initial marine carbonate sedimentation in the basin after subaerial exposure of the underlying Neogene volcanic basement. Unit 2 was deposited during transgression after a period of subaerial exposure and erosion following deposition of Unit 1. Deposition of Units 1 and 2 in the basin significantly modified the volcanic basement paleotopography by forming thick accumulations of sediment, particularly within the broad trough (Figure 2). The resulting ramp-like substrate topography, gently sloping to the east/southeast at 2 to 3 degrees, influenced distribution of subsequent deposits within the upper stratigraphic succession (Units 3-7) (Figure 2B; Chapter 2, this thesis).

Upper Stratigraphic Succession

Units 3 – 7 make up the upper succession and are composed of a fine-grained foraminifera-rich facies assemblage consisting of foraminiferal-, volcanic foraminiferal-, and skeletal foraminiferal wacke-packstone facies, and a coarse-grained facies assemblage consisting of graded skeletal packstone and carbonate breccia facies (Figure 4B). The fine-grained facies assemblage contains abundant carbonate mudstone, planktonic foraminifera and diatoms. Other constituents such as volcanic grains or skeletal fragments are typically less than 2 mm. Foraminiferal wacke-packstone deposits form dm-thick beds that are commonly heavily burrowed or finely laminated. Volcanic foraminiferal- and skeletal foraminiferal wacke-packstone deposits typically form cm- to dm-thick beds that display subtle normal gradation and scoured bases, however, massive bedding is also common within volcaniclastic foraminiferal wacke-packstone deposits.

The coarse-grained facies assemblage contains abundant skeletal grains (ranging from 2 to 6 mm) and typically displays less mud than the fine-grained facies assemblage. Graded skeletal packstone deposits form dm-thick beds that are normally graded and have distinct scoured bases. Underlying material is commonly incorporated into the basal portions of the coarser-grained deposits as mm- to cm-scale clasts. Carbonate breccia deposits form thick (meters to tens of meters) massive and chaotic beds with cm- to m-scale clasts of various foraminifera-rich wacke-packstones, graded skeletal packstones, and reefal boundstones (*Porites* and *Tarbellastreae*). Distinct scoured bases and basal and internal deformation structures are also characteristic of breccia deposits. Sediments underlying carbonate breccia deposits are commonly deformed and incorporated into the overlying bed as clasts or injection features. *Porites* and *Tarbellastreae* clasts within breccia matrices indicate that coral reefs had developed in upslope shallow-water locations.

Interstratified fine- and coarse-grained facies within Units 3 through 7 are interpreted as hemipelagic-pelagic sediments, low- and high-density turbidites, and debrites. These deep-water deposits overlie the shallow-water deposits of Units 1 and 2, and record inundation of the basin and development of reefs and associated platform sediments on surrounding paleohighs, particularly the extensive La Rellena platform bordering the western margin of the basin (Toomey, 1997). Sediment-gravity flows sourced from the platform followed two pathways into the basin: (1) they were focused into and along the large margin-parallel paleovalley and ultimately point-sourced into the basin, and (2) they were dispersed along a packstone-grainstone ramp-like surface north of the paleovalley (Figure 2B). The large paleovalley, which was not fully filled by Units 1 and 2 packstone-grainstone deposits, served as the dominant pathway for sediment-gravity flows into the basin. Mapping of stratigraphic units in the basin reveal that the focused-flow deposits within the paleovalley are time-equivalent with, but laterally isolated from the dispersed-flow deposits.

Focused-flow Versus Dispersed-flow Systems

Important differences in depositional geometries, distributions, thickness, and ratios of coarse- to fine-grained sediments exist between the focused-flow deposits and the dispersed-flow deposits. Focused-flow sediment gravity flow deposits within the large paleovalley display more complex geometries and greater ratios of coarse- to fine-grained sediment than dispersed-flow deposits. Coarse-grained sediment gravity flows within proximal paleovalley locations are influenced by local substrate topography from previous deposits and lateral confinement within paleovalley walls, and as a result, form irregularly shaped deposits with a high degree of internal erosion (Chapter 2, this thesis). Depositional geometries along the axis of the paleovalley reveal multiple backstepping debrites within Unit 4 that scour down into shallow-water packstone-grainstones. As distance from the platform increases and lateral confinement decreases within the focused-flow system, high-density turbidites and debrites form more tabular and laterally continuous deposits that display less erosion and lower ratios of coarse- to fine-grained sediment.

Dispersed flow deposits sourced along the ramp-like surface have sheet-like geometries that are more laterally continuous and display less internal erosion than deposits in the focused-flow system. Sediment gravity flow deposits along the ramp-like surface have a significantly lower ratio of coarse- to fine-grained sediment and are thinner than sediment gravity flow deposits within the paleovalley. In general, dispersed-flow deposits accumulate farther away from the platform margin than focused-flow deposits (or typical carbonate slope-apron deposits) due to the persistent and gentle slope along the packstone-grainstone ramp-like surface that connects the platform margin to the basin.

METHODOLOGY

Collection of Field and Lab Data

3-D outcrop exposures within the Agua Amarga basin allow for detailed correlation of stratigraphic architecture using measured stratigraphic sections and photomosaics. Hand samples for core plug petrophysical analysis (Appendix IV) and petrography (Appendix III) in the lab, as well as spectral gamma ray data (Appendix V), were collected in conjunction with measured sections. Field and lab data were integrated into Petra^{TM} in order to construct wells, well logs (synthetic lithofacies and porosity), and surface grids needed to populate a 3-D model.

Measured Sections and Photomosaics

Twenty-eight stratigraphic sections were measured with a jacob staff and brunton compass and recorded at a vertical scale of 1 cm = 1 m (Appendix I). Locations and elevations with respect to present-day sea level were noted using a hand-held GPS (Global Positioning System). The number and location of measured sections (Figure 2A) was based on outcrop accessibility, quality, and relative spatial distribution to other sections. Stratigraphic units were traced by walking out major contacts in the field, or correlated using photomosaics. The quality and coverage of photomosaics were important in documenting the complex geometries and lateral variability of sediment gravity flow deposits, particularly those located within the large paleovalley. Further, photomosaics were used to distribute pseudo wells spatially in Petra^{TM} in order to represent stratal and facies architecture accurately.

Petrophysical Data

Porosity and permeability data were compiled from core plugs taken from 421 hand samples of representative lithofacies. Hand samples were plugged at the Kansas Geological Survey in Lawrence, KS using an industrial drill press with a one-inch drill bit. The plugs were trimmed to quarter-inch increments between .5 and 2 inches in length. Some of the trimmed plug ends were later used to make petrographic thin sections. The majority of hand samples were plugged parallel to bedding; 13 of the 421 hand samples were plugged twice, resulting in a total of 434, 1-inch diameter core plugs.

The 434 plugs were weighed on an electronic balance after drying in an oven at ~ 90 degrees Celsius for approximately 24 hours. The average diameter (in) and length (in) of each plug was measured using a digital caliper to record plug dimensions and determine bulk volume. Bulk volumes were then calculated using the equation for the volume of a cylinder.

In addition to digital caliper measurements, the majority of the plugs were immersed in mercury to determine a more precise bulk volume (cc). The mercury immersion technique uses Archimedes Principal to calculate bulk volume of a plug. Mercury is an ideal liquid for this technique because its high surface tension generally inhibits contamination of the plug during immersion. Any plugs with deeply penetrating pore spaces, however, were excluded from mercury immersion measurements to avoid trapping mercury beads in visually concealed pore spaces. Bulk volumes calculated from mercury immersion measurements were used preferentially over the bulk volumes calculated from caliper measurements when determining porosity.

Helium porosity was measured in a Helium Porosimeter using a Boyle's Law technique ($P_1V_1 = P_2V_2$) on dry core plugs. Boyle's law uses the relationships between bulk volume, grain volume and pore volume to determine porosity (BV = GV+PV, ϕ = PV/BV). Porosity was measured to an accuracy of $\pm$ 0.1 porosity percent (Appendix IV). Given the uncertainty of exterior pores, the error range of these measurements is likely $\pm$ 0.5 porosity percent. The Helium Porosimeter was calibrated every 30 plugs, noting any changes in atmospheric pressure. Grain density was calculated by dividing the known dry weight into the grain volume of each plug (Appendix IV).

Routine air permeability measurements of core plugs were completed using an Air Permeameter with a Hassler-type confining pressure cell. Core plugs were subjected to a hydrostatic-confining stress of 500 psi, and permeability was calculated from the difference in upstream and downstream pressure, flow rate, and known diameter and length of each plug (Appendix IV).

DATA

Lithofacies

Synthetic lithofacies logs were constructed from measured sections by assigning major lithofacies a discrete integer value (Appendix VI). These facies include volcaniclastic skeletal packstone-grainstones and skeletal grainstones of the shallow-water Units 1 and 2, and foraminiferal-, volcanic foraminiferal- and skeletal foraminiferal wacke-packstones, graded (fine- to very coarse-grained) skeletal packstones, and carbonate breccias (fine- to very coarse-grained matrices) of the deep-water Units 3 though 7 (Table 1). Integer values represent the major lithofacies characterized in the field, including fine- to very coarse-grained lithologies within the graded skeletal packstone facies and carbonate breccia facies. Numerical facies logs do not, however, represent prominent sedimentary structures, tightly cemented horizons, and other features such as dominant pore types noted in petrographic analysis. A more detailed classification of facies, particularly one including porosity classification, would significantly increase the degree of heterogeneity within the model. Exclusion of these features simplifies the facies modeling process and increases the uncertainty associated with potential hydrocarbon volume (Russell et al., 2002; Borgomano et al., 2008).

Petrography

Petrographic analysis of the major lithofacies provided a more detailed understanding of porosity classification and pore-occlusion processes related to diagenesis and early compaction. Petrographic classification of porosity in this study is based on Choquette and Pray (1970). Interparticle and intraparticle porosity are the dominant pore types within the volcaniclastic skeletal packstone-grainstone, skeletal grainstone, graded skeletal packstone, and carbonate breccia facies (Figure 5A). Moldic porosity is present within the matrices of some carbonate breccias (Figure 5B). Intraparticle micro-porosity is the dominant pore type within the foraminiferal wacke-packstone facies (Figure 5C); interparticle, intraparticle and moldic porosity

Lithofacies	Lithofacies Integer	Depositional Mechanism	3-D Petrel Model
Foraminiferal ws/ps	2	Hemipelagic-pelagic sedimentation	Baffle Facies / Units
Volcaniclastic foraminiferal ws/ps	3	Hemipelagic-pelagic sedimentation or low-density turbidity currents	
Skeletal foraminiferal ws/ps	4	Low-density turbidity currents	
Graded fn-med skeletal ps	5	High-density turbidity currents	Reservoir Facies / Units
Graded crs skeletal ps	6		
Graded v.crs skeletal ps	7		
Breccia: fn matrix	8	Debris flows	
Breccia: med matrix	9		
Breccia: crs-v.crs matrix	10		
Volcaniclastic skeletal ps/gs	11	*In situ* shallow-water sedimentation	
Skeletal gs	11		

Table 1. The eleven major lithofacies characterized in the field (after Dunham, 1962) and their interpreted depositional mechanism. Each lithofacies was assigned an integer (2 – 11) in order to populate wells with synthetic lithofacies logs and stochastically distribute lithofacies within the model.

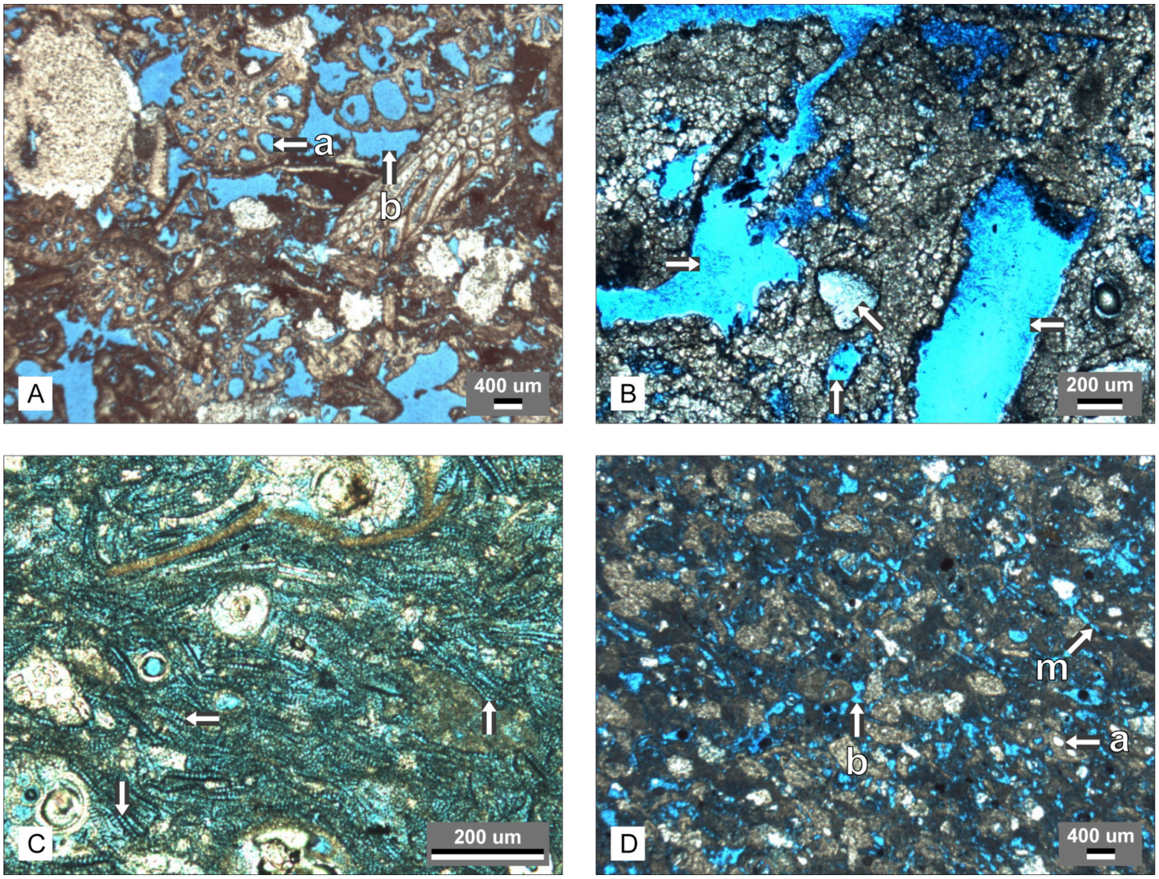

Figure 5. Examples of dominant pore types (white arrows) within modeled lithofacies. (A) Photomicrograph of volcaniclastic skeletal packstone-grainstone facies displaying intraparticle (a) and interparticle (b) porosity. Phi: 36.4%; k: 1438.7md. (B) Photomicrograph of carbonate breccia (coarse- to very coarse-grained matrix) facies displaying moldic porosity. Phi: 41.9%; 1785.9md. (C) Photomicrograph of foraminiferal wacke-packstone facies displaying intraparticle micro-porosity within diatom tests. Phi: 55.0%; k: 9.9md. (D) Photomicrograph of volcaniclastic foraminiferal wacke-packstone facies displaying intraparticle (a), interparticle (b), and moldic (m) porosity. Phi: 38.6%; k: 221.2md.

are present within the volcaniclastic foraminiferal and skeletal foraminiferal wacke-packstone facies (Figure 5D). Precipitation of syntaxial overgrowth and rim cements within intraparticle and interparticle pore spaces (Figure 6A) are the dominant pore-reducing processes within the volcaniclastic skeletal packstone-grainstone, skeletal grainstone, graded skeletal packstone, and to a lesser extent, carbonate breccia facies. Precipitation of dolomite (Figure 6B) variably reduces matrix porosity in all facies, but is especially abundant within the fine-grained foraminifera-rich facies and matrices of carbonate breccias. Dissolution of some skeletal grains and subsequent preservation of moldic porosity (Figure 6C) is most common within the breccia facies, however, molds of planktonic foraminifera tests (Figure 6D) are also common within the skeletal foraminiferal wacke-packstone and graded skeletal packstone facies. The degree of porosity occlusion by calcite or dolomite cement within a given lithofacies is variable but overall fairly minor. Additionally, fractured skeletal grains (Figure 6E) and over-packed grain fabrics (Figure 6E) occur to some extent within all facies but are particularly significant within volcaniclastic skeletal packstone-grainstone, skeletal grainstone, and graded skeletal packstone facies.

Core-plug Petrophysics

Petrophysical Results

Core plug petrophysical results indicate distinct porosity and permeability trends. High-permeability facies include volcaniclastic skeletal packstone-grainstones

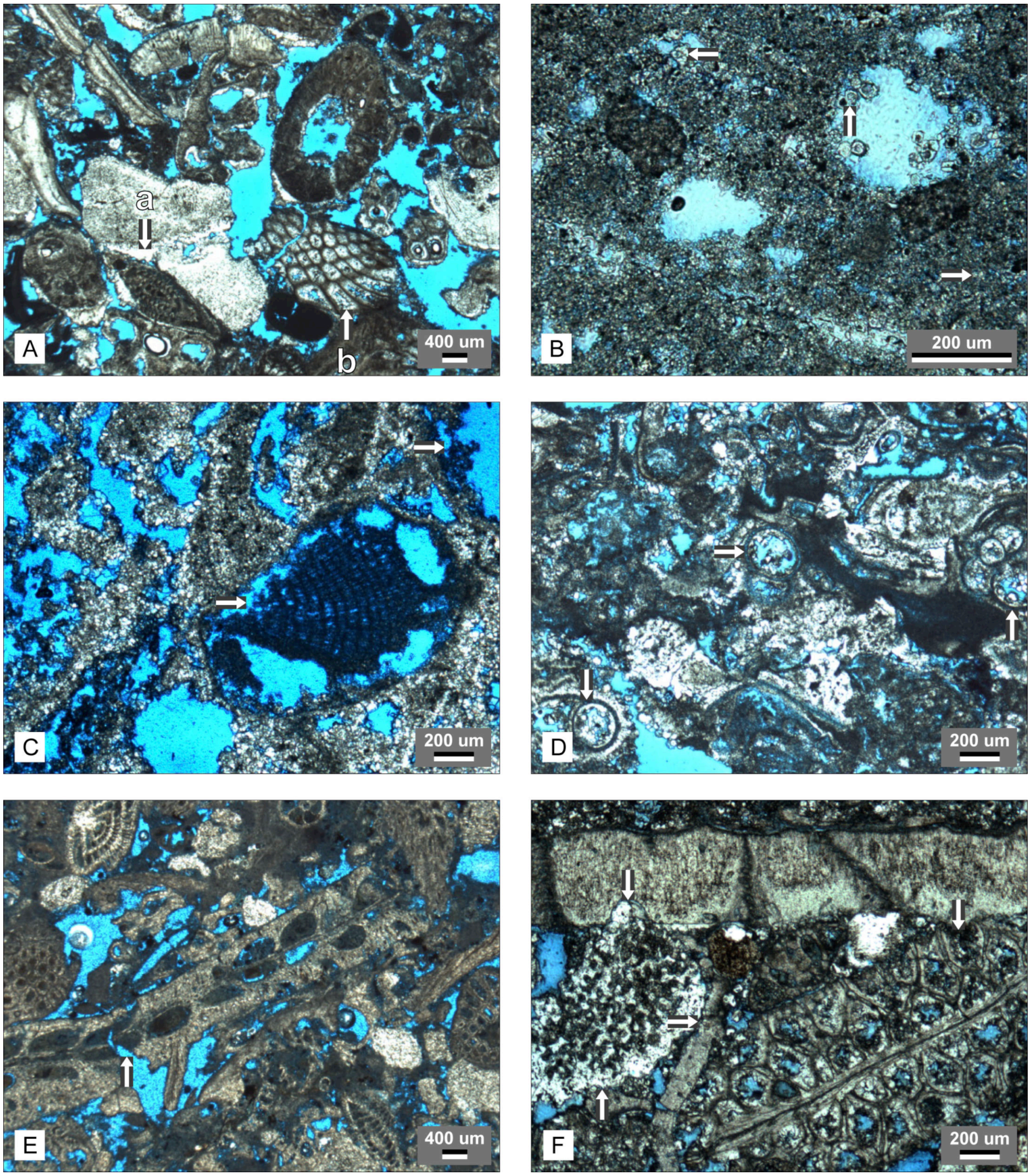

Figure 6. Photomicrographs demonstrating the effects of porosity-altering processes within modeled lithofacies. (A) Skeletal grainstone facies displaying syntaxial overgrowth (a) and rim (b) cement reducing interparticle and intraparticle porosity. Phi: 26.6%; k: 1613.9md. (B) Volcaniclastic foraminiferal wacke-packstone facies displaying dolomite cements reducing matrix porosity (arrows). Phi: 30.6%; k: 4.7md. (C) Carbonate breccia (medium-grained matrix) facies displaying dissolution of red algal grains and preservation of moldic porosity (arrows). Preserved matrix in this sample is predominantly dolomitized. Phi: 32.7%; k: 139.8md. (D) Skeletal foraminiferal wacke-packstone facies displaying molds of dissolved planktonic foraminifera (arrows). Phi: 32.8%; k: 254.6md. (E) Skeletal grainstone facies displaying fractured grain fabric (arrow). Phi: 27.7%; k: 870.7md. (F) Volcaniclastic skeletal packstone-grainstone facies displaying over-packed grain fabric and sutured grain contacts (arrows). Phi: 25.7%; k: 38.8md.

and skeletal grainstones (Units 1 and 2 shallow-water deposits), as well as graded fine- to very coarse-grained skeletal packstones and fine- to very coarse-grained breccia matrices (Units 3 through 7 deep-water high-density turbidites and debrites, respectively) (Figure 7A, 7C and 7D). Combined mean porosity and corresponding permeability is 26.3% and 81.1md for the shallow-water deposits, 30.5% and 136.1md for the high-density turbidites, and 30.1% and 64.6md for the debrites. High-permeability facies are termed reservoir facies in this study. Low-permeability facies include foraminiferal-, volcaniclastic foraminiferal-, and skeletal foraminiferal wacke-packstones (Units 3 through 7 deep-water hemipelagic-pelagic sediments and low-density turbidites) (Figure 7B). Combined mean porosity and corresponding permeability for these fine-grained deposits is 35.9% and 12.3md. Low-permeability facies are termed baffle facies in this study. Table 2 quantitatively summarizes the core plug porosity and permeability data by lithofacies as they were grouped in the model. Sampled reef and fine-grained foraminiferal clasts within breccia matrices dominantly have low permeability values, whereas clasts consisting of coarse skeletal fragments (likely from high-density turbidites) have significantly higher permeability values (Figure 8). Petrophysical results from reef clasts, however, are significantly biased due to the inability of the 1-inch diameter core plugs to reflect the ample storage potential and high permeabilities associated with the cm-scale moldic porosity within reef clasts.

Petrophysical data from reef and other clasts within breccia matrices were not incorporated into the breccia facies in the model due to the sampling size bias for the

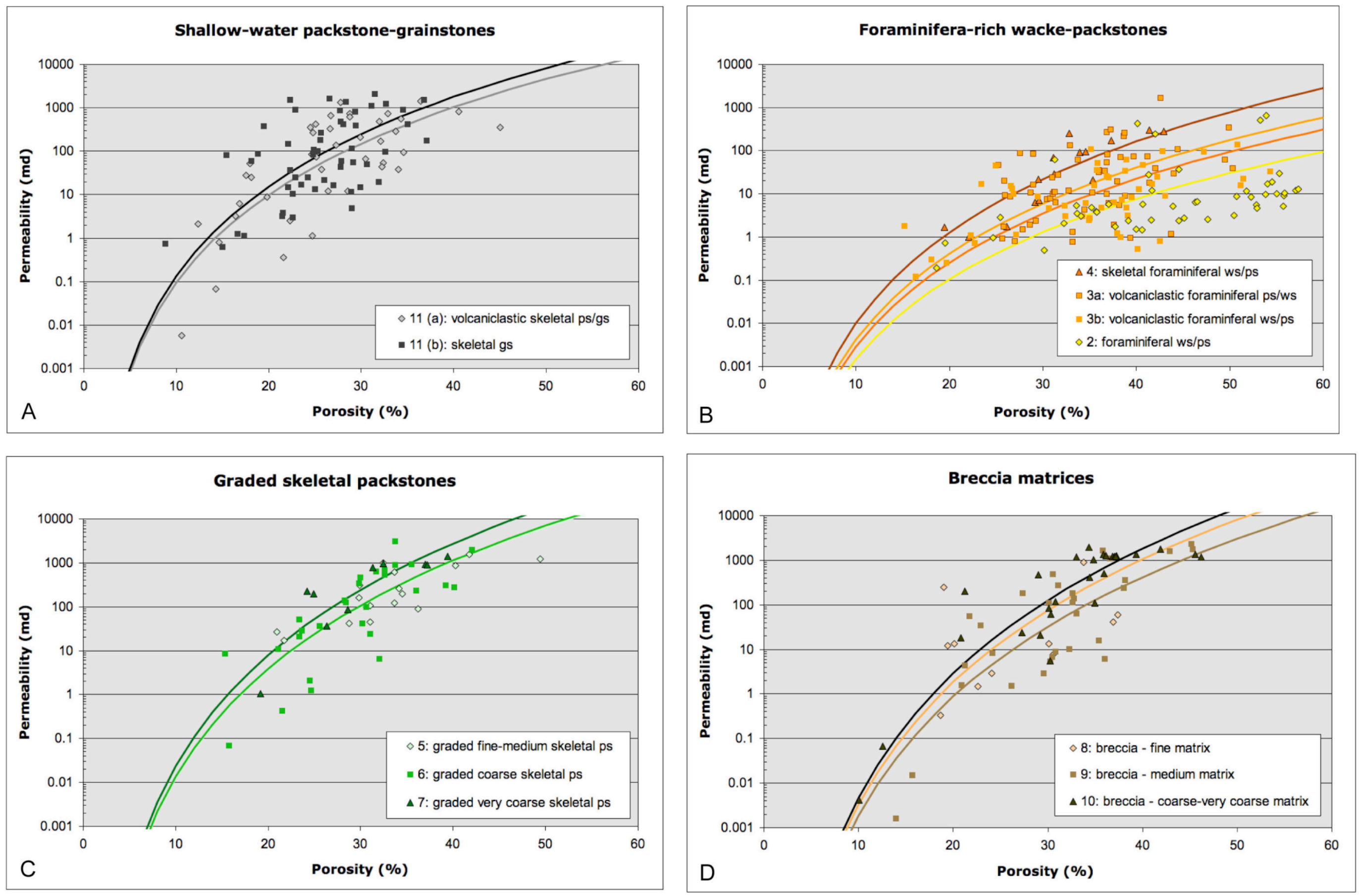

Figure 7. Porosity and permeability core plug data by lithofacies. (A) K-phi cross-plot of the volcaniclastic skeletal packstone-grainstone and skeletal grainstone facies of Units 1 and 2 shallow-water deposits. (B) K-phi cross-plot of the foraminifera-rich (foraminiferal-, volcaniclastic-, and skeletal-) wacke-packstone facies of Units 3 – 7 deep-water deposits. (C) K-phi cross-plot of the graded (fine- to very coarse-grained) skeletal packstone facies of Units 3 – 7 deep-water deposits. (D) K-phi cross-plot of the carbonate breccia (fine- to very coarse-grained matrices) facies of Units 3 – 7. The foraminifera-rich wacke-packstone facies display significantly lower permeability values than the other facies and are designated as baffle facies within the model. The remaining high-permeability facies are designated as reservoir facies in the model.

Facies Integer	Lithofacies	Median Porosity (%)	Mean Porosity (%)	Porosity Standard Deviation	Porosity at +2 Std Deviations (%)	Porosity at -2 Std Deviations (%)	Predicted Permeability at Mean Porosity (md)	Predicted Permeability at +2 Std Porosity (md)	Predicted Permeability at -2 Std Porosity (md)
	Foraminifera-rich Facies	**35.9**	**35.9**	**10.1**	**56.0**	**15.8**	**12.3**	**221**	**0.059**
2	Foraminiferal WS/PS	43.9	43.3	10.3	63.8	22.8	12.5	137	0.240
3a	Volcanic foraminiferal WS/PS	36.2	35.1	9.1	53.2	17.0	9.7	142	0.089
3b	Volcanic foraminiferal PS/WS	32.2	32.1	8.4	49.0	15.2	9.4	154	0.068
4	Skeletal foraminiferal WS/PS	31.2	31.8	6.4	44.5	19.0	32.6	347	0.896
	Graded fn-v.crs Skeletal PS Facies	**31.0**	**30.5**	**6.8**	**44.1**	**16.9**	**136.1**	**2797**	**1.081**
5	Graded fn-med skeletal PS	33.0	33.1	7.0	47.0	19.1	223.4	3953	2.545
6	Graded crs skeletal PS	30.2	29.3	6.6	42.5	16.1	82.3	1718	0.615
7	Graded v.crs skeletal PS	30.0	30.1	6.6	43.2	16.9	247.7	5253	1.955
	Breccia (fn-v.crs matrices) Facies	**30.8**	**30.1**	**8.7**	**47.5**	**12.8**	**64.6**	**4043**	**0.026**
8	Breccia – fn matrix	24.0	27.4	7.6	42.6	12.3	33.2	1852	0.021
9	Breccia – med matrix	30.7	29.5	9.0	47.5	11.5	27.6	1923	0.006
10	Breccia – crs-v.crs matrix	34.4	32.3	8.5	49.2	15.4	250.5	12600	0.252
	Shallow-water PS/GS Facies	**26.6**	**26.3**	**7.0**	**40.2**	**12.3**	**81.1**	**1460**	**0.475**
11a	volcaniclastic skeletal PS/GS	26.7	26.8	8.2	43.3	10.3	70.3	1745	0.117
11b	skeletal GS	26.0	25.9	5.8	37.6	14.2	90.5	1163	1.472

Table 2. Porosity and permeability statistics for each of the lithofacies modeled in this study. Implicit to these statistics is that data for each lithofacies is normally distributed. The foraminifera-rich (baffle) facies (2 – 4) display distinctly lower permeabilities than the reservoir facies (5 – 11).

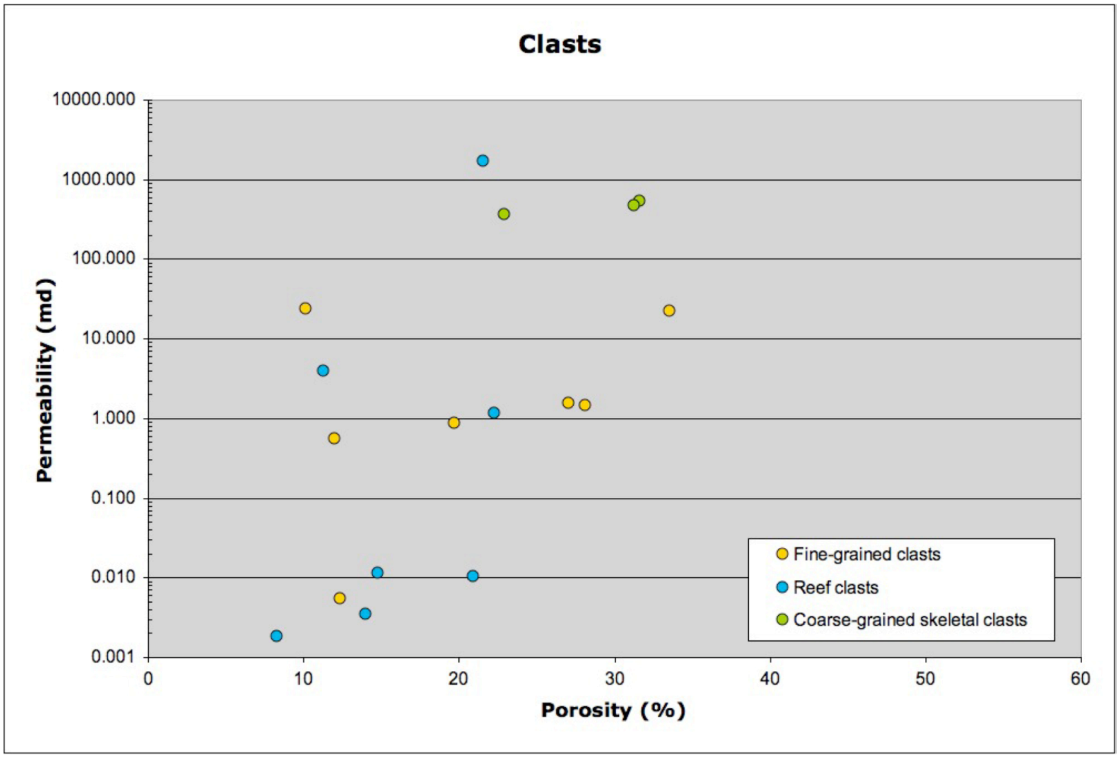

Figure 8. Porosity and permeability core plug data of clasts within breccia matrices. Reef and fine-grained foraminiferal clasts are tightly cemented and display significantly lower porosity and permeability values than coarse-grained skeletal clasts. Low porosity and permeability within reef clasts, however, is an artifact of sampling. Many reef clasts contained cm-to-dm-scale moldic porosity after reef framework, and such moldic porosity was impossible to sample at the scale of a one-inch core plug. Clasts were not modeled in this study, although they would likely play a significant role in predicting hydrocarbon storage potential and flow dynamics within breccia reservoir units.

reef clasts, as well as the uncertainty associated with representing the relative sizes, types, and abundance of clasts within a breccia deposit. Thus, porosities and permeabilities of the breccia deposits modeled in this study represent breccia matrix values only, which have to be considered as minimal values. Because of the exclusion of reef clasts, the modeling of porosity and permeability in the breccia facies is not as accurate as it is for the other reservoir facies.

Petrophysical Interpretations

Depositional environment and mechanisms of deposition are major controls on permeability and porosity. In general, permeability at any given porosity decreases with an increase in matrix mud, as reflected by Dunham's classification (e.g. grainstones display higher permeability than wacke-packstone) (Dunham, 1962). These predictable petrophysical characteristics are displayed within the resulting porosity-permeability trend lines (Figure 7A-D). Data outliers strongly influence lithofacies trends and help explain the following observations: (1) the foraminiferal wacke-packstone population trend is strongly influenced by several high-permeability samples (Figure 7B) and would likely exhibit a lower exponent value (Table 3) if the high-permeability values were eliminated; (2) The graded fine-to-medium-grained and coarse-grained skeletal packstone population trends are indistinguishable as a result of a few high-permeability samples within the graded fine-to-medium-grained skeletal packstone population (Figure 7C); (3) A few high-permeability samples within the fine-grained breccia matrix population (Figure 7D) resulted in a higher

Lithofacies Code #	Lithofacies	A	b	Standard Error Factor (x)
	Facies Group 1: shallow-water packstone-grainstones			95% SE=5.2x
11a	Volcaniclastic skeletal GS	1.9E-08	6.70	6.0
11b	Skeletal GS	1.9E-08	6.85	6.5
	Facies Group 2: foraminiferal-rich wacke-packstones			95% SE=4.1x
2	Foraminiferal WS/PS	1.0E-09	6.17	5.1
3a	Volcaniclastic foraminiferal WS/PS	1.0E-09	6.46	5.1
3b	Volcaniclastic foraminiferal PS/WS	1.0E-09	6.62	5.4
4	Skeletal foraminiferal WS/PS	1.0E-09	7.00	2.6
	Facies Group 3: graded fn - v crs skeletal packstones			95% SE=3.2x
5	Graded fn-med skeletal PS	8.9E-11	8.16	2.8
6	Graded crs skeletal PS	8.9E-11	8.18	4.7
7	Graded v.crs skeletal PS	8.9E-11	8.42	3.0
	Facies Group 4: fn - v crs breccias			95% SE=4.6x
8	Breccia – fn matrix	2.3E-12	9.15	6.6
9	Breccia – med matrix	2.3E-12	8.90	6.6
10	Breccia – crs-v.crs matrix	2.3E-12	9.30	3.8

Table 3. Power law porosity-permeability relationships from core plug data.

exponent value than the medium-grained breccia matrix population (Table 3); and (4) Within all facies, variable amounts of pore-filling calcite and dolomite cement and over-packed fabrics from mechanical compaction, resulted in some low-permeability samples that lower individual porosity-permeability trends.

The lower permeability trends of the carbonate breccia matrix facies compared to those of the other reservoir facies are likely due to the occlusion of matrix porosity by precipitation of dolomite. Destruction of interparticle pore networks from dolomitization in a given sample would dramatically reduce total permeability by reducing pore connectivity (Lucia, 1995), despite the persistence of other pore types such as intraparticle, moldic, and/or separate vugs. The higher permeability trends of the skeletal foraminiferal wacke-packstone facies compared to other baffle facies are likely due to an increase in the abundance of fine skeletal fragments, and thus interparticle, intraparticle, and moldic pore space (Lucia, 1995).

Petrophysical Data Limitations

Collection of petrophysical data from 1-inch diameter core plugs presents limitations on data accuracy from lithofacies containing heterogeneous fabrics. The most significantly effected lithofacies are those that contain skeletal grains in excess of 2 cm (very coarse-grained, high-density turbidites and breccia matrices), as well as lithofacies containing large moldic and/or vuggy pore space (commonly within breccia matrices and reef clasts; less commonly within high-density turbidites and shallow-water packstone-grainstone deposits). Large cm-scale skeletal grains (such as mollusk shells) within core plugs have the tendency to bias porosity/permeability measurements toward lower values than are representative of the lithofacies as a whole, particularly if the grain is oriented perpendicular to measured flow. Large moldic and vuggy pores within core plugs have the tendency to bias porosity/permeability measurements toward higher-than-average values. Large molds and vugs within a 1-inch diameter cylinder are commonly interconnected and dramatically increase measured petrophysical values. Within the context of the reservoir unit, however, molds and vugs may constitute a network of mostly separate pores, causing actual petrophysical values to be significantly lower (Lucia, 1995). Samples of *Porites* reef clasts within breccia matrices were the most significantly biased population: samples displayed very low-permeability values, with the exception of one sample containing touching vugs. Core plug samples of reef clasts were almost entirely composed of tightly cemented inter-coral matrix because the drill bit dimensions were too small to capture the large 2-6 cm *Porites* molds. Reef clasts have ample storage potential within a reservoir body, however, depending on their internal pore-network connectivity and overall size and abundance within a debrite, may accelerate or decelerate flow. Observations in the field suggest that the characteristically large pore networks within reef clasts would accelerate flow within modeled debrites.

Outlying porosity and permeability data points in this study are primarily the result of sampling-size biases discussed above. Rarely, however, outliers may be the result of intrinsic errors during the measurement process, or misclassification of lithofacies. Samples with anomalously low grain densities (primarily of the foraminiferal wacke-packstone facies) were not excluded from the data set as these samples are speculated to contain significant amounts of organic matter and opaline silica. Further, porosity and permeability results from these low-density samples do not indicate any significant problems with the measurement process.

RESERVOIR MODELING

2-D Framework in Petra^{TM}

Petra^{TM} was used in this study to manage field data and build the 2-D framework needed for 3-D modeling. Measured sections were imported as Raster images from Tiff files and positioned in X-Y space using the GPS coordinates (Global Positioning System) obtained at each section. Vertically, measured sections were tied to an arbitrary depth (500 m was set equivalent to present-day sea level) in order to place data into a subsurface context. Corresponding lithofacies and porosity logs (Appendix VI) tied to each section were imported from tabular Ascii files: lithofacies logs record facies integer values every 20 cm, and porosity logs record discrete porosity data points in conjunction with their sampled location within measured sections. In this way, data collected from outcrops around the basin were used to construct synthetic logs that serve as proxies for actual subsurface wire-line log and well data.

Stratigraphic Correlation

Stratigraphic correlations were completed in Petra™ to determine if correlation of geological, reservoir, or flow units would be the best approach for 3-D model construction (Tinker, 1996; Borgomano et al., 2008). The 3-D exposures in the Agua Amarga basin allowed for precise inter-well correlation of the major coarse-grained deposits within lithostratigraphic units, as well as contemporaneous coarse-grained deposits around the basin (litho and chronostratigraphy). Additionally, field observations and core-plug petrophysical results distinguish between reservoir and baffle facies and allow for accurate designation of deposits as either reservoir or baffle units in the model. It is assumed that all reservoir units determined in this study also behave as flow units. The probability that this assumption would hold true in the subsurface after significant burial is dependent on the burial and diagenetic history of the rocks (Schmoker and Halley, 1982; Schmoker, 1984; Enos, 1988; Goldhammer, 1997).

Designation of Reservoir Units

Reservoir units are composed of the shallow-water packstone-grainstone deposits of Units 1 and 2, as well as the major debrites and high-density turbidites within deep-water Units 3 – 7 (high-permeability facies). Shallow-water Units 1 and 2 were lumped together as one reservoir unit on the basis of their stratigraphic proximity and similar porosity-permeability characteristics (Figure 7A). High-density turbidites that evolved from debrites, or were approximately time-equivalent to debrites elsewhere in the basin, were assigned to the same reservoir unit. A few discrete high-density turbidites within the large paleovalley were not accurately modeled as reservoir units due to uncertainties concerning their lateral distribution. However, these deposits are represented in the model as higher-permeability streaks within interstratified baffle units. Baffle units, which are composed dominantly of low-density turbidites and hemipelagic-pelagic sediments (low-permeability facies) within deep-water Units 3 through 7, populate the space in between reservoir units. Over 100 pseudo wells were added in order to represent the complex inter-well geometries of the deep-water reservoir units accurately. Further, pseudo wells were used to extrapolate the existing outcrop data in proximal paleovalley locations into very proximal paleovalley locations (Figure 2A) where sediment gravity flow deposits are hypothesized to have pinched out in close proximity to the toe-of-slope.

Surface grids of the tops and bottoms of reservoir units (and thus the tops and bottoms of interstratified baffle units) were constructed using well top data and the minimum curvature gridding algorithm. Control points were used for construction of the volcanic basement surface in order to constrain elevations accurately. All surfaces were matched to the X-Y grid of the volcanic basement surface to maintain consistent grid dimensions. In order to avoid overlapping surfaces, surfaces were constructed from the bottom to the top of the model (stratigraphically oldest to youngest) by adding isopach (thickness) grids of the successive reservoir units to the surface grids of the previous reservoir units.

3-D Model in Petrel™

Structure Grid

The cellular grid for the model was constructed with an X-Y spacing of 5 meters, which is an extremely fine spatial scale compared to most subsurface models (Enge, 2007). Such high resolution was necessary, however, in order to capture the lithofacies architecture accurately in Petra™ (pseudo well X-Y spacing was commonly less than ten meters in the large paleovalley). Intersecting zones (reservoir and baffle units), as well as layers within those zones, define the Z dimension within the model. The base of the model is defined by volcanic basement and the top of the model is defined by the base of a zone of pre-Pliocene alteration, representing the top of the Miocene stratigraphic succession in the basin (Figure 3). Laterally, the model is contained within a polygon that encompasses all well and pseudo well data (Figure 9). The model contains in excess of 47 million cells.

Zones and Layers

Twenty-two zones represent reservoir and baffle units within the model and characterize the stratigraphy of the Agua Amarga basin (Appendix VII). Zones were created using well top data only; surface grids built in Petra™ were not used as input parameters during the zone-making process due to resulting surface errors and a significant increase in processing time. As a result, zones constructed solely from

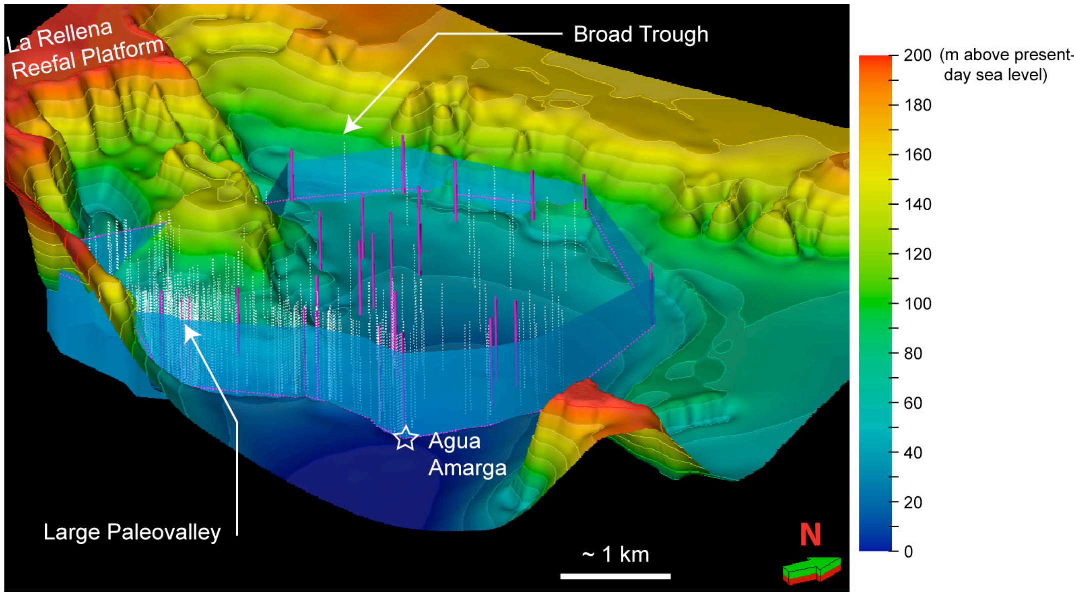

Figure 9. A detailed 3-D Petrel^{TM} image of the topography on the contact between Miocene carbonates and underlying volcanic basement constructed using well (from stratigraphic sections) and control point (from geologic map) data in Petra^{TM}. A simplified version of this surface serves as the lower bounding surface within the Petrel^{TM} model. The model is laterally contained within a polygon (light blue fence) that includes all wells (measured sections – pink/purple columns) and pseudo wells (dotted white columns) used to reconstruct carbonate depositional architecture in Petra^{TM}. Green/red arrow in bottom right corner points to the north. Basin is roughly 4km (N-S) by 8km (E-W). Vertical exaggeration is 7.5X.

well data are simplified but overall are representative of geometries observed in the field (Figure 10). Internal layers were added to zones in order to represent the vertical heterogeneity observed in lithofacies and porosity data from measured sections (Tinker, 1996). No internal layers were added to a few of the thin (less than 2 meter-thick) zones with limited lateral extent; porosity measurements were scarce or absent altogether in these zones.

Property Modeling: Facies

Both stochastic and deterministic methods were used to distribute facies (discrete data) within the model (Appendix VII). For the majority of zones, facies were spread randomly away from well centers either using sequential indicator simulation (SIS – common) (Deutsch and Journel, 1998) or indicator kriging (IK – less common) processes. Zones with only one facies were assigned that specific facies. Both IK and SIS processes utilize data variograms to describe increasing variances between discrete facies values as separation between them increase. Indicator kriging, however, is a deterministic process that yields smooth data interpolations (but does not describe small-scale heterogeneity), whereas sequential indicator simulation is a stochastic process that superimposes correlated noise onto smooth interpolations. (Corvi et al., 1992). Distribution of facies within zones was primarily done using the sequential indicator simulation process in order to procure realizations that most accurately reflected the gradational and patchy facies changes observed in the field. For zones that were laterally less extensive, and specific facies

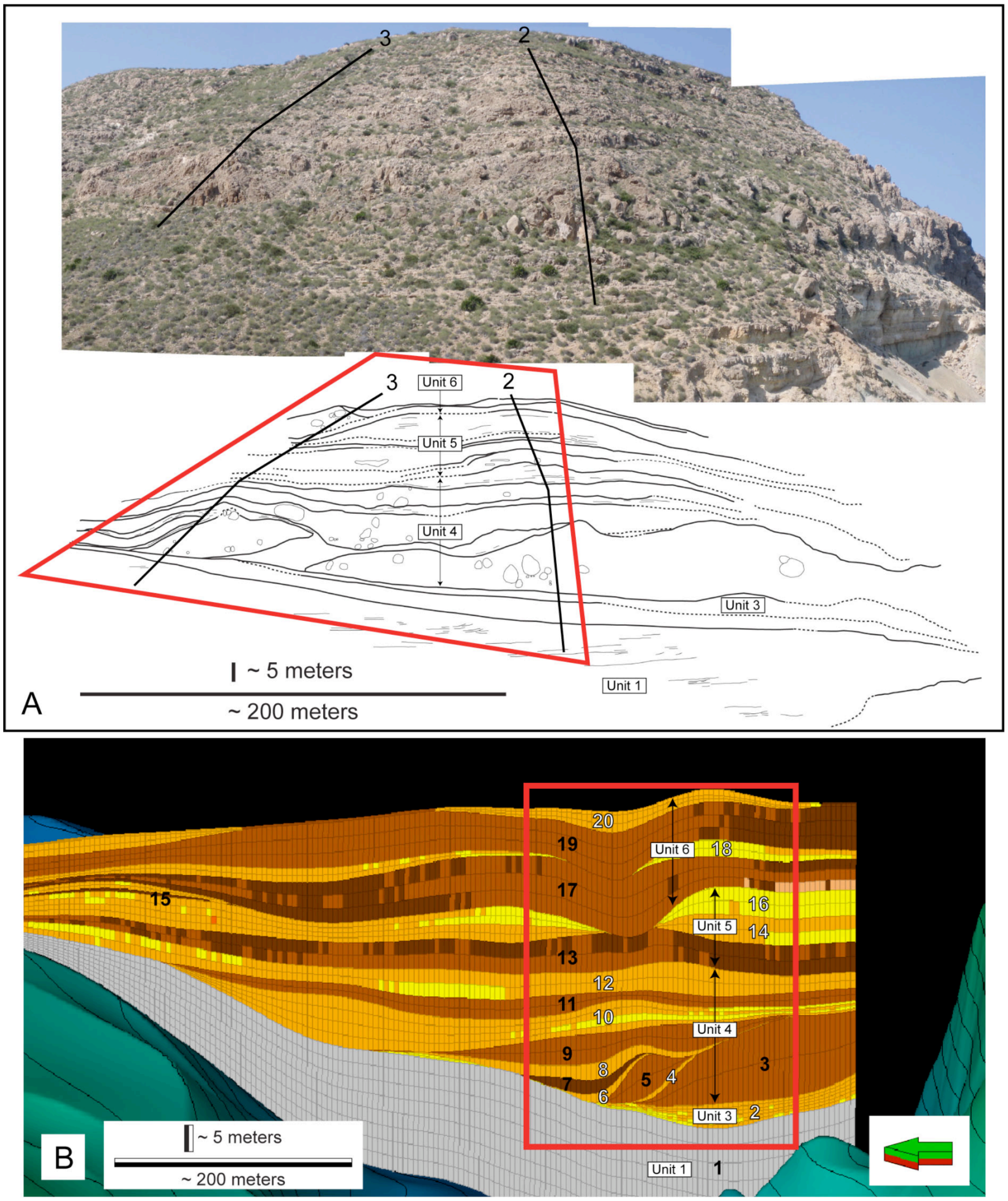

Figure 10. (A) Outcrop photograph displaying axial geometries of the major debrite subunits (Units 4, 5 and 6) within the proximal paleovalley at sections 2 and 3 (see Figure 2 for location). View to the northeast. (B) Same location within the Petrel™ model (red outline). Geometries observed in the field are accurately represented in the model. Numbers represent individual zones within the model (see Table 4). Zone 1 represents Units 1 and 2 shallow-water deposits. Zones 2 – 22 represent Units 3 – 7 deep-water deposits (zones 21 and 22 representing Unit 7 deposits and are not preserved within the paleovalley). Zones numbered in black are reservoir units containing debrites (brown) and high-density turbidites (green – not displayed in this location). Zones numbered in white are baffle units containing low-density turbidites and hemipelagic-pelagic sediments (orange and yellow). Arrow points to the north/northwest. Vertical exaggeration is 7.5X.

were known to exist, the indicator kriging process was used to conform to field observations.

Excellent understanding of facies distribution within the modeled zones of this study, however, necessitates some degree of control during the facies modeling process. Stochastic facies distribution for reservoir units consisting of both debrites and high-density turbidites was controlled by facies percentage polygons. Polygons were drawn to separate various portions of the zone, and facies were assigned an approximate percentage likelihood of occurring within each polygon on the basis field observations. In this way, the stochastic distributions of the graded skeletal packstones facies integer values (5, 6, and 7) were isolated from those of the carbonate breccia facies (8, 9, and 10).

Property Modeling: Porosity and Permeability

Stochastic and deterministic methods were also used to distribute porosity values (%) within the static model (Appendix VII). For the majority of zones, porosity was randomly spread away from well centers using the sequential Gaussian simulation process (Corvi et al., 1992; Deutsch and Journel, 1998). Stochastic porosity distribution was conditioned to facies, except for when a given facies lacked sufficient porosity data. Zones with limited porosity data (zero to one data point, a function of limited thickness and lateral distribution) were assigned a discrete value, either based on a porosity average of that facies within a different zone, or using the single porosity value attributed to that zone. Equations that related porosity to permeability by lithofacies were used to populate the static model's porosity values with corresponding permeability values (md) (Appendix VIII). Finally, multiple realizations resulted in similar property models, indicating that the model is stable overall. This is not surprising considering the array of deterministic approaches used during the model-making process.

Model Results

The basin is most reasonably divided into three play analogs, each of which would likely have a different exploitation strategy. The shallow-water play is composed of Units 1 and 2 packstone-grainstone deposits that accumulate on top of volcanic basement within the broad trough and elsewhere in the basin where paleotopographic slopes are low (Figure 11). Communication between the shallow-water play and the overlying deep-water plays is predicted to be low as a result of Unit 3 foraminifera-rich wacke-packstones at the base of the deep-water plays. These low-permeability fine-grained facies drape the shallow-water play everywhere in the basin except within portions of the large paleovalley, where Unit 4 debrite subunits truncate down into shallow-water packstone-grainstone deposits (Figure 12A).

Deep-water plays consist of the focused-flow and the dispersed-flow plays (Figure 11). The focused-flow play is located within and at the mouth of the margin-parallel paleovalley. Reservoir units consist of Units 3 through 7 turbidites and debrites. The dispersed-flow play is approximately coeval with the focused-flow play

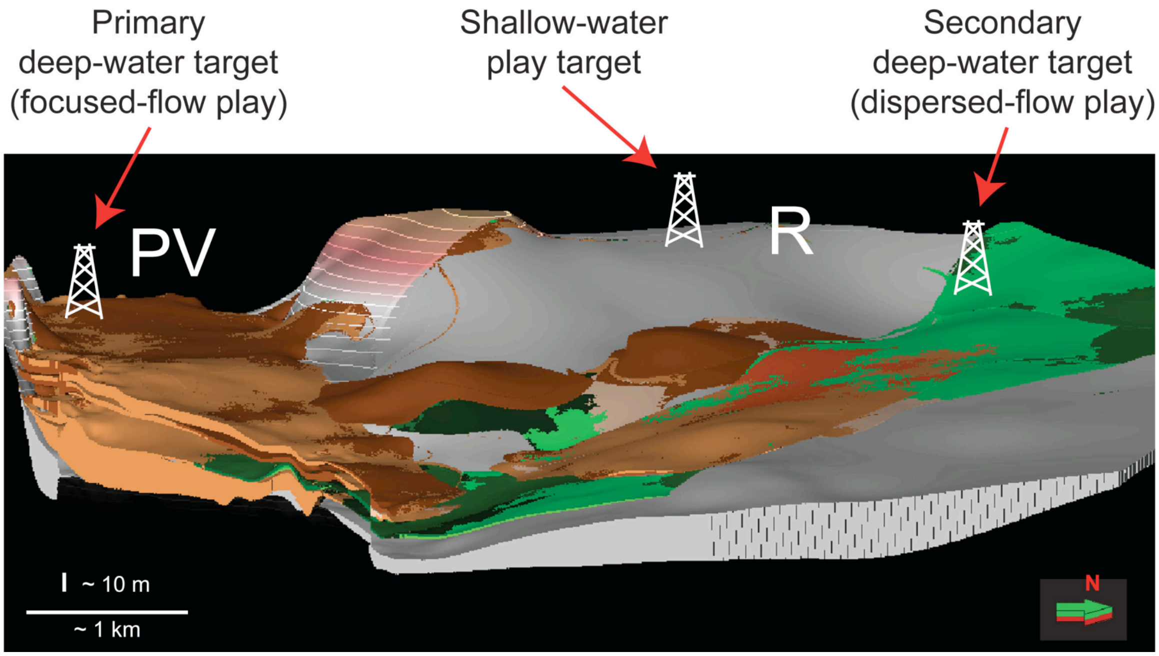

Figure 11. Reservoir targets within the shallow-water play (grey) and focused-flow and dispersed-flow deep-water plays (browns and greens). Targets occur in up-dip locations along the ramp-like surface (R) and within the large margin-parallel paleovalley (PV) where deposits pinch out against volcanic basement.

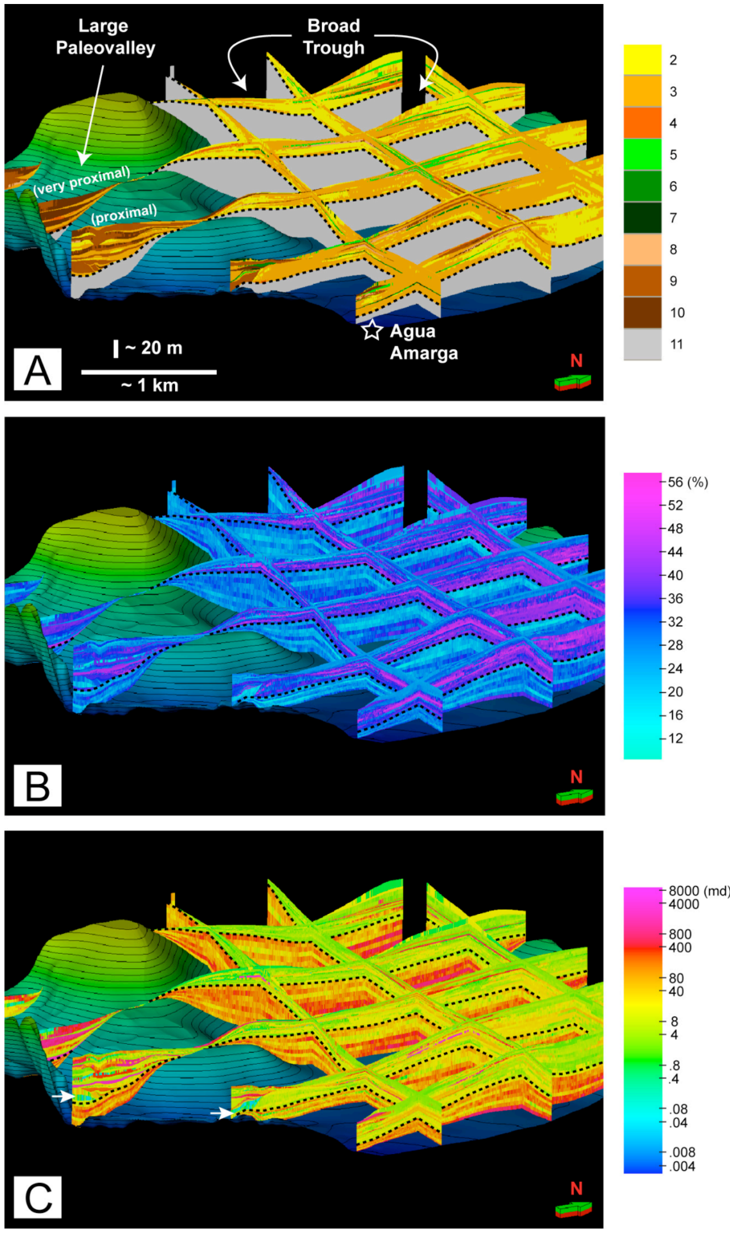

Figure 12. Fence diagrams of the 3-D model in Petrel^{TM}. Dotted black line separates Units 1 and 2 of the shallow-water play from Units 3 – 7 of the deep-water plays. Green/red arrows in bottom right corner of each diagram point to the north. (A) Lithofacies fence diagram representing the shallow-water play (grey) and the deep-water plays (browns, greens and yellows/oranges). Numbers represent specific lithofacies (see Table 1). Reservoir facies are represented by numbers 5 through 11, and baffle facies are represented by numbers 2 through 4. (B) Porosity fence diagram. Baffle facies typically have higher porosity values (purple/pink) than the reservoir facies (blues). (C) Permeability fence diagram. Baffle facies typically have lower permeability values (greens and yellows) than reservoir facies (oranges and reds). Unit 4 debrite subunit 4a within the large margin-parallel paleovalley display low permeability values (blues and greens) likely due to extensive dolomitization (white arrows). Distinguishing between reservoir and baffle units within the deep-water plays is difficult due to reservoir-quality petrophysical values within all modeled lithofacies.

and is located in the northern and central part of the basin overlying the preexisting ramp-like surface that resulted from deposition of Units 1 and 2 packstone-grainstone deposits. Reservoir units within the dispersed-flow play also consist of Units 3 through 7 turbidites and debrites. Although some inter-fingering of high-density turbidites and debrites occurs, reservoir units within the focused-flow play are mostly laterally isolated from those within the dispersed-flow play. Interstratified hemipelagic-pelagic sediments and low-density turbidites (baffle units) serve to inhibit vertical and lateral flow between these two deep-water plays.

Property Model

The property models display distinct differences in facies by zone; however, differences in porosity and permeability by zone are noticeably less distinct (Figure 12). The porosity and permeability models reveal reservoir-quality values for both reservoir and baffle units, however display notably higher permeability values within reservoir units. These results are not surprising considering that the model was constructed from outcrops that have not undergone significant burial.

Volumetric Calculations

Pore and bulk volumes were calculated for reservoir and baffle units within each reservoir play. Pore volume was calculated by creating a bulk volume property within the model and multiplying it by the porosity model (pore volume = bulk volume * porosity). This method assumes a net to gross ratio of 1, thereby rendering net volume equal to bulk volume. Pore volumes by zone were extracted from the statistics tab within the settings of the pore volume property; bulk volumes were similarly recorded from the bulk volume statistics tab (Table 4). In order to differentiate pore volumes within the focused-flow deep-water play from those within the dispersed-flow deep-water play, polygons were used to create Boolean properties that could then be applied as filters within the pore and bulk volume properties.

Reservoir facies within the shallow-water play have the greatest pore volume (97.7 million m^3), followed by reservoir facies within the focused-flow deep-water play (14.6 million m^3), and reservoir facies within the dispersed-flow deep-water play (5.71 million m^3) (Figure 12). These values convert to 614 million barrels, 91.7 million barrels, and 35.9 million barrels, respectively, and offer a high-end estimation for potential hydrocarbons in place. Volumes are similar (within an order of magnitude) to producing slope and basinal sandstone and carbonate reservoirs in the Permian basin (Dutton et al., 2005). Nevertheless, values reported here would be expectedly less in the subsurface when accounting for production recovery factors and other intrinsic reservoir properties not modeled in this study. Further, it is important to note that the calculated pore volumes for reservoir facies within the focused-flow play include a portion of extrapolated data that extend from proximal paleovalley locations (actual outcrop data at measured sections 1, 2, and 3) into very proximal paleovalley locations (Figure 2A). Calculated bulk volume of reservoir rock from outcrop data alone within the focused-flow play is 15.0 million m^3 and modeled volume is 46.5 million m^3 (see Table 4). Thus, volumetric calculations for the focused-flow play represent a modeled rather than an actually preserved scenario.

Oil-water Contacts

Oil-water contacts were added using elevation property filters at 35, 50 and 65 meters above present-day sea level to better understand the impact such contacts would have on reservoir play pore volumes at varying depth (Figure 13). As an oil-water contact moves upward, the shallow-water play displays the greatest relative loss in pore volume (62.5 million m^3) due to the significant volume of sediment that accumulated near present-day sea level along the coastline (Figure 12A). Within the deep-water plays, the focused-flow play displays a significantly greater relative loss in pore volume (7.30 million m^3) than the dispersed-flow play (.830 million m^3) as a result of its lower topographic position within the basin (the dispersed-flow deposits lie up-dip along the gently dipping packstone-grainstone ramp-like surface).

DISCUSSION

Subsurface Implications

Characterization and 3-D modeling of the shallow-water and deep-water carbonate plays within the Agua Amarga basin has created a useful analog for exploitation of similar subsurface petroleum reservoirs. Assuming a hypothetical seal

		Shallow-water Play		Focused-flow Play		Dispersed-flow Play	
Zone #	Zone Name	Bulk Volume (m3)	Pore Volume (m3)	Bulk Volume (m3)	Pore Volume (m3)	Bulk Volume (m3)	Pore Volume (m3)
22	7a_Fs	-	-	-	-	8658215	2446390
21	7a_Sgf	-	-	-	-	2256619	592451
20	6b_Fs	-	-	6120683	1554064	25934112	7788649
19	6b_Sgf	-	-	19736730	5755810	5306883	1519836
18	6a_Fs	-	-	9762632	2670065	20808545	5986633
17	6a_Sgf	-	-	14408831	4779812	7106764	2431630
16	5b_Fs	-	-	342078	97971	2059	575
15	5b_Sgf	-	-	234623	71196	-	-
14	5a_Fs	-	-	9280791	3033744	725512	237701
13	5a_Sgf	-	-	6120441	1921053	442070	139246
12	4e_Fs	-	-	4581162	1402092	-	-
11	4e_Sgf	-	-	2118189	966804	-	-
10	4d_Fs	-	-	14054982	5772543	52744145	19805655
9	4d_Sgf	-	-	336246	121130	-	-
8	4c_Fs	-	-	132348	44867	-	-
7	4c_Sgf	-	-	56109	16932	-	-
6	4b_Fs	-	-	41425	9565	-	-
5	4b_Sgf	-	-	124644	39317	-	-
4	4a_Fs	-	-	65632	19033	-	-
3	4a_Sgf	-	-	3382251	905217	3454204	1031184
2	3	-	-	21845970	7757842	87637579	34007513
1	1&2	357682541	97689627	-	-	-	-
				TOTALS		TOTALS	
			Reservoir Units (Sgf)	46518064	14577271	18566540	5714347
			Baffle Units (Fs)	66227703	22361786	196510167	70273116

* Sgf = Sediment-gravity flow

* Fs = Fine sediment

Table 4. Calculated bulk and pore volumes (m^3) by zone for the shallow-water play and the deep-water focused-flow and dispersed-flow plays. Zones were constructed by separating stratigraphic units (1 – 7) into sediment gravity flow (Sgf) and fine-grained sediment (Fs) deposits as reservoir and baffle units, respectively.

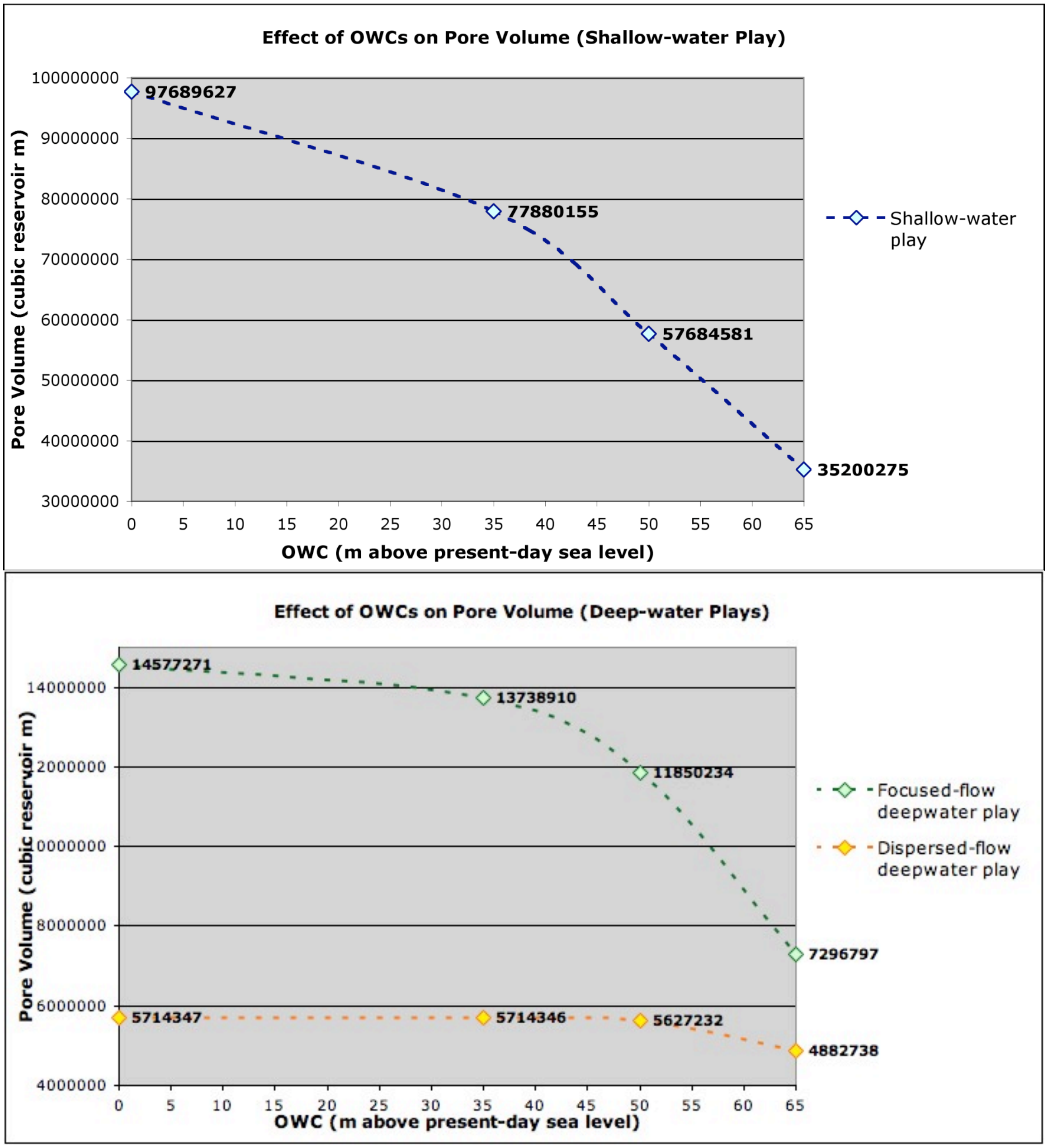

Figure 13. Reservoir pore volumes for the shallow-water play (A), and the focused-flow and dispersed-flow deep-water plays (B). Pore volumes calculated without an oil-water contact are displayed at 0 meters. Oil-water contacts at successively greater elevations (35, 50 and 65 meters above present-day sea level) within the model results in a decrease of pore volumes for all plays. The shallow-water play displays the greatest relative pore volume loss as a result of its greater overall reservoir volume. Within the deep-water plays, the focused-flow play displays a significantly greater relative loss in pore volume than the dispersed-flow play as a result of its overall lower topographic position within the paleovalley.

facies, source rock, and sufficient burial conditions allowing for the development of hydrocarbons, the best places to exploit the shallow-water and deep-water plays are in stratigraphically up-dip locations where unit pinch-outs occur. The foraminiferal wacke-packstone facies, interpreted as hemipelagic-pelagic sediments (and likely consisting of significant amounts of organic matter), would serve as the dominant source rock in the basin. Similarly, these deposits, as well as volcaniclastic- and skeletal foraminiferal wacke-packstones, interpreted as low-density turbidites, have the potential to serve as seal facies where they overlie the reservoir rocks.

Pore volume results indicate that the shallow-water play has the greatest potential reservoir volume (Table 4). This play may be affected by its stratigraphic (and topographic) position below the deep-water source rock (although migration from another downdip source would be likely). Combined, Units 1 and 2 shallow-water deposits have thickest accumulations in the broad trough (Figure 2A) and thin down-dip toward the present-day coastline, in the large paleovalley, and updip where there are basement paleotopographic highs. The well with greatest potential in the shallow-water play analog (Figure 11) would be in up-dip locations north of the paleovalley along the basin margin where shallow-water deposits lap out against volcanic basement and are sealed by fine-grained carbonates.

As discussed in the foregoing sections, pore volume results also reveal significant reservoir volume within the deep-water plays (Table 4). The best deep-water reservoir target would be in the focused-flow play (Figure 11). Greatest recovery would likely be within very proximal paleovalley locations, where the greatest thicknesses of reservoir facies are predicted. Although there is little actual preserved outcrop in very proximal locations within the large paleovalley, preserved geometries within debrite subunits in proximal paleovalley locations suggest that high-density turbidites and debrites onlap against volcanic basement and earlier deposits at the toe-of-slope in very proximal paleovalley locations (Figure 2A). Thus, the focused-flow deep-water deposits modeled within the large paleovalley are detached from adjacent (upslope) reef/forereef slope material.

High-density turbidites and debrites within the dispersed-flow play are isolated from the focused-flow deposits and thus form their own reservoir play. Volumetric calculations reveal that the dispersed-flow reservoir units have lesser volumes than the focused-flow reservoir units (Table 4) but serve as a secondary deep-water target play analog in the basin (Figure 11). The well with greatest potential would likely occur in up-dip locations, assuming sufficient lateral communication between reservoir facies.

Controls on the Shallow-water Play

Vertical and lateral continuity of reservoir units within each play and between plays is largely controlled by paleotopography and relative sea-level history. The shallow-water play is composed of Units 1 and 2 packstone-grainstone deposits that accumulate on top of volcanic basement within the broad trough and elsewhere in the basin where paleotopographic slopes are low. Deposition of Units 1 and 2 on low-angle paleo-substrates during periods of inundation facilitated widespread accumulation of laterally continuous units with low internal facies variability. Petrophysical properties for Units 1 and 2 are very similar (Figure 7A) and suggest that communication between units in the subsurface would be high. The presence of volcaniclastic grains within Unit 1, however, may introduce a mobile clay component within the subsurface that would complicate production. Additionally, the subaerial exposure surface separating these units may significantly restrict flow dynamics between units if this interval were to become tightly cemented during burial diagenesis (porosity and permeability values in this interval are currently high).

Controls on the Deep-water Plays

The most significant control on bulk volume of reservoir facies within each of the two deep-water play analogs is likely the area of shallow-water carbonate production and its transport into the basin. The linear dimension of carbonate shelf margin that each deep-water system drains, however, is hypothesized to be a good proxy for the area of shallow-water carbonate production, and can be used to predict reservoir bulk volumes. The substrate paleotopographic map (Figure 2) shows that the focused-flow deep-water play is sourced by approximately 5.07 km of carbonate shelf margin, whereas the dispersed-flow system is sourced by only approximately 2.14 km (a ratio of 2.37). Volumetric calculations reveal that the bulk volume of modeled reservoir facies within the focused-flow system (including extrapolated data in the very proximal paleovalley) is approximately 2.5 times that of the dispersed-flow system (Table 4). Further, the ratio of reservoir bulk volume to linear dimension of shelf margin is 9200 m^3/m for the focused-flow play and 8700 m^3/m for the dispersed-flow play (Table 4). The similarity between these ratios suggests that the linear dimensions of shelf margin sourcing a deep-water play can be used to predict the bulk volume of reservoir rock within a given deep-water carbonate play.

Vertical and lateral communication between high-density turbidites and debrites varies depending on the abundance of interstratified hemipelagic-pelagic sediments and low-density turbidites, as well as the erosive tendencies of the high-density turbidites and debrites at any given location. Thicker accumulations of hemipelagic-pelagic sediments and low-density turbidites exist during periods of high relative sea level, resulting in decreased vertical and lateral communication between reservoir units. During periods of low relative sea level, or after sustained high sea level, however, there is a greater abundance of high-density turbidites and debrites, resulting in increased potential for vertical and lateral communication between these deposits. Considering the presence of variably abundant interstratified fine-grained and low-permeability deposits, however, the erosive tendency of high-density sediment gravity flows is likely a significant control on reservoir continuity within each play.

Erosion of hemipelagic-pelagic sediments and low-density turbidites by high-density turbidites and debrites is greater in locations with lateral confinement and proximity to steeply dipping substrate slopes than it is in locations with gentle substrate slopes and an absence of lateral confinement. The ratio of total reservoir unit bulk volume to baffle unit bulk volume in the two deep-water systems supports this idea. In the focused-flow system (including extrapolated data) the ratio is 0.70, and in the dispersed-flow system the ratio is 0.09, indicating that paleotopographic focus of sediment-gravity flows improves reservoir character in a predictable way. Again, it must be pointed out that these ratios are those modeled, and that the actual ratios calculated from the outcrop alone would differ, but show a similar relationship.

Within the focused-flow deep-water play, vertical and lateral communication between reservoir units is greatest in very proximal and proximal paleovalley locations and decreases down-dip as proximity to steeply dipping platform slopes and lateral confinement within paleovalley walls decreases. This trend is a result of greater concentrations of high-density turbidites and debrites with complex geometries in very proximal and proximal paleovalley locations, as well as a greater tendency for these deposits to erode interstratified hemipelagic-pelagic sediments and low-density turbidites. In other words, topographic confinement of flows and focusing of large amounts of platform debris into a small area works in favor of the best reservoir properties. Additionally, location of the toe-of-slope adjacent to steeply dipping platform slopes within very proximal and proximal paleovalley locations results in significantly thicker accumulations of reservoir facies than found within the dispersed-flow play.

Within the dispersed-flow deep-water play, vertical and lateral communications between reservoir units is uniformly low. Low vertical communication is a result of thick accumulations of hemipelagic-pelagic sediments and low-density turbidites in between reservoir units. Gentle slopes, a small linear dimension shelf margin (and therefore a small area) of source, and an absence of lateral confinement all result in thinner sheet-like geometries that display significantly less truncation of underlying fine-grained deposits and high percentages of baffle units. These characteristics are largely due to a continuous and gently sloping substrate topography that increases lateral flow distribution and dissipates internal flow energy as distance from the platform margin increases.

CONCLUSIONS

Outcrop examples of shallow-water and deep-water carbonate deposits serve as important analogs for the exploration and development of similar systems in the subsurface. Outcrop characterization of late Miocene carbonates in the Agua Amarga basin, southeast Spain, followed by construction of a whole-field cellular model, indicates ample reservoir potential within three play analogs. These play analogs in order of decreasing hydrocarbon storage potential are a shallow-water play, a focused-flow deep-water sediment-gravity flow play, and a dispersed-flow deep-water sediment-gravity flow play. The shallow-water play is composed of high-energy shallow subtidal skeletal packstone-grainstone deposits (Units 1 and 2) that display well-preserved interparticle and intraparticle porosity. These deposits have high porosity and permeability values (a combined mean porosity of 26.3% and corresponding permeability of 81.1md) and are designated as reservoir facies within the model. The deep-water plays are composed of interstratified hemipelagic-pelagic sediments and fine and coarse-grained sediment gravity flow deposits (Units 3 through 7). Coarse-grained sediment gravity flow deposits (high-density turbidites and debrites) have abundant interparticle, intraparticle and moldic porosity. These deposits have high porosity and permeability values and are designated as reservoir facies in the model. High-density turbidites have a combined mean porosity of 30.5% and corresponding permeability of 136.1md, and debrites have a combined mean porosity of 30.1% and corresponding permeability of 64.6md. Hemipelagic-pelagic sediments and low-density turbidites display interparticle, intraparticle and moldic porosity (as well as characteristic intraparticle micro-porosity within the foraminiferal wacke-packstone facies). These fine-grained deposits have high porosity and low permeability values (a combined mean porosity of 35.9% and corresponding permeability of 12.3md) and are designated as baffle facies in the model.

The static reservoir model constructed in this study implements field and lab data in order to make general predictions about potential hydrocarbon volume within the shallow-water and deep-water plays. Pore volumes calculated for each play suggest considerable subsurface reservoir potential. Volumetric calculations reveal 97.7 million m^3 of pore volume within the shallow-water play, 14.6 million m^3 within the focused-flow deep-water play, and 5.71 million m^3 within the dispersed-flow deep-water play. Despite these high initial predictive pore volumes, dynamic reservoir modeling through flow simulation is needed in order to more accurately constrain reservoir volume and hydrocarbon exploitation potential. Specifically, incorporating key reservoir parameters such as water saturation, capillary pressure, relative permeability and the potential for multiple fluid phases are crucial for meaningful flow simulation results. Considering the number of cells within the current whole-field model (in excess of 47 million) construction of individual models for each reservoir play would be advised prior to flow simulation.

Paleotopography and relative fluctuations in sea level are the dominant controls on the internal architectures and distributions of reservoir facies. The effect of paleotopography is particularly noteworthy for high-density turbidites and debrites within the deep-water plays. The majority of resedimented platform sediments were focused into and along the axis of a large margin-parallel paleovalley and ultimately point-sourced into the basin. The geometries and distributions of the focused-flow coarse-grained sediment-gravity flows are significantly different from those dispersed along the gently dipping ramp-like surface that developed from accumulation of Units 1 and 2. Focused-flow deposits in very proximal and proximal paleovalley locations display the most complex geometries with the greatest ratio of coarse-grained reservoir facies to fine-grained baffle facies. Complexity of reservoir facies and ratio of coarse- to fine-grained sediment decreases with decreasing lateral confinement within paleovalley walls, and increasing distance from the platform margin and steeply dipping platform slopes. Dispersed-flow sediment-gravity flows along the ramp-like surface display uniform sheet-like geometries with lower coarse- to fine-grained sediment ratios than those within the focused-flow system due to an absence of lateral confinement and continuous and gently dipping substrate slopes. The focused-flow and dispersed-flow deep-water carbonate deposits in this study differ significantly from traditional line-sourced slope-apron deposits and offer new insight into models for deposition of carbonate sediment-gravity flows.

Paleotopography is likely an important control on the accumulation of volumetrically significant deep-water carbonate reservoir bodies. The static model results from this study suggest that where known focusing topographic features are located sufficiently close to carbonate-producing platforms, reservoir location, size and heterogeneity can be predicted. Deposits within the focused-flow play (using model results) have a significantly higher bulk volume ratio of reservoir-to-baffle facies compared to deposits within the dispersed-flow play (0.70 versus 0.09). These coarse- to fine-grained sediment ratios are indicative of reservoir heterogeneity and suggest that paleotopographic focus of sediment-gravity flows improves reservoir character. Additionally, the linear dimension of shelf margin sourcing the reservoir appears to be an important predictor of reservoir volume within each play. The focused-flow play is sourced by approximately 5.07 km of shelf margin and the dispersed-flow play is sourced by approximately 2.14 km of shelf margin, an approximate ratio of 2.37. Bulk volume calculations (using extrapolated data within the focused-flow play) reveal that the total deep-water reservoir volume within the focused-flow play is approximately 2.5 times greater than that of the dispersed-flow play. Another way to consider this relationship is to calculate the ratio of reservoir bulk volume to linear dimension of shelf margin for each deep-water system, 9200

m^3/m for the focused-flow play and 8700 m^3/m for the dispersed-flow play. The resulting ratios are strikingly similar and indicate that knowing the linear dimension of shelf margin sourcing a deep-water play may be useful in predicting subsurface reservoir volumes.

References Cited

Adams, E. W., J. P. Grotzinger, W. A. Watters, S. Schroder, D. S. McCormick, and H. A. Al-Siyabi, 2005, Digital characterization of thrombolite-stromatolite reef distribution in a carbonate ramp system (terminal Proterozoic, Nama Group, Namibia): AAPG Bulletin, v. 89, p. 1293-1318.

Borgomano, J., F. Fournier, S. Viseur, and L. Rijkels, 2008, Stratigraphic well correlations for 3-D static modeling of carbonate reservoirs: AAPG Bulletin, v. 92, p. 789-824.

Borgomano, J., J. P. Masse, and S. Al Maskiry, 2002, The lower Aptian Shuaiba carbonate outcrops in Jebel Akhdar, northern Oman: Impact on static modeling for Shuaiba petroleum reservoirs: AAPG Bulletin, v. 86, p. 1513-1529.

Choquette, P. W., and L. C. Pray, 1970, Geologic nomenclature and classification of porosity in sedimentary carbonates: American Association of Petroleum Geologists Bulletin, v. 54, p. 207-250.

Corvi, P., K. Heffer, P. King, S. Tyson, and G. Verly, 1992, Reservoir Characterization Using Expert Knowledge, Data and Statistics: Oilfield Review, Schlumberger, p. 25-39.

Deutsch, C. V., and A. G. Journel, 1998, GSLIB: Geostatistical software library and user's guide, 2d ed.: New York, Oxford University Press, 369 p.

Dillett, P. M., 2004, Paleotopographic and sea-level controls on the sequence stratigraphic character of a heterozoan carbonate succession: Pliocene, Carboneras basin, southeast Spain: Unpublished M.S. thesis, University of Kansas, Lawrence, KS, 116 p.

Dunham, R. J., 1962, Classification of carbonate rocks according to depositional texture, *in* W. E. Ham, ed., Classifications of carbonate rocks - a symposium: AAPG Memoir, p. 108-121.

Dutton, S. P., E. M. Kim, R. F. Broadhead, W. D. Raatz, C. L. Breton, S. C. Ruppel, and C. Kerans, 2005, Play analysis and leading-edge oil-reservoir development methods in the Permian basin: Increased recovery through advanced technologies: AAPG Bulletin, v. 89, p. 553-576.

Enge, H. D., S. J. Buckley, A. Rotevatn, and J. A. Howell, 2007, From outcrop to reservoir simulation model: Workflow and procedures: Geosphere, v. 3, p. 469-490.

Enos, P., 1977, Tamabra Limestone of the Poza Rica Trend, Cretaceous, Mexico, *in* Deep-water carbonate environments: Special Publication - Society of Economic Paleontologists and Mineralogists p. 273-314.

Enos, P., 1988, Evolution of pore space in the Poza Rica trend (Mid-Cretaceous), Mexico: Sedimentology, v. 35, p. 287-325.

Esteban, M., 1996, An Overview of Miocene Reefs from Mediterranean Areas: General Trends and Facies Models, *in* E. K. Franseen, M. Esteban, W. C. Ward, and J. M. Rouchy, eds., Models for Carbonate Stratigraphy from Miocene Reef Complexes of the Mediterranean Regions: SEPM Concepts in Sedimentology and Paleontology 5, p. 3-54.

Esteban, M., J. C. Braga, J. Martin, and C. Santisteban, 1996, Western Mediterranean Reef Complexes, *in* E. K. Franseen, M. Esteban, W. C. Ward, and J. M. Rouchy, eds., Models for Carbonates Stratigraphy from Miocene Reef Complexes of Mediterranean Regions: SEPM Concept in Sedimentology and Paleontology 5, p. 55-72.

Francis, B. P., L. J. Weber, S. Batchel, P. M. Harris, D. Fisher, and J. A. M. Kenter, 2004, Prediction and mapping of deep-water slope carbonate reservoirs using seismic data, Tengiz Field, western Kazakhstan: Annual Meeting Expanded Abstracts - American Association of Petroleum Geologists, p. 47.

Franseen, E. K., and R. H. Goldstein, 1996, Paleoslope, Sea-level and Climate Controls on Upper Miocene Platform Evolution, Las Negras Area, Southeastern Spain, *in* E. K. Franseen, M. Esteban, W. C. Ward, and J. M. Rouchy, eds., Models for Carbonates Stratigraphy from Miocene Reef Complexes of Mediterranean Regions: SEPM Concept in Sedimentology and Paleontology 5, p. 159-176.

Franseen, E. K., R. H. Goldstein, and M. Esteban, 1997, Controls on Porosity Types and Distribution in Carbonate Reservoirs: A Guidebook for Miocene Carbonate Complexes of the Cabo de Gata Area, SE Spain: American Association of Petroleum Geologists Education Program, p. 1-150.

Franseen, E. K., R. H. Goldstein, and M. R. Farr, 1998, Quantitative Controls on Location and Architecture of Carbonate Depositional Sequences: Upper Miocene, Cabo de Gata Region, SE Spain: Journal of Sedimentary Research, v. 68, p. 283-298.

Franseen, E. K., R. H. Goldstein, and T. E. Whitesell, 1993, Sequence stratigraphy of Miocene carbonate complexes, Las Negras area, southeastern Spain: implications for quantification of changes in relative sea-level, *in* R. G. Loucks, and J. F. Sarg, eds., Carbonate Sequence Stratigraphy: Recent Developments and Applications: AAPG Memoir 57, p. 409-434.

Gibbons, W., and M. T. Moreno, eds., 2003, The Geology of Spain: Geological Society of London, 649 p.

Goldhammer, R. K., 1997, Compaction and Decompaction Algorithms for Sedimentary Carbonates: Journal of Sedimentary Research, v. 67, p. 26-35.

Harris, P. M., R. A. Garber, and M. E. Clark, 2000, Geologic framework for Korolev Field, Kazakhstan; a Carboniferous isolated carbonate platform: Annual Meeting Expanded Abstracts - American Association of Petroleum Geologists, p. 65.

Lucia, F. J., 1995, Rock-Fabric/Petrophysical Classification of Carbonate Pore Space for Reservoir Characterization: AAPG Bulletin, v. 79, p. 1275-1300.

Mankiewicz, C., 1996, The Middle to Upper Miocene carbonate complex of Nijar, Almeria Province, southeastern Spain, *in* E. K. Franseen, M. Esteban, W. C. Ward, and J. M. Rouchy, eds., Models for Carbonates Stratigraphy from Miocene Reef Complexes of Mediterranean Regions: SEPM Concept in Sedimentology and Paleontology.

Mapa Geologico de Espana, 1981, (1:50,000): Instituto Geologico y Minero de Espana.

Martin, J. M., J. C. Braga, and C. Betzler, 2003, Late Neogene - Recent uplift of the Cabo de Gata volcanic province, Almeria, SE Spain: Geomorphology, v. 50, p. 27-42.

Payros, A., and V. Pujalte, 2008, Calciclastic submarine fans: An integrated overview: Earth-Science Reviews, v. 86, p. 203-246.

Payros, A., V. Pujalte, and X. Orue-Extebarria, 2007, A point-sourced calciclastic submarine fan complex (Eocene Anotz Formation, western Pyrenees): facies architecture, evolution and controlling factors: Sedimentology, v. 54, p. 137-168.

Pranter, M. J., A. I. Ellison, R. D. Cole, and P. E. Patterson, 2007, Analysis and modeling of intermediate-scale reservoir heterogeneity based on a fluvial point-bar outcrop analog, Williams Fork Formation, Piceance Basin, Colorado: AAPG Bulletin, v. 91, p. 1025-1051.

Russell, S. D., M. Akbar, B. Vissapragada, and G. M. Walkden, 2002, Rock types and permeability prediction from dipmeter and image logs: Shuaiba reservoir (Aptian), Abu Dhabi: AAPG Bulletin, v. 86, p. 1709-1732.

Sanz de Galdeano, C., and J. A. Vera, 1992, Stratigraphic record and palaeogeographical context of the Neogene basins in the Betic Cordillera, Spain.: Basin Research, v. 4, p. 21-36.

Schmoker, J. W., 1984, Empirical Relation Between Carbonate Porosity and Thermal Maturity: An Approach to Regional Porosity Prediction: The American Association of Petroleum Geologists, v. 68, p. 1697-1703.

Schmoker, J. W., and R. B. Halley, 1982, Carbonate Porosity Versus Depth: A Predictable Relation for South Florida: AAPG Bulletin, v. 66, p. 2561-2570.

Tinker, S., 1996, Building the 3-D Jigsaw Puzzle: Applications of Sequence Stratigraphy to 3-D Reservoir Characterization: AAPG Bulletin, v. 80, p. 460-485.

Toomey, N., 1997, Controls on Sequence Stratigraphy in upper Miocene Carbonates of Cerro de Ricardillo, southeastern Spain: Unpublished M.S. thesis, University of Kansas, Lawrence, KS, 145 p.

Weber, L. J., B. P. Francis, P. M. Harris, and M. S. Clark, 2003, Stratigraphy, lithofacies, and reservoir distribution; Tengiz Field, Kazakhstan: Annual Meeting Expanded Abstracts - American Association of Petroleum Geologists, p. 178.

Appendices

Appendix I

Measured Stratigraphic Sections

Thirty-one stratigraphic sections were measured to document lithofacies and lithofacies architecture in the Agua Amarga basin, however only twenty-eight sections were used for stratigraphic correlation and 3-D reservoir-analog modeling. Elevation (meters above sea-level) and location (GPS coordinates) for each section was noted using a hand-held GPS and topographic map. Three of the sections listed below (sections A, AA-E and CEP-3_a & _b) were excluded from this study based on the following reason: section A only documents a few meters of Unit 1; section AA-E represents deposits sourced from Mesa Roldan, not the La Rellena reefal platform; section CEP-3 is almost entirely altered by pre-Pliocene subaerial exposure. *All measured sections are available electronically in their original file format (Adobe Illustrator).*

Measured Section		Elevation (m above sl)	GPS Location	
A*	Agujero	46	30S 0592678	4090172
AA-E*	Agua Amarga E	0	30S 0595254	4088864
AA-W	Agua Amarga W	4	30S 0594714	4088740
CE/NE-1	Cala de Enmedio NE	10	30S 0593961	4088190
CE/NE-2	Cala de Enmedio NE	10	30S 0593838	4088255
CE/SW	Cala de Enmedio SW	22	30S 0593865	4088105
CEP-2	Cortijo del Plomo	8	30S 0592961	4087036
CEP-3_a*	Cortijo del Plomo	18	30S 0593101	4086927
CEP-3_b*	Cortijo del Plomo	97	30S 0592968	4086788
CH-1	Cerro de la Higuera	43	30S 0593207	4087715
CH-2	Cerro de la Higuera	4	30S 0593216	4087123
CH-3	Cerro de la Higuera	27	30S 0593173	4087220
CLJ-2	Cortijada la Joya	77	30S 0592472	4089634
CLJ-3	Cortijada la Joya	78	30S 0592458	4089929
CLT-2	Casas los Torres	94	30S 0592273	4091188
CM-2	Canada Mendez	44	30S 0593552	4089149
CU-1	Cerro del Cuartel	32	30S 0593928	4089021
CU-2	Cerro del Cuartel	60	30S 0593328	4088481
CU-3	Cerro del Cuartel	6	30S 0594495	4088598
EP	El Palmar	78	30S 0594468	4091427
L15	Location 15	37	30S 0592795	4089299
L15 (RAD)	Location 15	78	30S 0592854	4089136
L19	Location 19/La Gorra	66	30S 0592138	4090224
L20	Location 20/Los Pacos	110	30S 0591106	4090375
L21	Location 21	73	30S 0591794	4090606
L26	Location 26	67	30S 0590920	4089307
L27	Location 27/Los Viruegas	20	30S 0594439	4089831
LC-1	Las Cordilleras	94	30S 0592008	4089545
LdlT-2	Llanos de los Torres	91	30S 0592569	4091594
LM-2	La Mesa	28	30S 0594814	4089610
LP-2	Los Pollos	58	30S 0594592	4089968
RA-2	Rellena Artesica	49	30S 0592157	4089039

* not included in 3-D PetrelTM model

Appendix II

Coastline Photomosaics

Two photomosaics of the present-day coastline in the Agua Amarga basin document depositional units and lithofacies architectures of focused-flow deposits along depositional dip. The first photomosaic, *App_II_A.ai*, is of outcrop from Cala del Plomo to Cala de Enmedio. The second photomosaic, *App_II_B.ai*, is of outcrop from Cala de Enmedio to Agua Amarga. *Photomosaics are available electronically in their original file formats (Adobe Illustrator).*

Appendix III

Petrography

Eighty-four thin sections were prepared for petrographic analysis of representative lithofacies in the Agua Amarga basin. Seventy-seven of these thin sections were examined in detail; seven were excluded on the basis that they were not crucial to lithofacies characterization. Sample names, lithofacies classifications, skeletal & non-skeletal constituents, sedimentary structures, dominant pore types & cements, and photomicrograph IDs were recorded in an excel spreadsheet, *App_III.xls (available electronically).*

Appendix IV

Core Plug Petrophysical Data

One-inch diameter core plugs from collected hand samples of representative lithofacies in the field were measured for helium porosity (%), air permeability (md), and grain density (g/cc). Plug IDs with an asterisk are from hand samples collected from previous work in the basin. Petrophysical values were recorded in an excel spreadsheet, *App_IV.xls (available electronically).*

Appendix V

Spectral Gamma Ray Data

Spectral gamma ray data was collected every meter in conjunction with measured stratigraphic sections using a hand-held spectral scintillometer. Potassium (%), uranium (ppm), thorium (ppm) and total gamma ray (API) values were recorded in an excel spreadsheet and imported into Petra™ as well log data, *App_V.xls (available electronically).*

Appendix VI

Synthetic Lithofacies & Porosity Logs

Synthetic lithofacies and porosity logs were constructed in conjunction with measured sections and collected hand samples and imported into Petra™ as well log data. Integer values were assigned to corresponding lithofacies every twenty cm and discrete porosity data points (%) were recorded at their sampled stratigraphic horizon. Lithofacies and porosity values were recorded in an excel spreadsheet, *App_VI.xls (available electronically)*.

Appendix VII

Table of Zone Data (Petrel™ Model)

Summary table describing the input characteristics and simulation processes for each zone within the reservoir-analog model.

Zone	Lithostratigraphic Units	Quality	Layers / zone	Facies present (code #)	Facies Simulation	Polygons	Porosity Simulation
22	7a_Fs	Baffle	0	2,3	SIS	No	SGS
21	7a_Sgf	Reservoir	2	5,6,10	SIS	Yes	SGS
20	6b_Fs	Baffle	2	2,3,4,5,6,7	SIS	No	SGS
19	6b_Sgf	Reservoir	3	3,4,5,6,9,10	SIS	Yes	SGS
18	6a_Fs	Baffle	2	2,3,4,5,6,7	SIS	No	SGS
17	6a_Sgf	Reservoir	3	4,5,6,8,9,10	SIS	Yes	SGS
16	5b_Fs	Baffle	2	2,3	SIS	No	SGS
15	5b_Sgf	Reservoir	0	6,7,9,10	IK	No	SGS
14	5a_Fs	Baffle	4	2,3,4	SIS	No	SGS
13	5a_Sgf	Reservoir	2	5,6,7,9,10	SIS	Yes	SGS
12	4e_Fs	Baffle	2	2,3,4	SIS	No	SGS
11	4e_Sgf	Reservoir	2	5,9,10	IK	No	SGS
10	4d_Fs	Baffle	4	2,3,5,6,7	SIS	No	SGS
9	4d_Sgf	Reservoir	2	9	AV	No	SGS
8	4c_Fs	Baffle	0	3	AV	No	SGS
7	4c_Sgf	Reservoir	0	10	AV	No	SGS
6	4b_Fs	Baffle	0	3	AV	No	SGS
5	4b_Sgf	Reservoir	2	9	AV	No	SGS
4	4a_Fs	Baffle	0	3	AV	No	AV
3	4a_Sgf	Reservoir	2	3,4,5,6,7,8,9,10	SIS	Yes	SGS
2	3	Baffle	6	2,3,6	SIS	No	SGS
1	1&2	Reservoir	8	11	AV	No	SGS

Sgf	Sediment gravity flows
Fs	Fine-grained sediments
SIS	Sequential Indicator Simulation (Stochastic)
IK	Indicator Kriging (Stochastic)
AV	Assigned Value (Deterministic)
SGS	Sequential Gaussian Simulation (Stochastic)

Facies & code number

2	foraminiferal ws/ps
3	volcaniclastic foraminiferal ws/ps, ps/ws
4	skeletal foraminiferal ws/ps
5	graded fn-med skeletal ps
6	graded crs skeletal ps
7	graded v.crs skeletal ps
8	breccia: fn matrix
9	breccia: med matrix
10	breccia: crs-v.crs matrix
11	volcaniclastic skeletal ps/gs & skeletal gs

Appendix VIII

Table of Permeability Input Equations (Petrel^{TM} Model)

Table of equations that relate porosity (phi_pct) to permeability (perm) by lithofacies (FACIES). These equations were constructed from core-plug petrophysical data and were used to build the permeability model within Petrel^{TM}.

```
perm=U
perm =IF(FACIES=2,Pow(10,(2.87*Log(phi_pct)-3.99)),perm)
perm =IF(FACIES=3,Pow(10,(4.33*Log(phi_pct)-5.59)),perm)
perm =IF(FACIES=4,Pow(10,(8.18*Log(phi_pct)-10.77)),perm)
perm =IF(FACIES=5,Pow(10,(5.30*Log(phi_pct)-5.73)),perm)
perm =IF(FACIES=6,Pow(10,(8.29*Log(phi_pct)-10.22)),perm)
perm =IF(FACIES=7,Pow(10,(8.42*Log(phi_pct)-10.05)),perm)
perm =IF(FACIES=8,Pow(10,(3.62*Log(phi_pct)-3.89)),perm)
perm =IF(FACIES=9,Pow(10,(10.09*Log(phi_pct)-13.37)),perm)
perm =IF(FACIES=10,Pow(10,(8.32*Log(phi_pct)-10.18)),perm)
perm =IF(FACIES=11,Pow(10,(5.89*Log(phi_pct)-6.48)),perm)

PermeabilityZ=0.1*perm
```

Appendix IX

Dip Angle Maps

Dip angle maps of volcanic basement topography and modified basin topography after deposition of Units 1 and 2 shallow-water packstone-grainstones.

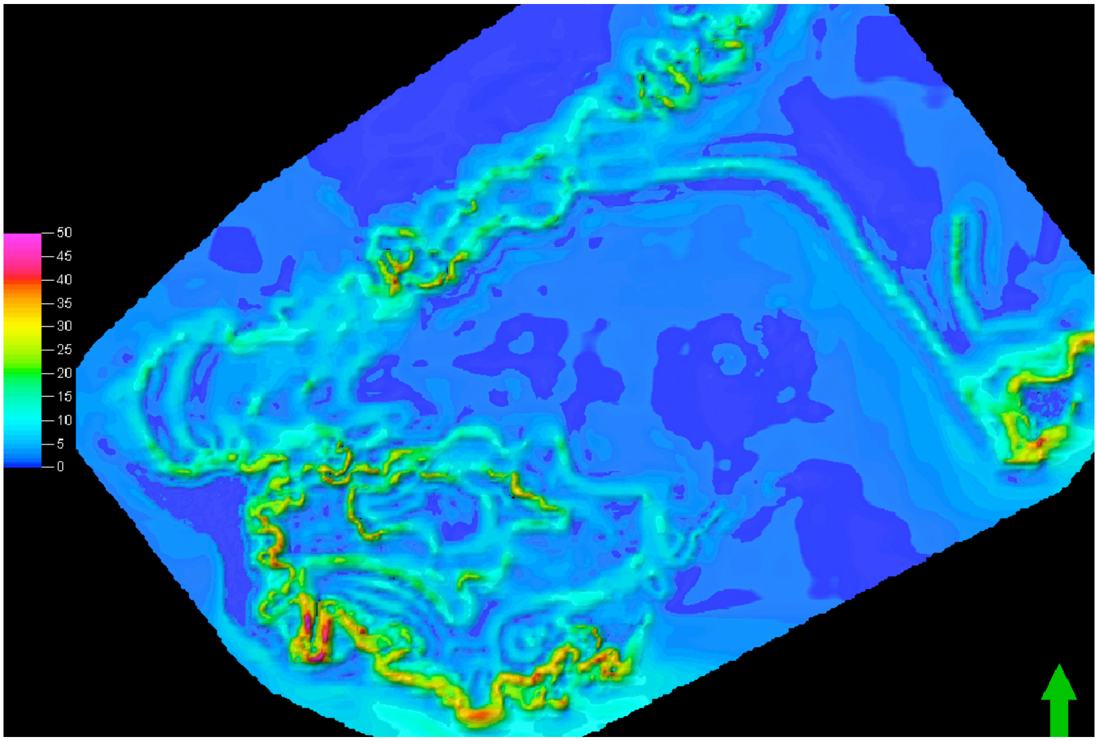

Volcanic basement topography dip angle map.

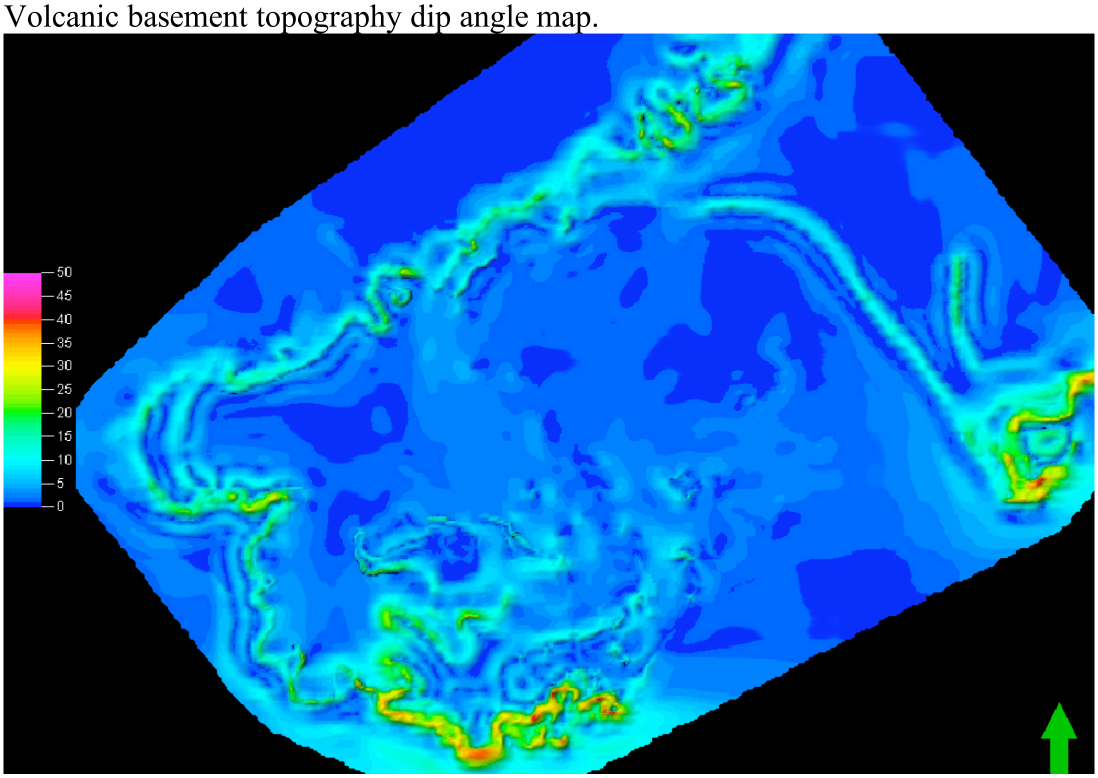

Shallow-water packstone-grainstone topography dip angle map.

Appendix X

Porosity Evolution

Petrographic analysis of the major lithofacies modeled in this study revealed that sediments in the Agua Amarga basin were subjected to variably amounts of diagenetic alteration. Variably abundant calcite and dolomite cement, dissolution of skeletal grains, and mechanical compaction features are all common processes indicative of diagenesis within the eogenetic realm (Mazzullo and Harris, 1992; Scholle and Ulmer-Scholle, 2003). High porosity and permeability values, however, suggest minimal alteration of original depositional fabrics for the majority of facies. Considering that the lithofacies in the Agua Amarga basin have not been subjected to burial conditions, the evolution of outcrop porosity and permeability values to their respective values in the subsurface is crucial in predicting reservoir-analog potential.

A decrease in porosity and permeability is widely predicted for lithofacies that are subjected to increasing burial (Schmoker and Halley, 1982; Schmoker, 1984; Amthor et al., 1994; Goldhammer, 1997; Budd, 2001; Ehrenberg and Nadeau, 2005). The lithofacies with the best potential for preserving reservoir-quality porosity and permeability in the subsurface are those with the highest initial percentages of interparticle porosity and least tendency for rapid diagenetic alterations (Budd, 2001; Ehrenberg and Nadeau, 2005). Grain size also plays an important role in the initial reduction of porosity and permeability. Fine-grained carbonate sediments often undergo significant thickness reduction during early burial, dramatically reducing pore-throat sizes, whereas coarser-grained sediments compact more slowly, preserving depositional porosity and permeability at greater depths (Goldhammer, 1997). Higher initial permeability values within coarser-grained sediments, however, commonly results in greater early cementation and associated porosity occlusion (Goldhammer, 1997). Within this study, the foraminifera-rich facies have the lowest reservoir potential in the subsurface due to initially small pore throats and a strong likelihood for porosity reduction through compaction and cementation during burial. The packstone-grainstones of the shallow-water play and the graded skeletal packstones of the deepwater plays have the best reservoir potential. Both of these facies preserve significant interparticle and intraparticle porosity despite evidence for early cementation. Breccia matrices of the deepwater plays also have good reservoir-potential, however, the greater tendency for dolomitization and dissolution of grains producing moldic porosity within this facies could be exacerbated in the subsurface and potentially limit reservoir quality if pore structure was reduced to separate molds encased in an impermeable matrix (Lucia, 1995). On the other hand, dolomite reservoirs formed in the eogenetic realm have a greater tendency to preserve porosity and permeability during burial than limestone reservoirs as a result of increased resistance to the effects of mechanical and chemical compaction (Amthor et al., 1994). Additionally, dolomite reservoirs have a greater tendency to form extensive, permeability-enhancing fracture networks with increasing depth, often making them better reservoirs than limestone reservoirs despite lower matrix porosity and permeability values (Schmoker et al., 1985).

Reference Cited

Amthor, J. E., Mountjoy, E.W., and Machel, H.G., 1994, Regional-Scale Porosity and Permeability Variations in Upper Devonian Leduc Buildups: Implications for reservoir Development and Prediction in Carbonates: AAPG Bulletin, v. 78, p. 1541-1559.

Budd, D. A., 2001, Permeability loss with depth in the Cenozoic carbonate platform of west-central Florida: AAPG Bulletin, v. 85, p. 1253-1272.

Ehrenberg, S. N., and Nadeau, P.H., 2005, Sandstone vs. carbonate petroleum reservoirs: A global perspective on porosity-depth and porosity-permeability relationships: AAPG Bulletin, v. 89, p. 435-445.

Goldhammer, R. K., 1997, Compaction and Decompaction Algorithms for Sedimentary Carbonates: Journal of Sedimentary Research, v. 67, p. 26-35.

Lucia, F. J., 1995, Rock-Fabric/Petrophysical Classification of Carbonate Pore Space for Reservoir Characterization: AAPG Bulletin, v. 79, p. 1275-1300.

Mazzullo, S. J., and Harris, P.M., 1992, Mesogenetic Dissolution: Its Role in Porosity Development in Carbonate Reservoirs: AAPG Bulletin, v. 76, p. 607-620.

Schmoker, J. W., 1984, Empirical Relation Between Carbonate Porosity and Thermal Maturity: An Approach to Regional Porosity Prediction: The American Association of Petroleum Geologists, v. 68, p. 1697-1703.

Schmoker, J. W., Krystink, K.B., and Halley, R.B., 1985, Selected Characteristics of Limestone and Dolomite Reservoirs in the United States: The American Association of Petroleum Geologists Bulletin, v. 69, p. 733-741.

Schmoker, J. W., and Halley, R.B., 1982, Carbonate Porosity Versus Depth: A Predictable Relation for South Florida: The American Association of Petroleum Geologists v. 66, p. 2561-2570.

Scholle, P. A, and Ulmer-Scholle, D. S., 2003, A Color Guide to the Petrography of Carbonate Rocks: Grains, textures, porosity, diagenesis, AAPG Memoir 77, Tulsa, Oklahoma, The American Association of Petroleum Geologists.